國立臺灣大學工學院土木工程學系

碩士論文

Department of Civil Engineering
College of Engineering
National Taiwan University

Master's Thesis

以經濟可行性為核心的電動公車 V2G 最佳化系統分析

Optimization Analysis of the Electric Bus V2G System Focused on Economic Feasibility

王竣平

Chun-Pin Wang

指導教授：詹瀅潔 博士

Advisor: Ying-Chieh Chan, Ph.D.

中華民國 114 年 7 月

July, 2025

doi:10.6342/NTU202502274

國立臺灣大學碩士學位論文
口試委員會審定書

NATIONAL TAIWAN UNIVERSITY
MASTER'S THESIS ACCEPTANCE CERTIFICATE

以經濟可行性為核心的電動公車V2G最佳化系統分析

Optimization Analysis of the Electric Bus V2G System Focused on Economic Feasibility

本論文係 王竣平 (R12521701) 在國立臺灣大學土木工程學系營建工程與管理組完成之碩士學位論文，於民國114年06月25日承下列考試委員審查通過及口試及格，特此證明。

The undersigned, appointed by the Department of Civil Engineering Construction Engineering and Management on 06/25,2025 have examined a Master's Thesis entitled above presented by WANG, CHUN PIN (R12521701) candidate and hereby certify that it is worthy of acceptance.

口試委員 Oral examination committee:

詹瀅潔 詹瀅潔

(指導教授 Advisor)

謝依芸 謝依芸

紀乃文 紀乃文

系主管 Director： 葛宇甯 葛宇甯

doi:10.6342/NTU202502274

誌謝

本論文得以順利完成離不開詹瀅潔老師的悉心指導。感謝老師在研究方向、資料分析與論文撰寫上提供寶貴的建議與耐心指導，讓我在研究過程中能夠不斷進步，並培養出更嚴謹的學術態度與思考能力。老師不僅在專業知識上給予我莫大的幫助，也在研究態度與人生方向上給予我許多啟發與鼓勵，使我在遇到困難時仍能保持信心與毅力。誠摯感謝口試委員謝依芸老師與紀乃文老師撥冗擔任本論文的審查委員，並提供寶貴的建議與回饋。在口試中，兩位老師提出的問題與觀點，幫助我從不同角度重新思考研究內容與方法，也讓我有機會釐清研究架構中的不足之處，使本論文更加完整。您們的專業指導與鼓勵，對我而言受益良多，深表感謝。感謝洪梓航、顏永裕、蔡承耘和顏偉哲等同學，在我撰寫本研究程式碼最感到無助的時刻，總是耐心地指導我解決技術上的問題。你們不僅協助我排除一個又一個錯誤，更幫助我建立起獨立解決問題的思維與信心。感謝詹 lab 的同學彭子庭、楊舜宇、顏偉哲以及郭銘晉同學，在過去兩年的研究歷程中，謝謝你們的陪伴與合作，讓研究室的生活不再只是冷冰冰的程式與數據。從討論研究議題到日常的交流與歡笑，這段時光成為我碩士生涯中最珍貴的回憶之一。感謝營管組的同學們，這兩年來一起經歷了無數次的吃飯、出遊、研究討論與上課時光，無論是學術上的交流還是日常的相處。最後感謝支持一路過來的家人朋友們提供的支持，使學習無後顧之憂。

王竣平 謹誌

中華民國一百一十四年七月

doi:10.6342/NTU202502274

中文摘要

近年來，城市電動化與淨零排放政策推動下，電動公車不僅是潔淨載具，更逐漸展現作為電網儲能單元的潛力。然而，V2G（車連網）系統的實際運作牽涉高度複雜性，其必須同時整合公車排班、太陽能發電變化、時間電價制度（TOU）、電池衰退成本與充電樁設施配置等多重因素，並考量這些因素之間的交互影響與時序關聯。由於傳統的操作方法無法處理這類動態、非線性且離散的調度問題，因此本研究提出一套混合整數線性規劃（MILP）模型，作為最佳化運算框架，以提升整體營運與能源管理效益。本研究以臺北市為場域，結合三座主要電動公車場站、九條路線與周邊學校屋頂太陽能系統進行模擬分析。模型結果顯示，在基線情境下，導入 V2G 系統每月可降低營運成本約新台幣 22 萬元，惟若初期投資過高，回收期仍可能超過 36 年。透過 Latin Hypercube Sampling（LHS）與 Sobol 全域敏感度分析，本研究發現”建物售電價格”與”尖峰時間電價”為關鍵政策參數；而電池衰退成本與太陽能轉換率亦具次要但不可忽視的影響。在參考政策與技術組合下，如建物售電價格 NT$2/kWh、TOU 尖峰電價 NT$10/kWh、電池容量 500kWh、衰退成本 NT$0.26/kWh，回收期可縮短至 6 年內。研究亦指出，當車隊電動化比例達 75%、並採取 1:2.22 的車樁配置時，可進一步縮短投資回收期並提升經濟效益。本研究提供一套具實證基礎的策略架構，協助政府與運輸單位在資源有限情境下，有效推動具經濟韌性的電動公車能源系統整合與永續城市轉型。

關鍵字: 車連網系統、電動公車、場站基礎設施、太陽能系統、經濟可行性、混合整數線性規劃、敏感性分析

doi:10.6342/NTU202502274

Abstract

As cities worldwide move toward transportation electrification and carbon neutrality, electric buses are increasingly recognized not only as clean transport solutions but also as distributed energy storage units through Vehicle-to-Grid (V2G) systems. However, managing a large-scale V2G operation presents considerable complexity. It involves simultaneously coordinating bus dispatch schedules, solar generation fluctuations, time-of-use (TOU) electricity peak prices, battery degradation, and infrastructure constraints. These factors require careful alignment between charging, discharging, and route needs. As such, simple rule-based strategies are insufficient; an optimization-based framework is essential for maximizing cost-effectiveness while maintaining operational feasibility. To address this challenge, this study proposes an optimization-based framework that integrates V2G operations with rooftop solar photovoltaic (PV) systems in an urban transit context. A mixed-integer linear programming (MILP) model is developed to minimize total operational costs while considering real-world bus schedules, depot constraints, and solar generation from adjacent school rooftops in Taipei City. The model simulates 3 bus depots and 9 routes under various energy and policy scenarios. Baseline results show V2G can reduce monthly operational costs by NT$220,000, though the payback periods payback period exceeds 36 years hdue to high initial investment. Sensitive analyses using Latin Hypercube Sampling (LHS) and Sobol methods identify building solar electricity selling price which usually considering as feed in tariff (FIT) and TOU rates as dominant policy leverages. When some favorable conditions are applied NT$2/kWh solar feed-in price, NT$10/kWh TOU peak rate, 500 kWh battery capacity, and NT$0.26/kWh degradation cost the payback periods can be reduced to under six years. The model also finds that V2G becomes viable only when at least 75% of the fleet is electrified and recommends a

doi:10.6342/NTU202502274

charger-to-bus ratio of 1:2.22 to minimize capital investment. These insights provide a data-driven foundation for transit agencies and policymakers to design scalable, cost-effective, and policy-responsive V2G deployment strategies for sustainable urban transportation.

Keywords: Vehicle-to-Grid (V2G), Electric Buses, Depot Infrastructure, Solar Photovoltaics, Economic Feasibility, Mixed-Integer Programming, Sensitive Analysis

doi:10.6342/NTU202502274

Contents

doi:10.6342/NTU202502274

doi:10.6342/NTU202502274

doi:10.6342/NTU202502274

doi:10.6342/NTU202502274

List of Figures

doi:10.6342/NTU202502274

doi:10.6342/NTU202502274

doi:10.6342/NTU202502274

doi:10.6342/NTU202502274

List of Tables

doi:10.6342/NTU202502274

List of Appendix Tables

doi:10.6342/NTU202502274

Nomenclature

	Symbol	Description	Category
0	t (period)	Time index (1 hour per time step)	Indices & Sets
1	i (unit)	Index for electric bus units	Indices & Sets
2	nperiods	Set of all time periods	Indices & Sets
3	units	Set of all electric bus units	Indices & Sets
4	field	Charging site	Indices & Sets
5	fields	Set of all charging sites	Indices & Sets
6	α_{ist}	1 if unit i is operating at time t, 0 otherwise	Binary Variables
7	β_{ist}	1 if fast charging is active for unit i at time t	Binary Variables
8	γ_{ist}	1 if slow charging is active for unit i at time t	Binary Variables
9	η_{ist}	1 if V2G discharging is active for unit i at time t	Binary Variables
10	FC_{ist}	Fast charging amount (grid)	Energy Variables
11	SC_{ist}	Slow charging amount (grid)	Energy Variables
12	SFC_{ist}	Solar-powered fast charging amount	Energy Variables
13	SSC_{ist}	Solar-powered slow charging amount	Energy Variables
14	D_{ist}	V2G discharging amount	Energy Variables
15	C_{ist}	V2G charging amount (battery input)	Energy Variables
16	$Consump_{ist}$	Operational energy consumption	Energy Variables
17	SOC_{ist}	State of charge	Energy Variables
18	$ISOC_{ist}$	Increase in SOC	Energy Variables
19	$DSOC_{ist}$	Decrease in SOC	Energy Variables
20	P_t	Electricity price (TOU)	Cost & Price Parameters
21	TP_t	Tiered TOU electricity price	Cost & Price Parameters
22	$EVCP_t$	TOU price for EV charging	Cost & Price Parameters

	Symbol	Description	Category
23	SP_t	Solar generation cost	Cost & Price Parameters
24	BC	Battery degradation cost per kWh	Cost & Price Parameters
25	BD_{ist}	Battery degradation cost	Cost & Price Parameters
26	SP	Total cost of slow grid charging	Cost & Price Parameters
27	FP	Total cost of fast grid charging	Cost & Price Parameters
28	SSP	Total cost of slow solar charging	Cost & Price Parameters
29	SFP	Total cost of fast solar charging	Cost & Price Parameters
30	DP	Revenue from V2G discharging	Cost & Price Parameters
31	BDP	Battery degradation total cost	Cost & Price Parameters
32	FSC	Fast/slow grid charging price ratio	Cost & Price Parameters
33	SFSC	Fast/slow solar charging price ratio	Cost & Price Parameters
34	BSoP	Selling price of surplus solar power	Cost & Price Parameters
35	UCap	Infrastructure capital cost	Capital & Maintenance Costs
36	CharCap	Capital cost for V2G chargers	Capital & Maintenance Costs
37	UO&M	Monthly O&M cost of infrastructure	Capital & Maintenance Costs
38	CharO&M	Monthly O&M cost of V2G chargers	Capital & Maintenance Costs
39	BATCost	Battery replacement cost	Capital & Maintenance Costs
40	Rev	Profit from operational cost reduction	Economic Indicators
41	ROI	Return on investment	Economic Indicators
42	DoDCycle	Battery life cycle (DoD cycles)	Economic Indicators
43	η_{pv}	Solar transfer efficiency	Solar Parameters
44	roof	Rooftop area	Solar Parameters
45	I	Solar irradiance (Wh/m²)	Solar Parameters
46	T	Temperature	Solar Parameters

doi:10.6342/NTU202502274

1. Introduction

Unlike traditional vehicle operations, Vehicle-to-Grid (V2G) systems must simultaneously manage charging and discharging timing, energy cost, solar variability, and battery degradation behavior. These multidimensional interactions make simple scheduling infeasible and require an optimization framework to achieve cost-effectiveness and operational feasibility.

1.1 Background and Motivation

In this era of rapid urban development, the swift growth of has led to a significant decline in the energy self-sufficiency of urban communities. Rely on the traditional way with the electricity system is not sustainable anymore, therefore we are urge to find an innovative way to refresh it. At the same time, the increasing adoption of electric buses (EVs) in cities presents new opportunities to leverage EVs batteries as distributed energy storage resources. Our research purpose aims to explore how electric vehicles resources can be integrated existing power grid to support the planning and development of future urban energy systems. Therefore, this research will try to give a possible future planning for Taipei area by 2030.

In terms of development for sustainable city in the future, the National Development Council (NDC) of Taiwan has pointed out a strategy. First of all, in the energy field the NDC set 35% of decarbonization by renewable energy like solar energy and advanced technology for storage energy from 2023. About transportation field, NDC outlined 16% of decarbonization by applying green transportation like electric public transportation. This plan includes fully electrifying urban bus fleets by 2030. As of January 2024, a total of 630 electric buses have been deployed in Taipei City. However, With the increase of the electrified fleet may cause higher pressure on grid. Accordingly,

doi:10.6342/NTU202502274

we believe that Taipei possesses a sufficient number of electric buses that can serve as energy storage units within a V2G system and have the positive interaction effect with the solar system located in the urban city area [1].

In Taiwan, despite policy efforts to electrify urban bus fleets, limited depot charging infrastructure, lack of dynamic dispatch systems, and underutilization of rooftop solar resources pose challenges for scalable, economically viable deployment. A data-driven V2G strategy is urgently needed to bridge this gap.

1.1.1 Urban Transportation Electrification Trends and Challenges

In response to the global push for carbon neutrality, countries are accelerating the electrification of public transportation. An urban bus system is not a plug-and-play process. Operators must coordinate vehicle dispatch schedules, solar energy fluctuations, time-of-use (TOU) electricity peak prices, battery degradation profiles, and charging infrastructure limits. These variables interact across time and space, making the system too complex for heuristic or rule-based scheduling. Therefore, a robust optimization framework is necessary to identify feasible and cost-effective operation strategies under real-world constraints. There are several foreign studies focus on urban electric buses development we also want to review, some mentioned the electric buses faced the longer charging time than diesel fuel buses which created the challenge of scheduling[2], some paper mentioned robust optimized schedule can help for formulating[3], some research urge for integrating with closing depot renewable energy[4, 5]. Some paper mentioned to conduct incentive policy[6], and utility design of the buses depot are also matter [7]. These gave us an incentive to dig out the Taiwan's urban electric buses status and policy for us to form our model and recommendations.

To expand upon the complex plan in the green urban transportation plan in Taiwan, several documents have served as guiding lights in the darkness. For example,

doi:10.6342/NTU202502274

Automotive Research & Testing Center (ARTC) did a guideline, they imply that European Union has plans to reduce carbon dioxide emissions with electrify its all the public bus fleet by 2030. In contrast, Taiwan, due to the background of its bus industry developing history, has initially prioritized the electrification of urban bus systems which has been highlighted as the main transportation resources in our future planning. With this ambitious, Taiwan's Ministry of Economic Affairs (MOEA) and Ministry of Transportation and Communications (MOTC) have jointly launched a three-year national project focused on the domestic production of ten major components, aiming to strengthen local design and development capabilities and ultimately support the local manufacturing of electric buses in Taiwan. Aligned with the broader objectives of transport electrification, the Forward-looking Infrastructure Development Program, approved by the Executive Yuan, has designated green energy infrastructure as a priority. As part of our thesis initiative, MOEA and MOTC are collaboratively implementing the "DMIT Program" (Design, Manufacturing, Integration, and Testing) for intelligent electric buses with green transportation which include V2G system. Under this program, MOEA is tasked with coordinating industry collaboration for the development of key systems and complete vehicle designs, accelerating the localization of entire vehicles and four major subsystems which gave a great opportunity to develop energy management system for electric buses. Consequently, a large number of electric buses are expected to be deployed across Taiwan's urban areas. This study, therefore, provides an important contribution to the development of auxiliary systems for electric buses in the near future [8].

However, the rapid growth of electrified buses, if not supported by effective energy management and the integration of renewable energy, may lead to increased dependence on grey energy electricity generated from fossil fuels thus undermining the intended goals

doi:10.6342/NTU202502274

of green energy transition. Therefore, it is essential to consider the operational demands and constraints of domestic electric bus systems. Here is study from Taiwan government aims to shave peak-time charging pressure through scheduling strategies. MOTC induce the TOU pricing and capacity contracts with buses for encourage operators to adjust charging schedules in response to grid demand. The study further argues that refresh the traditional sequence charging, smart charging strategies should be prioritized. Additionally, the integration of solar photovoltaic (PV) systems is recommended by the government as well [9].

Lee interviewed several bus companies, including Taoyuan and Hsinchu Bus operators, to explore suitable scheduling patterns for electric buses. Her research helped clarify how electric buses operate differently from diesel buses, especially in terms of charging behavior. Most operators charged buses at night during off-peak hours, but many also added charging at noon to ensure full-day operation. This strategy matches well with solar power generation at midday, which improves energy efficiency. The study also pointed out that scheduling must follow Taiwan's labor regulations on driver working hours. This requirement encourages more discussion about integrating electric buses with intelligent vehicle systems [10]. Lin used a simulated annealing algorithm to optimize electric bus operations. His results showed that adjusting charging schedules through optimization could reduce extra costs, such as overtime and early returns. This finding highlights the potential of algorithm-based scheduling to improve operational efficiency in electric public transport [11]. Chen analyzed the economic conditions of electric bus operations in Taiwan. He noted that, with government subsidies, electric buses currently have a short-term cost advantage over diesel buses. However, he emphasized that long-term sustainability depends on how well operators adopt clean energy technologies, such

doi:10.6342/NTU202502274

as green electricity. Without such measures, electric buses may lose their competitiveness when subsidies end [12].

Another topic is incentive from previous is to utilized optimization model to optimize the idle time with these electric buses, in order to this opinion we survey several studies have investigated the idle periods of electric buses. For example, in California's bus system, vehicles typically experience 14 to 16 hours of idle time per day, particularly between 20:00 and 06:00. To accommodate peak-hour demands, a portion of the fleet also remains idle during daytime hours. In cases where buses are designated for school transport or other lower needed area, the idle duration can extend to 18 to 20 hours per day [13].

1.1.2 Renewable Energy Policy and Power Grid Trends and Challenges

Speak of the energy policy, since 1979 Taiwan Power Company (Taipower) has implemented demand side management strategies aimed at encouraging users to shift electricity consumption away from peak periods. By offering electricity rate discounts, Taipower incentivizes users to participate in load shifting which can solve the fluctuations of renewable energy for energy generation to meet the balance from generation and using.

In these regions, TOU pricing mechanisms have proven effective in reducing peak demand by increasing electricity prices during high-load hours like winter evenings or summer nights. In Taiwan, our peak time of the grid usually in the summer night which Taipower are trying focus on.

Taiwanese government also provided a Renewable Energy Development Act, requiring that at least 30% of the rooftop area of new or renovated buildings be used for installing solar panels. According to estimates from the Ministry of Economic Affairs, every 20 square meters of rooftop space can support about 1 kilowatt of photovoltaic (PV) capacity. Based on this policy, we expect that Taipei City holds strong potential for

doi:10.6342/NTU202502274

decentralized solar development, opening new opportunities for sustainable urban energy solutions. Taipei City Government previously conducted studies on solar energy potential across different parts of the city. Before 2019, they estimated an installable capacity of around 29 megawatts. In addition, research by the Taiwan Green Productivity Foundation in 2008 suggested that if all schools under the Taipei City Department of Education installed solar PV systems, they could collectively generate at least 2.7 MWp of electricity. With ongoing improvements in solar PV technology, we believe that Taipei's potential for solar power generation will continue to grow [14].

To better understand the structural challenges of electricity transmission in northern Taiwan, this study takes a closer look at the 2023 power grid situation as shown in **Figure 1**. We found that most of the base load electricity supply in the region has shifted from natural gas. We assumed that the V2G can set as a replacement of the natural gas base load energy. Therefore, this research began by analyzing the grid systems in Taipei City, New Taipei City, Keelung, and Taoyuan. This helps us evaluate the possible limitations of a centralized power grid and lays the foundation for discussing the potential of developing a V2G system in this area. We used data provided by Taipower to examine the grid conditions in northern Taiwan, especially focusing on the northeastern and northwestern power systems. The region faces a power shortfall of about 3,500 MW, while its electricity demand typically ranges between 10,000 and 11,000 MW. About 66% of the electricity comes from thermal power plants, while the remaining 27% is supplied from central and southern Taiwan. Further analysis of thermal power generation shows that most of the electricity comes from the Tatan Natural Gas Power Plant located in Taoyuan. Electricity is transmitted into Taipei through two major extra-high voltage substations: Dinghu and Xiandu. This setup reveals a potential weakness in the grid. Therefore, developing decentralized and self-sufficient energy systems appears necessary

doi:10.6342/NTU202502274

for improving energy security in northern Taiwan. According to the international energy agency the grid distribution cost up to NT$0.5/kWh, no to say the cost of massive power failure. With this understanding we can see the opportunity of decentralized grid which is involved V2G.

We used web-scraped data to analyze the power grid over a one-day period, focusing on the four private natural gas power plants that supply electricity to the Taipei area. The data shows that these plants reach their peak generation between 16:00 and 23:00. This generation pattern aligns with the peak demand period defined by the time-of-use pricing system discussed earlier. This finding is organized in **Figure 2**. In the appendix we based on the the emission profiles of northern Taiwan's electricity mix and pollutant factors [15], gived the estimated health externality cost is approximately NT$1.8 per kilowatt-hour, demonstrating the public health value of V2G systems through air pollution reduction.

doi:10.6342/NTU202502274

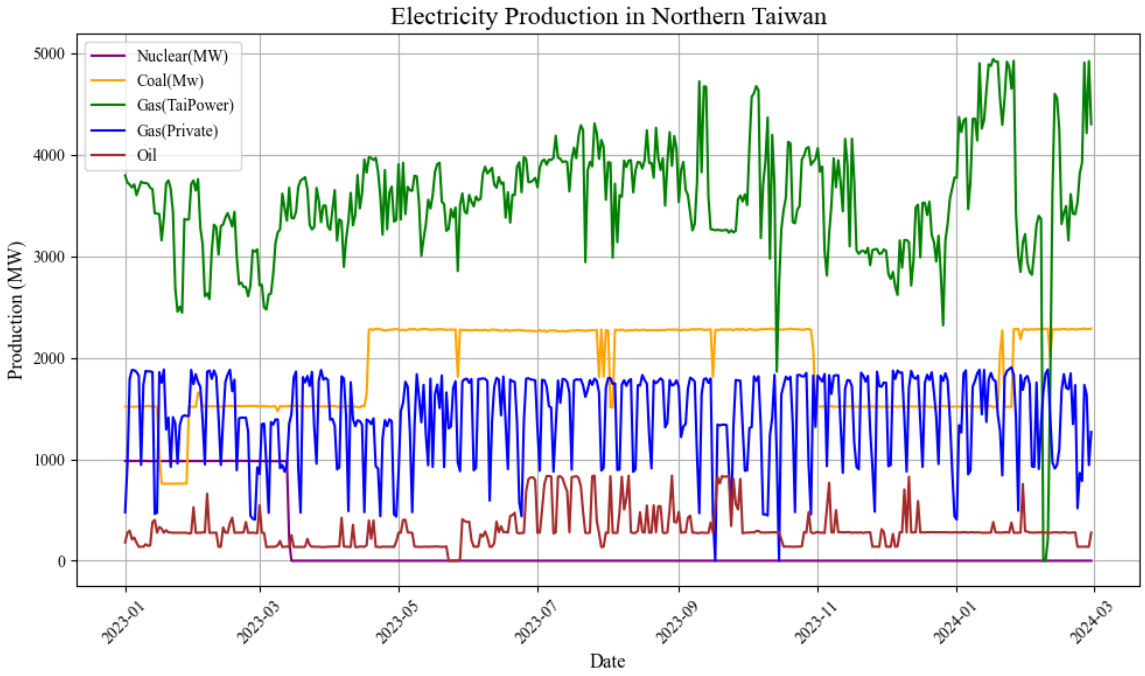

Figure 1 Power Generation Profile of Northern Taiwan in 2023

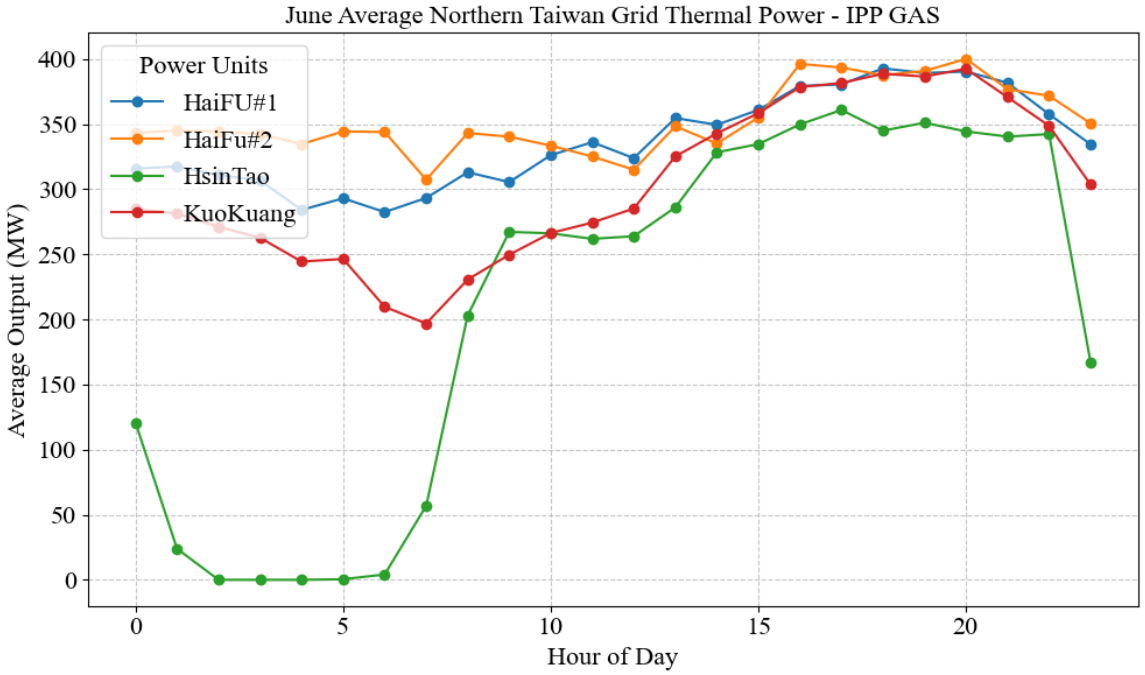

Figure 2 Average Thermal Power Output of Private Natural Gas Plants

in Northern Taiwan, June 2024

doi:10.6342/NTU202502274

1.2 Literature review with V2G Applications

Several recent studies have explored how V2G and Vehicle-to-Building (V2B) systems can optimize energy usage across various scenarios. In general, many studies focus on the societal benefits of V2G systems, particularly how they integrate with transportation networks to promote decarbonization. About seasonal effect, He applied clustering analysis to classify power usage patterns across different seasons. They examined how electric vehicle (EV) integration could be optimized in commercial buildings by evaluating the effects of EV quantity on both electricity cost and grid demand. The results showed that when accounting for seasonal solar generation, building load curves, and electricity pricing, the ideal number of EVs varied by season with 25 vehicles in summer and 9 in winter. Their model demonstrated that electricity costs could be reduced by at least 50% during the summer, providing strong empirical support for applying smart energy strategies in buildings [16]. There are also V2B experiment here in Taipei, Taiwan with optimization model to determine using stand battery system and electric vehicles and show it has economy and environmental benefit [17].

For instance, V2G load shifting has been shown to reduce carbon emissions by 1.1% [18], while V2G systems using school buses can contribute to a 0.36% reduction in the state fleet located [19]. Other studies, such as Yang's research, emphasize the role of V2G in achieving carbon neutrality [20]. Some studies also examine the impact of local electricity generation systems on carbon emissions by analyzing charging patterns, which is useful for urban energy planning incorporating V2G systems [15]. Additionally, some papers explore the potential of V2G systems working with islanded microgrids to facilitate black start capabilities, in cooperation with existing electricity generation systems [21]. Furthermore, other research delves into how charging patterns influence the V2G system and its interaction with electricity loads [13]. In summary, V2G systems are

doi:10.6342/NTU202502274

a multifaceted area of research, involving a range of perspectives, parameters, and methods for energy optimization. The following literature review will examine studies that build on these foundational concepts, providing further insights into the application and future directions of V2G research.

Liao demonstrated that over a 30-year operational period, an EV fleet in Michigan, USA, could achieve an economic return of up to 30% of the initial operating costs in Net Present Value (NPV) terms. They also noted that larger EV batteries present better opportunities for V2G applications [22]. In economic analysis with V2G studies goes back to Shirazi [23] conducted a NPV analysis of electric school buses operating under a V2G system, using school buses in Pennsylvania as their case study. The study estimated that the cost per seat for electric buses, compared to diesel buses, was approximately USD 7,200 (NT$216,000) higher. One key finding was that temperature had a significant impact on both the operation and economic benefit of the V2G system. Specifically, if the system did not include thermal management and was shut down at temperatures below -6.7°C, the potential revenue could drop by 22%. Based on this, the authors suggested that V2G systems are more suitable for warmer climates. In this paper, it supposed bigger electric buses has more potential with V2G system due to scale effect. Hsu, Kuo, Tsai, and Yeh conducted a NPV analysis to examine the economic benefits of integrating electric buses with the power grid in the Taipei area. The study compared three operational models: diesel buses, electric buses, and electric buses combined with a V2G system. It considered fixed costs, variable costs, and tax-related expenses, while also testing different TOU electricity peak pricing levels at NT$8, NT$10, and NT$12 per kWh. The results confirmed the economic feasibility of electric bus operations under these scenarios. From a financial perspective, electric buses demonstrated better cost-effectiveness than diesel buses. When including government subsidies and V2G revenue,

doi:10.6342/NTU202502274

the net present value of electric buses reached up to NT$277.4 million, significantly higher than the diesel bus model, which peaked at around NT$201.9 million. However, the study did not include data on battery degradation, which presents a valuable research gap. Our study builds upon their findings by incorporating a broader range of hidden costs and operational scheduling benefits [24]. Compared to Shirazi, who based their evaluation on a 14-year bus depreciation period in the U.S., Hsu et al.'s study used Taiwan's standard 8-year depreciation. This difference highlights the importance of considering depreciation period as a key parameter, which we include in our model. Through reviewing literature that applies the NPV method, we find consistent evidence supporting the overall effectiveness of V2G systems. In transportation engineering, applying optimization models allows researchers to extract more precise parameter changes, which are critical for sensitive analysis. Some studies have already attempted to define and evaluate key V2G parameters through simulation and comparison. Based on Shirazi we found three essential factors that shape the economic viability of V2G which is initial capital cost, battery, and TOU pricing. These elements serve as the foundation for our upcoming review of optimization based V2G models [23].

Taking TOU pricing as an example, Moradipari's research showed that focused on the TOU price can leads to 62.5% of operation reduction, if it can combine with solar PV system even can reduce 91.3% operation cost, there method will be shifting the charging schedule into night and have free charging with solar energy in V1G scenario (No discharging)[25]. Onsite solar PV system with V2G system in Italian scenario can approximately cut total annual cost up to 5.6% ~ 17.1% with Mixed Integer Linear Programming (MILP) approach for the optimization in Italian electricity market [26].

Fei pointed out that different electricity market mechanisms can lead to varying economic outcomes. In their comparison between Frequency Control Reserve (FCR) and

doi:10.6342/NTU202502274

Sale by Market Price (SbMP) models, they found that the SbMP model makes more aggressive use of arbitrage strategies like buying electricity at low prices and selling at higher prices. However, this also results in more frequent battery discharging, which increases the risk of battery degradation. Our study will focus on the SbMP model, optimizing power dispatch based on TOU pricing while also accounting for battery degradation [27]. Based on Fei findings, we also consider that fleet-scale plays a role in profitability. Specifically, a minimum of 14 vehicles is needed for the operator to benefit from adjusting service hours to match price differentials in the electricity market. This consideration will be included when designing the fleet configuration in our model [27]. Tian also used TOU pricing as a core parameter to optimize the timing of electric vehicle (EV) charging and discharging, aiming to improve grid stability. In his optimization model, the objective function was designed around a TOU-based V2G power control strategy, with the goal of minimizing electricity costs for EV owners while reducing stress on the grid. The strategy analyzed electricity price fluctuations throughout the day to determine the most efficient charging and discharging times, optimizing overall energy usage. The results showed that the V2G system significantly improved both grid stability and operational efficiency. In case studies conducted in Beijing and Jilin, the model reduced peak grid load by up to four times. Given Taiwan's long-standing implementation of TOU pricing, this study will adopt insights from Tian's work and incorporate the local TOU scheme into our optimization model to evaluate the applicability of V2G strategies in the Taiwanese context [28]. Arsalan analyzed the use of household vehicles in V2G operations through market transactions with the Japan Electric Power Exchange (JEPX). The study simulated the potential profits and challenges arising from daily V2G operations. It found that shifting the original charging time from 8:00–12:00 and discharging time from 0:00–3:30 to a new schedule of 9:00–15:00 for charging and

doi:10.6342/NTU202502274

17:00–21:00 for discharging could significantly increase short-term revenue. However, this new strategy may lead to faster battery degradation over the long term. Therefore, the study highlighted the need to balance profit gains with battery life in long-term operations. It is also worth noting that Arsalan's research did not account for the upfront capital investment required to implement the system. In contrast, our study will include initial capital costs as part of the model to better reflect real-world financial conditions [29].

The study also proposed an optimization model that considers the actual operating conditions of electric buses. It integrates the planning of charging infrastructure with scheduling strategies based on real-world bus operations. By aligning planning with real service patterns, the model can effectively reduce both total operational costs and peak electricity charges. In particular, optimizing infrastructure during the planning phase can lower costs by around 20%, while optimizing charging strategies during the operational phase can further reduce operating costs by 68%. In this study, the initial investment cost for high-power charging equipment was defined as over USD 25,000 (NT$750,000), and battery costs were estimated at USD 700/kWh (NT$21,000/kWh). These values are adopted as key reference parameters in the present research [30].

Battery degradation is also a common focus in optimization models. Borge-Diez defined and formulated the cost calculation for battery degradation within their model assumptions [31]. Ager-Wick Ellingsen studied electric vehicle batteries made of different chemical compositions and conducted destructive testing to verify battery cycling behavior, particularly within the 20% to 80% state-of-charge range [32].

Lee highlighted the critical role of battery degradation in V2G system design, outlining various parameters and relationships involved in battery degradation, such as "Cycle Degradation," "Temperature," and "Voltage." [33]. Zeng emphasized that, based on simulation results, if charging control is not properly managed, the degradation cost

doi:10.6342/NTU202502274

of EV batteries could exceed the actual charging cost by more than ten times or 87.26% of total operation cost [34]. Manzolli conducted a case study in Coimbra, Portugal, where battery degradation was incorporated into both the objective function and constraints of their optimization model. Their results showed that when battery prices dropped below EUR 100/kWh (NT$3,700/kWh), the cost-effectiveness of electric buses improved significantly. By comparing the 30-year total cost of ownership (TCO) between electric and diesel buses, they found that electric buses could reduce overall costs by up to 38% [35]. Also, there is a research reveal that under RMB 600/kWh can reduce 75.32% of total operational cost [36].

1.3 Research Gap

Based on the literature review studies, it is evident that V2G systems hold promising potential to address urban energy challenges and support transportation electrification in Taiwan. However, several critical research gaps remain, limiting the practical applicability of V2G solutions, especially for urban electric bus fleets. These gaps can be summarized as following context.

1. Lack of integrated multi-factor optimization frameworks

   Most existing studies focus on single-dimensional analyses are consider only one or two variables in analysis, failing to capture the complex interdependencies among technical, economic, and policy factors. For example, TOU peak pricing, solar generation, and battery degradation are often modeled independently or under simplified assumptions, which reduces realism and decision-making relevance.

2. Gap related to urban localization

   Many studies are conducted in suburban, low density urban contexts or focus on private electric vehicles. They often neglect localized conditions prevalent in dense East Asian cities like Taipei, such as rooftop solar availability on public facilities,

doi:10.6342/NTU202502274

inflexible bus scheduling, and Taiwan's unique TOU electricity peak pricing. This limits the transferability of findings to such urban environments.

3. Perspective gap regarding public transit operators

   Existing research tends to emphasize macro-level social benefits, such as carbon mitigation and grid support, while overlooking the operational constraints and economic incentives of public transit operators. Since these stakeholders are crucial for real-world V2G implementation, neglecting their perspective can lead to impractical or infeasible strategies.

These gaps hinder the development of actionable, location-specific V2G strategies for electric bus systems, and reduce the utility of current models for public-sector infrastructure planning. Without addressing these challenges, policy recommendations and infrastructure planning risk remaining conceptual rather than operationally robust.

1.4 Research Objectives

To address these issues, this study aims to investigate the economic feasibility and sensitive-driven optimization of integrating rooftop solar energy with V2G systems in urban electric bus operations. The specific objectives are list here.

- To develop a mixed-integer linear programming (MILP) model that incorporates real-world operational constraints, including bus dispatch schedules, rooftop solar potential, battery degradation, and TOU electricity peak pricing.
- To quantify the impact of key policy-related and science-oriented parameters on total operational costs and payback periods using Latin Hypercube Sampling (LHS) and Sobol sensitive analyses.
- To identify cost-effective and policy-feasible parameter combinations that minimize payback periods while ensuring energy sustainability.

Therefore, this thesis is structured as follows.

doi:10.6342/NTU202502274

- Chapter 2 presents the overall modeling framework, including the formulation of the mixed-integer linear programming (MILP) model, key assumptions, and constraint design.
- Chapter 3 describes the simulation results under baseline and sensitive conditions, including cost-saving potential, optimal parameter settings, and scenario comparisons.
- Chapter 4 concludes the study by discussing key findings, model limitations, policy implications, and recommendations for future research and implementation in Taiwan.

doi:10.6342/NTU202502274

2. Methodology

2.1 Research Framework and Scope

This study follows the overall framework shown in **Figure *3***. First, data related to energy, transportation, and electricity policies are collected and fed into a Gurobi-based optimization model to obtain preliminary results. Next, key model parameters are projected to the year 2030 to build an interval-based parameter model. In the sensitive analysis stage, the first phase uses Latin Hypercube Sampling (LHS), which has faster convergence, to perform the initial optimization analysis. A regression analysis is then applied to the optimized results to evaluate the impact of each parameter on total system cost. In the second phase, Sobol sampling and global sensitive analysis are used to capture both second-order effects and variance contributions, allowing for a more complete understanding of parameter interactions and their influence on overall system performance.

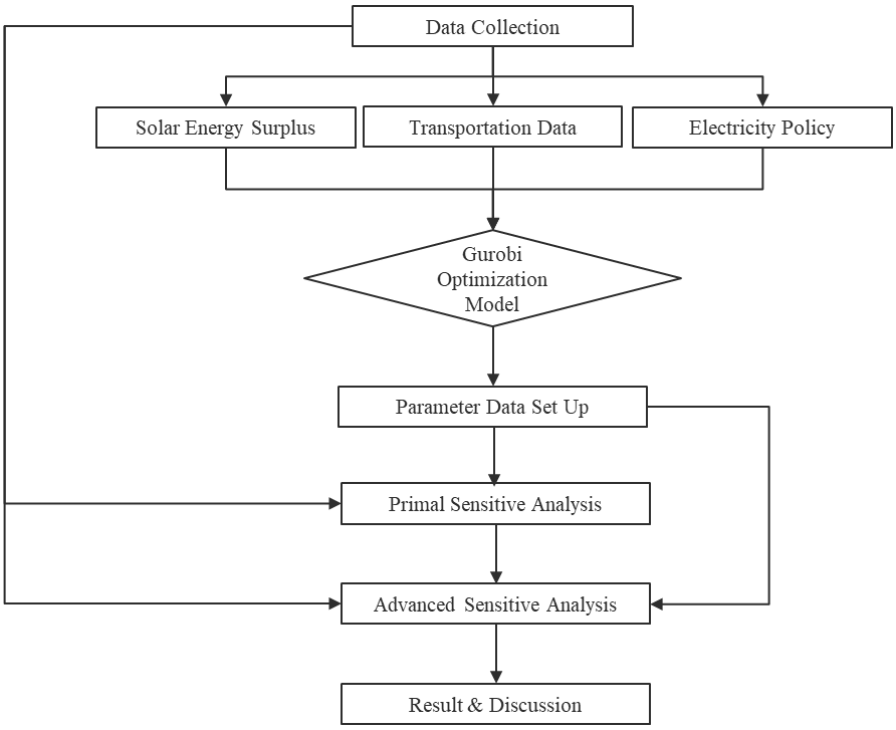

Figure 3 Overall Research Scope

doi:10.6342/NTU202502274

In this study, we integrate three major bus depots and their associated routes into our research framework, using nearby schools as representative sites for solar energy generation and scheduling, as illustrated in **Table 1** and **Figure 4**. Our scope includes a total of 110 electric buses operating across 9 different routes in Taipei City, with the fleet distributed among three major depots, 44 buses at the Songzhi Depot, 39 at the Jiuzhuang Depot, and 27 at the Wuxing Depot. Each depot is strategically paired with nearby educational facilities identified as having rooftop solar energy potential. Specifically, the Songzhi Depot is linked to both Songshan Vocational High School and Yongchun High School provide 20510 m^2 rooftop availability and 82040 m^2 floor area, the Jiuzhuang Depot is associated with Jiuzhuang Elementary School which offers 4028 m^2 rooftop space and a total floor area of 16112 m^2, and the Wuxing Depot is paired with Wuxing Elementary School with 6428 m^2 rooftop availability and 25712 m^2 floor area. These depot-school pairings form localized renewable energy clusters that support integration with the V2G system. Each depot manages its own energy transactions with its corresponding solar source, while all depots collectively aim to minimize total operational cost through optimized dispatching and coordinated energy scheduling.

Table 1 Depots-Schools Integration Information

	Songzhi Depot	Jiuzhuang Depot	Wuxing Depot	Total
Operating routes (routes)	3	3	3	9
Buses Amount (buses)	44	39	27	110
Available school rooftop area (m^2)	20,510	4,028	6,428	30,966
School floor area (m^2)	82,040	16,192	25,712	123,944

doi:10.6342/NTU202502274

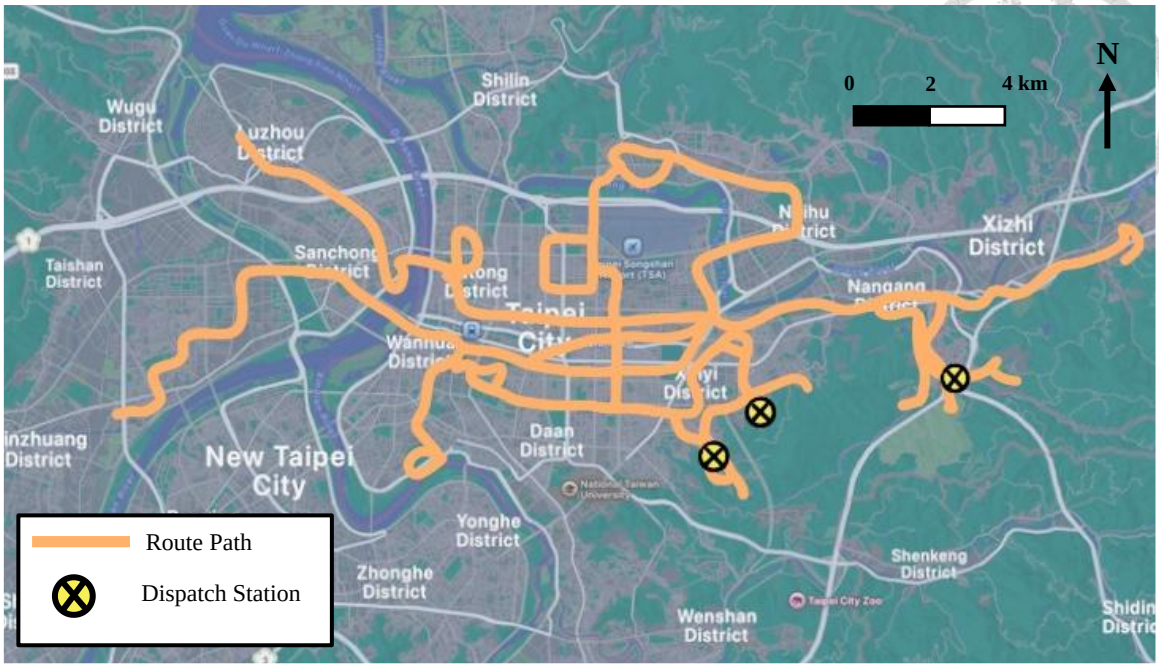

Figure 4 Scope of Research on Taipei's Map

doi:10.6342/NTU202502274

2.2 Estimation of Urban Solar Energy Potential

To assess the renewable energy surplus, we evaluate the solar power generation potential of rooftop areas located near bus depots. Smart meters installed by National Taiwan University are used to estimate each building's electricity self-sufficiency rate. By calculating this self-sufficiency, we are able to determine the amount of surplus solar energy available for potential integration with the V2G system. The overall structure of this evaluation process is illustrated in **Figure 5**.

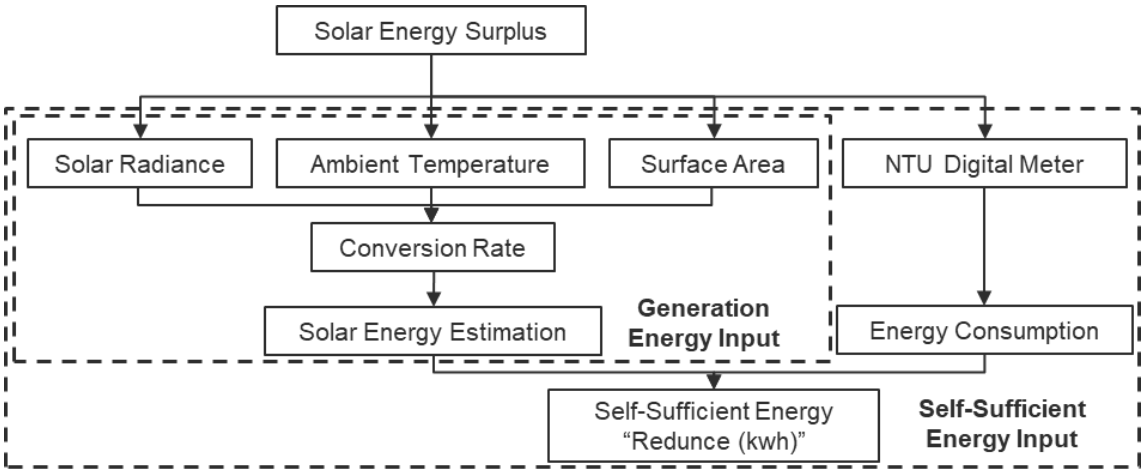

Figure 5 Solar Energy Research Scope

2.2.1 Estimation Method for Urban Rooftop Solar Energy Potential

For solar power estimation, this study uses Equation 1, which requires inputs including the solar conversion efficiency, rooftop area, solar irradiance, and ambient temperature [37].

$$Solar_{generation} = \eta_{PV} * roof * I * (1 - 0.005 * (T - 25)) \quad \textbf{(1)}$$

Studies on Taipei City's overall rooftop solar power potential whether based on geographic information system (GIS) modeling or building-type extrapolation

doi:10.6342/NTU202502274

consistently indicate strong potential across the Greater Taipei region. Han used geographic information system (GIS) modeling to analyze solar irradiance patterns in selected areas of Taipei and estimate their corresponding solar power generation potential [38]. An assessment of illegal rooftop structures in Taipei also revealed significant untapped potential for solar power generation due to the large total surface area of these rooftops [39]. Beyond generation potential, building electricity usage data can also be used to estimate the solar self-sufficiency rate of buildings in Taipei [40]. In this study, we calculate solar self-sufficiency rates and validate them using the method proposed which takes into account regional differences, seasonal variations, and the number of building floors to ensure the robustness of our estimation. For solar irradiance and temperature data, we use publicly available datasets from the Central Weather Administration's CODIS meteorological observation network in Taiwan, which we preprocess and adapt for modeling purposes.

2.2.2 Identification of Solar Building Locations Near Bus Depots

This study focuses on three schools located near bus depots in Taipei City as the main research sites: Songshan High School of Commerce and Home Economics in Xinyi District, Jiuzhuang Elementary School in Nangang District, and Wuxing Elementary School in Daan District. These three schools, along with Fanghe Experimental High School in Daan District which has installed rooftop solar panels and operates its own solar power generation facility are all located along the southern edge of the Taipei Basin. The actual solar generation data from Fanghe Experimental High School is used as a reference to validate the accuracy and feasibility of the solar potential estimates developed in this study. In our estimation, the total rooftop is around 1200 m^2 with the equation of **Equation 1** we get 25519 kWh. According to Fanghe Experimental High School offered us data, it has an installed solar capacity of 169.92 kWp in Phase I and 43.56 kWp in

doi:10.6342/NTU202502274

Phase II, totaling 213.48 kWp. With Intensity set about 3.25 kWh/m2/day [41], it will be about 20814 kWh in June. is quite close to the real situation with the data they've offered us in June shown as **Figure 7**. This mean the calculation system on our hand is quite mature enough and it can really work in a real site.

Figure 6 Taipei Exist Feng-He High School Rooftop Solar Farm

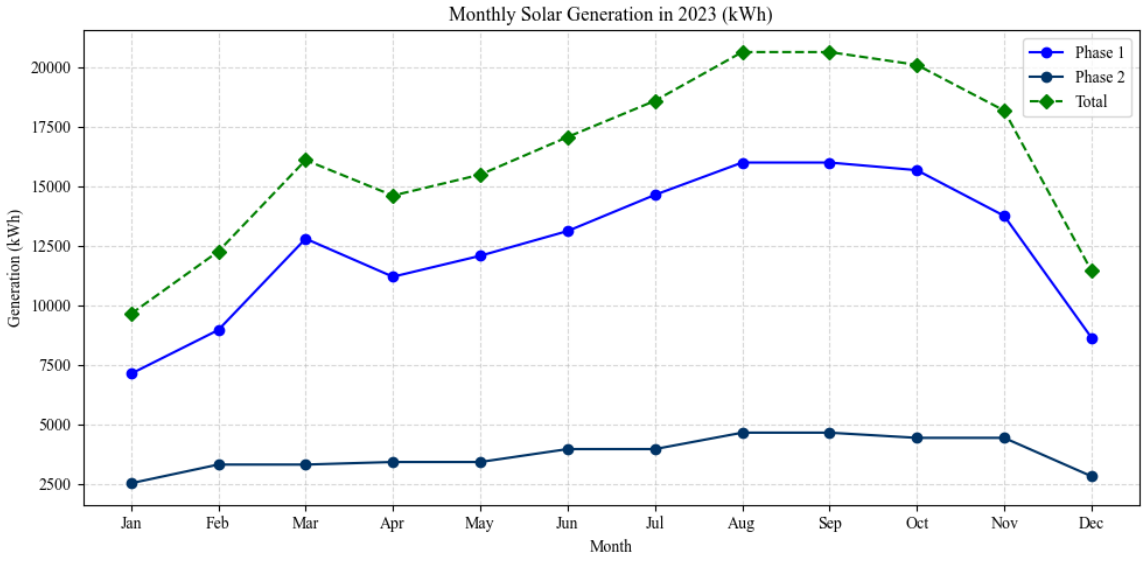

Figure 7 Feng-He High School Rooftop Solar Farm Generation Data

doi:10.6342/NTU202502274

The rooftop area of the three selected school campuses in this study was analyzed using a geographic information system (QGIS). As shown in **Figure 8**, Jiuzhuang Elementary School serves as an example of how this spatial analysis was conducted. We selected school buildings located near bus depots as the target sites for potential solar panel installation, in order to enhance the feasibility of early-stage pilot implementation.

As illustrated in **Figure 9**, we overlaid the Taipei City map and building footprint data provided by the Taipei City Government within QGIS to perform rooftop area calculations. Once the target area was identified, we used the GIS model to compute the total rooftop surface area within the selected boundary. In the case of Jiuzhuang Elementary School, the original zoned area was approximately 40,067 square meters, while the total rooftop area of the selected buildings was calculated to be 3,212 square meters. This rooftop area was then used as input in Equation 1 to estimate the expected hourly solar power generation.

Figure 8 School – Bus Station Location's Relationship

doi:10.6342/NTU202502274

Figure 9 GIS information for School Sample

In our research, we compare the three depots based on their solar energy potential and the energy use intensity of the nearby schools integrated with each depot. **Table 2** below shows the solar potential and school energy usage conditions for each depot-school combination. These indicators help us understand how much solar energy can be used locally and how the school buildings may influence energy distribution in the integrated system. According to Energy Administration, the elementary school EUI should around 14~27 kWh/year-m^2 and high school should around 23~34 kWh/year-m^2 which make the data here become reasonable.[42]

doi:10.6342/NTU202502274

Table 2 Energy Generation and Consumption of three depots Information

	Songzhi Depot & Schools	Jiuzhuang Depot &Schools	Wuxing Depot &Schools
Solar potential (kWp)	3,692	725	1,157
Solar potential (kWh/month)	604,874.83	119,000.25	189,573.04
Consumption of School (kWh/month)	343,050.50	67,711.71	107,515.01
EUI of School (kWh/month-m^2)	4.18		
EUI Guide (kWh/year-m^2)	23-34	14-27	
Self Sufficient Rate (%)	104		
Li & Han et al.(2022) Self Sufficient Rate (%)	123		

2.2.3 Estimation of Building Electricity Demand Based on Function

For electricity usage estimation, this study uses the Civil Engineering Research Building at National Taiwan University as a reference and applies a floor area-based scaling method to estimate the electricity consumption of the target buildings during specific time periods. Taking Jiuzhuang Elementary School as an example, the building has four floors and a rooftop projected area of 3,212 square meters, giving a total floor area of 12,848 square meters. Since typical elementary and junior high school buildings in Taiwan do not use centralized chilled water systems and mainly rely on individual air conditioning units, we assume a rooftop utilization rate of 100%. According to data from Lo [37], the Civil Engineering Research Building has a projected area of 2,300 square meters and nine floors, giving an estimated total floor area of approximately 20,700 square meters. Based on this ratio, we adjust the electricity usage using data from NTU's campus digital smart meter monitoring system to estimate the expected electricity demand of the selected teaching buildings during specific time periods. This method

doi:10.6342/NTU202502274

allows us to simulate electricity use characteristics of educational buildings throughout different timeframes such as summer and winter breaks, class hours, and idle periods ensuring that the power demand estimations in this study reflect realistic usage patterns with school type building.

2.2.4 Estimation of Building Solar Self-Sufficiency and Surplus Energy Potential

Based on the previously estimated solar generation and electricity demand of each building, this study calculates both the building's solar self-sufficiency rate and the surplus energy generated. The surplus energy at each time step is determined based on the excess generation from the previous hour. However, due to current Taiwan Power Company's (Taipower) policies, which offer feed-in tariff (FIT) for building selling solar energy, many buildings sell their solar energy back to the grid rather than utilizing it locally such as Fanghe Experimental High School. With this concept, the study also explores alternative ways to set building solar energy that could better support progressive policies for community-based microgrids.

Using Jiuzhuang Elementary School as an example, the building's solar self-sufficiency rate in June is calculated to be 103.87%. This result aligns reasonably well with the value provided by [40], which estimated a June solar self-sufficiency rate of 123% for four-story residential buildings in Taipei. This comparison demonstrates the feasibility and validity of the self-sufficiency estimation method used in this study, providing a reliable foundation for future research.

2.3 Electric Bus Operation Pattern Analysis

When electric buses depart from the designated depot sites, their operations follow the unique characteristics of public transportation systems. This study also investigates the surrounding bus stations operated by Metropolitan Transport Corporation (大都會客運) near the selected sites namely Songzhi Station, Jiuzhuang Station, and Wuxing

doi:10.6342/NTU202502274

Station and provides an analysis of current operations along with future planning perspectives. Taking Jiuzhuang Station as an example, it serves four routes: Route 276, Route 306, Minibus Route 6, and Route 823. Among these, Routes 276, 306, and 823 are currently operated using diesel-powered Daewoo BS120CN buses from South Korea, while Minibus Route 6 is operated through a joint-operation minibus system. Based on a 2023 survey of the domestic electric bus market, the electric buses currently used by Metropolitan Transport Corporation commonly include the Master Bus MB120SE by Master Transportation, the Model T by Foxtron (Horizon Plus), the RACE150 by RAC Electric Vehicles, and the K9 by BYD. However, due to the larger wheelbase and width of these models, they are not suitable for the narrow roads and turning radii required for operating Minibus Route 6. Therefore, for Jiuzhuang Station, electric bus replacement planning focuses on Routes 276, 306, and 823. This study refers to manufacturer provided specifications for the above mentioned electric bus models. Considering that key factors such as battery capacity and energy consumption per kilometer have a significant impact on the performance of V2G systems, and given the ongoing trend toward domestic production of electric buses, the Foxtron Model T is selected as the representative model for this study. All replacement scenarios assume substituting the current South Korean Daewoo BS120CN diesel buses with the Foxtron Model T on the identified routes in our research assessment. Based on the above assumptions, a total of 39 diesel buses from Routes 276, 306, and 823 are considered for electrification. The operational schedule of these electric buses is based on the public timetable released by Metropolitan Transport Corporation. Taking Route 276 from Jiuzhuang Station as an example, its service hours run from 6:00 AM to 9:00 PM. During weekday peak periods, buses operate every 15 to 20 minutes, while off-peak and weekend periods follow a fixed schedule. This study uses Python for data processing. Given the fixed time intervals between departures, we model

doi:10.6342/NTU202502274

the bus dispatches on an hourly basis using probabilistic methods. A Poisson distribution is applied to estimate the expected number of electric bus dispatches per hour. For example, during weekday peak and off-peak periods on Route 276, we simulate the random arrival of electric buses at intervals of 15–20 minutes. This method is similarly applied to Routes 306 and 823, producing 24-hour Poisson-based dispatch distributions for each route shown as **Figure 10**.

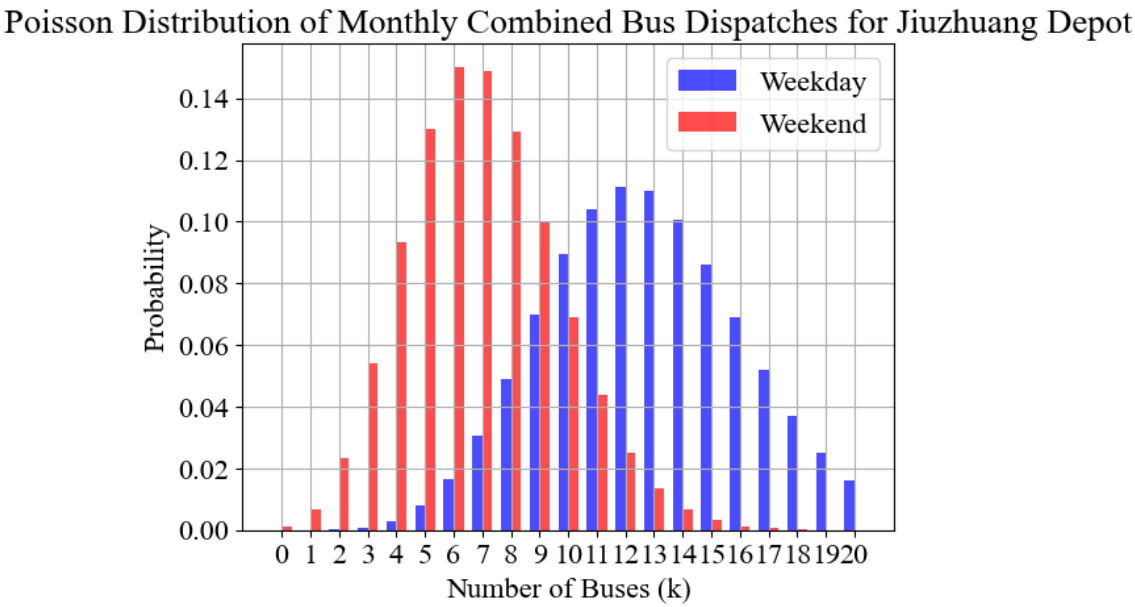

Figure 10 Poisson Distribution of Combined Bus Dispatches for Jiuzhuang Depot

Similarly, after calculation, we derive the expected number of bus dispatches per hour, as shown in **Figure 11**. This expected simplified how a depots to deal with transportation need, in this graph it can echo to previous study that sometime the electric buses will stay in the depot and being idle [13]. The average idle time for electric buses will be 58% ~ 83% depends on different route. In our research it will be around 78% for idle time in the JiuZhuang depot according to the estimation which means this bus operation has relative low departure rate.

doi:10.6342/NTU202502274

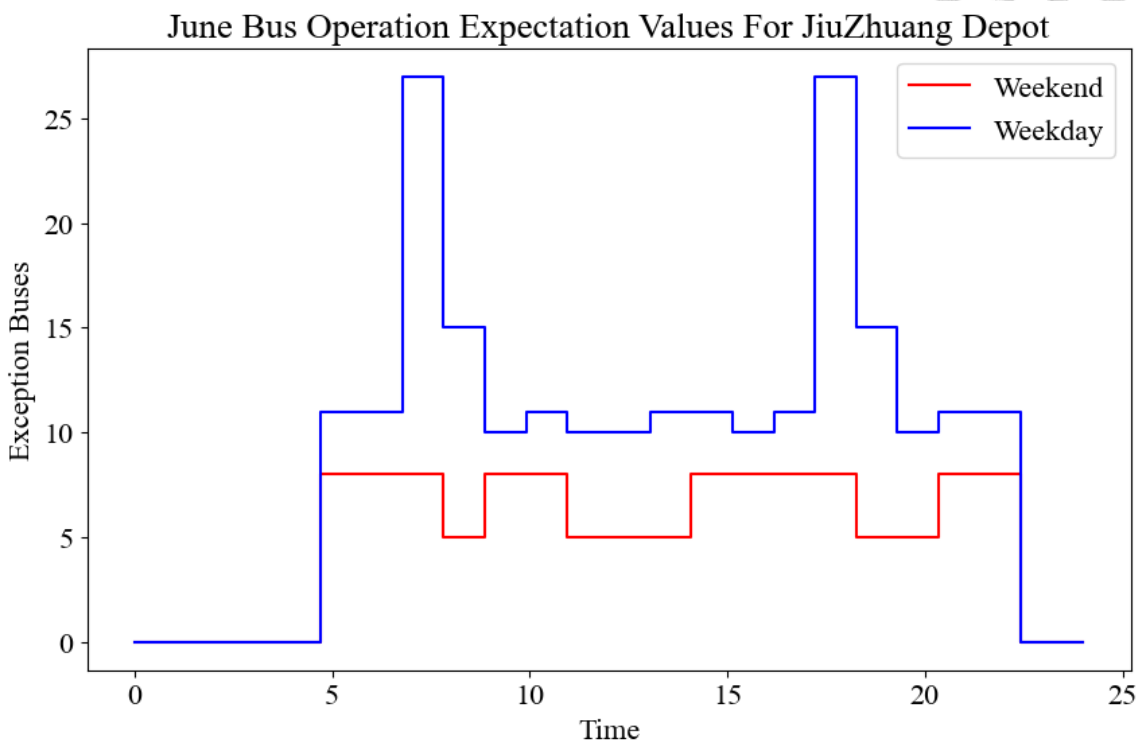

Figure 11 June Bus Operation Expectation Values for JiuZhuang Depot

This result supports the subsequent development of the optimization model. Once the solar self-sufficiency of the selected buildings and the dispatch patterns of the electric bus depots are confirmed, we map their spatial relationships based on geographic proximity. This allows us to establish the connections among depots, buildings, and electric buses, forming the foundational structure of this study's site-to-bus allocation model.

2.4 Optimization Model Development

In optimization modeling, there are two models one is linear and mixed-integer linear programming methods, and another one is gradient-based nonlinear optimization techniques. The following section compares these two approaches and explains the reason for adopting mixed-integer linear programming methods in this study. **Figure 12** is the

doi:10.6342/NTU202502274

scope of the optimization model in our research to build up what we want to optimized while we want to form a V2G model.

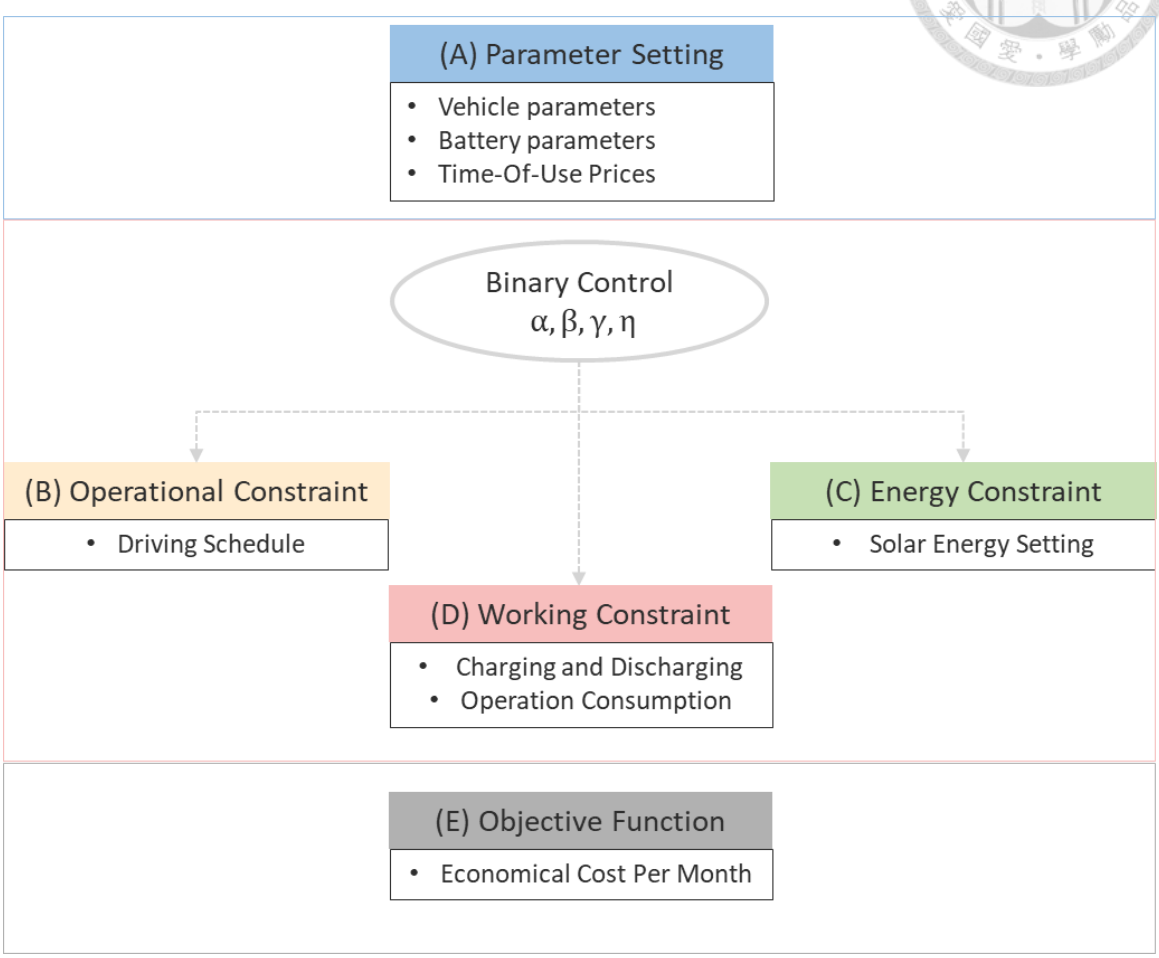

Figure 12 Scope of Model

2.4.1 Overviews of Gradient-Based Nonlinear Optimization Methods

A wide range of optimization algorithms can be broadly categorized into derivative-based and derivative-free methods. Derivative-based techniques utilize gradient information, such as the first-order derivative ∇f, to determine the search direction and guide to the optimization results. One example is the Conjugate Gradient (CG) method, which is suited for solving large-scale unconstrained linear minimization problems. This method accelerates convergence by searching along conjugate directions rather than simply following the steepest descent of -∇f. It iteratively updates the gradient -∇f to reach

doi:10.6342/NTU202502274

the optimal solution. Second-order methods extend this idea by introducing the Hessian matrix ($\nabla^2 f$), which allows for more precise convergence based on curvature information. These methods are more accurate for scientific computation but come with significantly higher computational costs. In contrast, derivative-free methods operate like black-box optimizations, requiring only function values. One well-known example is the Nelder-Mead method, which compares function values at multiple points ex., f(-1), f(1), ..., f(n) to gradually move away from high-value regions and approach the minimum. However, both derivative-based and derivative-free methods are prone to getting stuck in local minima, which may distort the final results. Additionally, because these algorithms rely heavily on continuous derivatives, they are not suitable for solving mixed-integer linear programming (MILP) problems [43].

2.4.2 Overviews of Mixed-Integer Linear Programming Methods

In the Mixed-Integer Linear Programming Methods, there is a useful package called gurobi which primarily uses the Branch-and-Bound algorithm, supplemented by various heuristic methods, to solve optimization problems and obtain optimal solutions. In this study, mixed-integer formulations are frequently encountered. For example, the number of buses is treated as an integer variable, while power-related behaviors like energy flow are modeled as continuous variables. These two types of variables need to be optimized together within a single integrated model. For linear problems, feasible regions defined by constraints and objective functions can be solved using the simplex method. This approach iteratively swaps basic and non-basic variables at the vertices of the feasible region to identify the optimal solution. For solving mixed-integer problems, Gurobi applies the Branch-and-Bound algorithm to find the optimal solution. The process begins by relaxing the integrality constraints and solving the corresponding linear programming (LP) problem to obtain an optimal LP solution. If the solution contains fractional values

doi:10.6342/NTU202502274

in integer variables, the algorithm selects one of these variables and branches on it, rounding it up and down to create two new subproblems. If a solution is found where all integer variables take integer values, the algorithm terminates. If a node is infeasible or the current solution's objective value is worse than an existing feasible solution, that branch is pruned. This process continues until all branches have either been solved to optimality or pruned due to infeasibility or minor than current integral solution. In this study, many optimization tasks involve mixed-integer formulations, where both discrete decisions (such as the number of buses) and continuous variables (such as energy consumption) must be solved together. Gurobi's hybrid method is well-suited to efficiently handle such mixed-variable problems like V2G problem [44].

2.4.3 Comparative Analysis of Gradient-Based and MILP Optimization Approaches

Based on the literature review and the needs of this study, a commercial solver designed for mixed-integer linear programming was selected. Compared to nonlinear optimization methods that rely on derivatives, mixed-integer linear programming offers several advantages. It is especially suitable for large-scale problems involving both integer and continuous variables, which matches the structure of urban energy scheduling models used in this research. Following are several for choosing mix-integer linear programming method.

1. Mixed-Variable Modeling Capability

   Mixed-integer programming methods are specifically designed to solve problems that involve both integer and continuous variables. These models are commonly encountered in practical scheduling and planning tasks. Compared to such approaches, gradient-based nonlinear optimization techniques are typically limited to continuous variable problems. When applied to models with discrete decisions,

doi:10.6342/NTU202502274

these methods often require additional relaxations or transformations, which can increase the complexity and computational cost.

2. Solution Stability and Initialization Robustness

   Gradient-based methods rely on derivatives to guide the search process, making them effective for nonlinear and non-convex problems. However, they are often sensitive to initial values and may converge to local minima. In contrast, mixed integer programming methods use structured algorithms such as branch and bound, which explore multiple solution paths and are less affected by initial conditions, offering greater reliability in finding global optima in well formulated models.

3. Application Suitability for Grid Scheduling

   Problems involving grid scheduling and energy dispatch commonly feature binary or fixed allocation decisions. Mixed integer programming methods are well optimized for such discrete models, allowing accurate representation of practical constraints like unit requirement, charging schedules.

4. Urban Scale and Computational Efficiency

   The selected solver incorporates advanced features such as automatic method selection, multithreaded computation, and presolve routines, which enhance performance in solving large scale optimization problems. These features are essential in urban-scale applications, where models may include hundreds of thousands of variables and constraints. Without such enhancements, convergence speed and memory usage would become critical problem.

5. Solution Interpretability and Sensitive Analysis

   In addition to computational performance, mixed integer programming methods provide structured output, including optimality conditions, dual values, and shadow

doi:10.6342/NTU202502274

prices. These results are useful for post-analysis, scenario evaluation, and policy interpretation, especially in planning and decision-support contexts.

To conclude, MILP method give us more robust, reliable optimization model to conduct with V2G analysis.

With this understanding, and given Mixed-Integer Linear Programming Method's reliance on multi-core processor performance, this study was conducted using high-performance CPUs: the AMD Ryzen 9 7950X and the Intel i7-12650H. In each optimization scenario, the model contains approximately 600,000 constraints and around 320,000 variables. A single optimization run takes approximately 10 minutes, while sensitive analysis can require more than one week of continuous computation.

2.4.4 Design the V2G model with MILP Optimization Approaches

To complement the insights illustrated in the **Figure 12**, we introduce a pseudocode that outlines the optimization goal and relevant parameters as shown in **Figure 13**.

```
Algorithm : Monthly V2G Economic Cost Optimization

Input:
    Bus fleet data, PV generation, TOU pricing,
    Battery capacity, SOC_initial, charging power,
    Gurobi optimization constraints

Output:
    Optimal charge/discharge schedule with cost minimization

1  Initialize model with parameters:
    - SOC_initial, Bus_Capacity, Fast/Slow charging
    - TOU electricity prices, PV generation profile, Buses dispatch schedule profile
2  For each bus in each depot (Songzhi, Jiujuang, Wuxing):
3      For each time step (1 hour as a time step):
4          Estimate solar power generation and load
5          Calculate demand and storage states
6          Apply constraints on:
             - SOC range
             - Charging/discharging power
             - Grid selling/buying cost
             - Battery degradation cost
7          Formulate MILP with:
             - Objective: minimize net operation cost
8      Solve MILP via Gurobi
9      Record dispatch result and cost
10 Aggregate and compare across depots
11 Return optimized strategy and cost analysis
```

Figure 13 V2G optimization model Pseudocode

doi:10.6342/NTU202502274

2.5 Baseline Parameter Settings

In the V2G operation setup, this study assumes the use of the Foxtron Model T electric bus, with a standard battery capacity of 300 kWh. The initial state of charge (SOC) is set at 50%. According to historical interview data from the Institute of Transportation, Ministry of Transportation and Communications, the average operating speed of electric city buses in Taiwan is 20 km/h, and the average energy consumption is 0.9 kWh per kilometer. Under the baseline setting, fast charging is defined with a maximum power of 135 kW, and slow charging with a maximum power of 7 kW. The optimization model determines the best allocation of resources using mixed-integer programming. For grid electricity pricing, the model adopts the time-of-use charging rates announced by Taipower in November 2024 for electric vehicle charging stations [45]. Peak-time electricity is priced at NT$9.34 per kWh, and off-peak at NT$2.29 per kWh. Peak periods are defined as weekdays from 16:00 to 22:00, all other hours are considered off-peak. Regarding the baseline solar feed-in tariff, we follow Taipower's solar energy buy-back rate of NT$3 per kWh. For the pricing gap between fast and slow charging, the model adopts a baseline price multiplier of 2.41, based on comparisons with domestic and international EV charging tariffs [46-48]. Additionally, for the sale of electricity back to the grid, this study follows the three steps time-of-use pricing scheme announced by Taipower in November 2024. The electricity rates are defined as follows: NT$6.92 per kWh during peak periods (weekdays 16:00–22:00), NT$4.54 per kWh during mid-peak periods (weekdays 9:00–16:00), and NT$1.96 per kWh during off-peak hours (all other times). The baseline battery degradation cost is set at NT$0.45 per kWh, based on the typical cost of lithium titanate (LTO) batteries used in electric buses. Further details and equations related to battery degradation will be explained in the battery sensitive analysis section.

doi:10.6342/NTU202502274

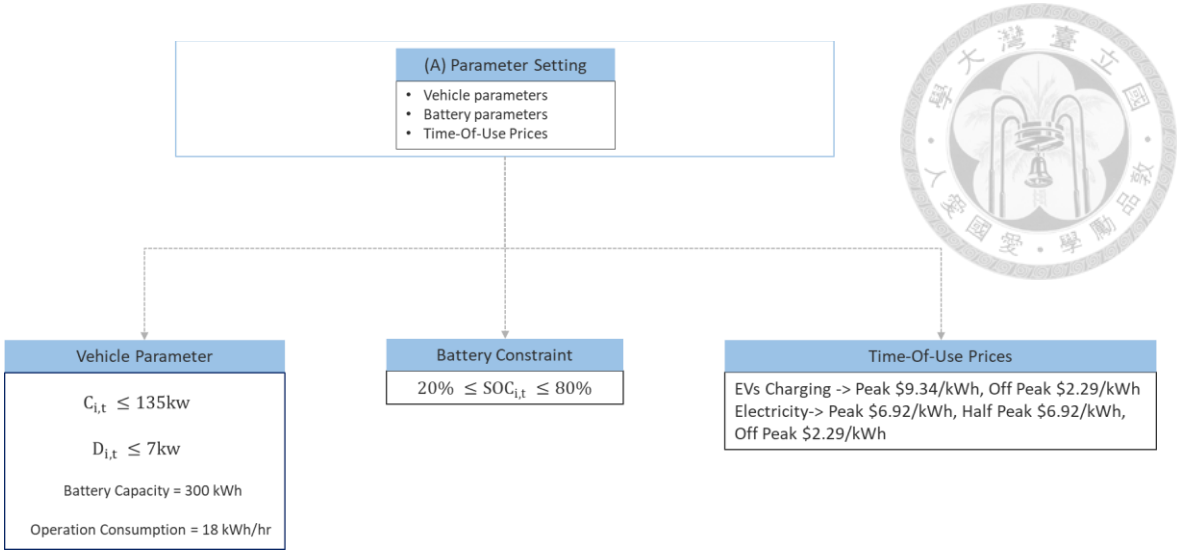

Figure 14 The Road Map of operation model's parameter

The following initialization constraints are derived from the physical limitations of the electric bus systems and must be considered in the simulation. To account for battery health and realistic operation, we set both upper and lower bounds on the battery state of charge (SOC). According to battery-related literature, such as [32], the typical operating range for battery charge should be constraint. Our research definition is between 20% and 80% of total capacity, as shown in Equation 2. In addition, we acknowledge limitations imposed by basic charging infrastructure particularly for V2G discharge rates. To reflect the capabilities of real-world systems, the maximum discharging power for slow charging is set at 7 kW, as shown in Equation 3. The maximum fast charging power is set at 135 kW, as shown in Equation 4. This ensures that the simulation remains within feasible hardware boundaries.

Battery Boundary Constraint:

$$20\% \leq SOC_{i,t} \leq 80\% \quad \textbf{(2)}$$

doi:10.6342/NTU202502274

Charging Pile Discharging Constraint:

$$Ci,t \leq 135kW \tag{3}$$

Charging Pile charging Constraint:

$$Di,t \leq 7kw \tag{4}$$

2.6 Model Constraints

2.6.1 Binary Constraints for Bus Operational States

In formulating the mathematical model for electric bus operation strategies, it is essential to ensure that each bus performs only one activity at any given time. This exclusivity of operation is enforced through a set of binary variables: α, β, γ, and η each representing a distinct operational mode: in-service operation, fast charging, slow charging, and discharging, respectively.

$$\forall period \in nperiods, \forall unit \in units, \quad \alpha + \beta + \gamma + \eta \leq 1 \tag{5}$$

2.6.2 Constraints on Solar-Powered Charging Availability

This constraint ensures that, at any given time, the total energy used by the solar charging system does not exceed the available surplus energy generated by the solar panels. Specifically, the sum of solar-powered fast charging and slow charging must remain within the solar surplus capacity at that time. Mathematically, this is enforced by limiting the combined solar slow charging amounts $SSC_{i,t}$ and solar fast charging

doi:10.6342/NTU202502274

amounts$SFC_{i,t}$ based on the available surplus energy. The binary variables β and γ indicate whether fast charging or slow charging is activated, respectively.

$$\sum_{unit=1}^{units} SFCi,t * \beta + SSCi,t * \gamma \leq \text{Building Solar Energy Surplus} \quad \textbf{(6)}$$

2.6.3 Constraints on Electric Buses Dispatch Requirements

To ensure that the bus system maintains its transport efficiency while operating under a V2G framework, it is necessary to guarantee that a sufficient number of buses remain in service during scheduled operation hours. The following describes how operating time periods across a one-week schedule are defined and how the corresponding dispatch of buses is managed. Let P represent the set of time periods, with d = 24 periods per day. The variable $\alpha_{\text{unit,period}}$ denotes the operational status of a specific bus unit at a given time period whether it is in active service.

The operation-level constraint is defined as follows:

$$\forall \text{period} \in \text{nperiods}, \sum_{\text{unit}=1}^{\text{units}} \alpha_{\text{unit,period}} \geq \text{Dispatch Demand} \quad \textbf{(7)}$$

In practice, most bus dispatches typically last longer than one hour. However, implementing detailed dispatch duration constraints can significantly increase the computational load of the optimization model. To address this, a sub study is conducted to compare two scenarios: one with a minimum dispatch duration constraint of three hours and one without such a restriction. The goal is to observe whether this real dispatch situation constraint has a significant impact on the optimized operational cost or not.

doi:10.6342/NTU202502274

. This study modifies Equation 7 by adding a constraint that enforces a minimum dispatch duration of three hours like Equation 8. To avoid logical conflicts in the model, the original time-based dispatch restriction is adjusted. When a dispatch is initiated identified by the condition (period − period−1) = 1, the sum of dispatch indicators over the current and following two periods (period, period + 1, period + 2) must exceed 3. This ensures that once a vehicle begins service, it remains in operation for at least three coming hours, aligning the model close to world scheduling behavior.

$$\forall \text{period} \in \text{nperiods} - 2, \sum_{\text{unit}=1}^{\text{units}} \alpha_{\text{unit,period}} \geq \text{Dispatch Demand} \quad \textbf{(8)}$$

$$\alpha_{\text{unit,period}} + \alpha_{\text{unit,period+1}} + \alpha_{\text{unit,period+2}} \geq 3 * (\alpha_{\text{unit,period}} - \alpha_{\text{unit,period-1}}) \quad \textbf{(9)}$$

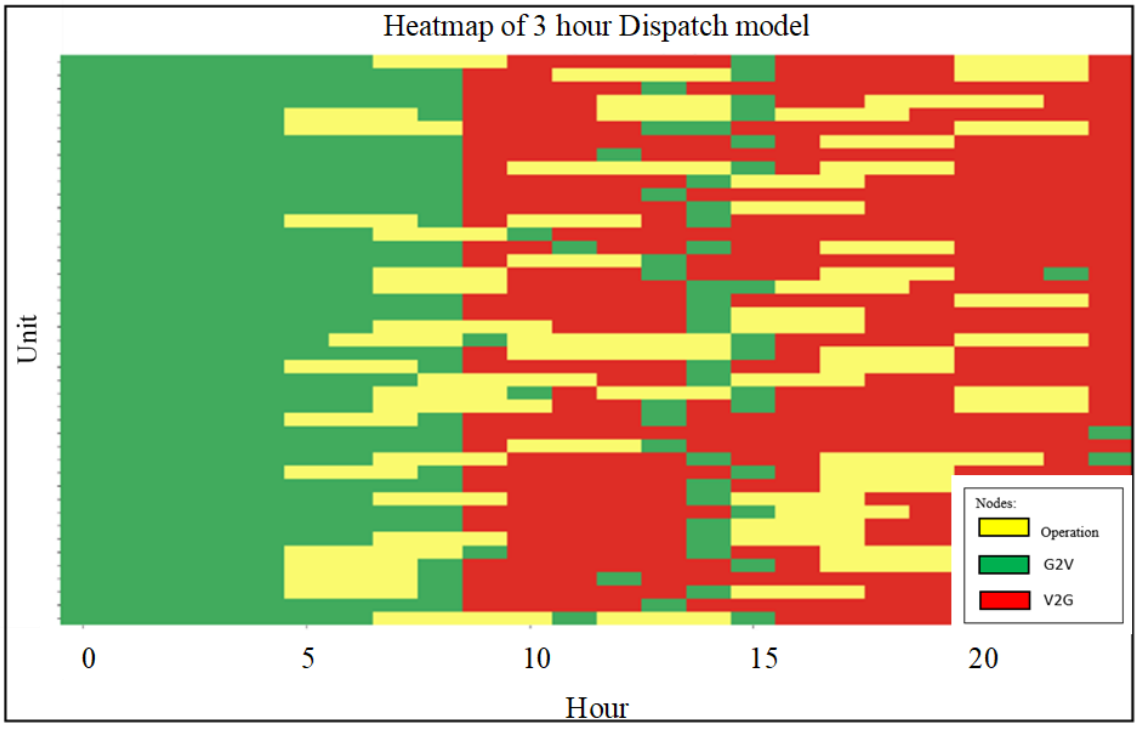

Figure 15 3-hour Dispatch Model

doi:10.6342/NTU202502274

When this constraint was added, the optimized operating cost was NT$433,070, which is within the margin of error compared to NT$422,615 without the constraint. However, the computation time increased by more than 10 to 20 times. Therefore, in the subsequent setup, this study simplified the operating time constraint.

2.6.4 Battery Scheduling and State-of-Charge Constraints

To initialize the system, this study defines the state of charge (SOC) at time period zero for each bus SOC_i as 50%. Based on the assumption that the battery's full capacity is 300 kWh, each electric buses start with an initial energy level of 150 kWh for calculation and optimization purposes.

$$\mathrm{SOC}_{\mathrm{unit},0} = 50\% * \text{ Battery Capacity} \quad \textbf{(10)}$$

To prevent the electric bus operation systems from being excessively affected by the V2G discharging process, this study imposes a condition that every three days, the state of charge (SOC) must be reset to its initial level.

$$\mathrm{SOC}_{\mathrm{unit,n}} = \mathrm{SOC}_{\mathrm{unit,n-3}} = \mathrm{SOC}_{\mathrm{unit},0} \quad \textbf{(11)}$$

To define the system's behavior and ensure continuity between time periods, this study forms the battery state of charge (SOC) dynamics based on Equation 12. The SOC at time period n is determined by the SOC at time period n−1, plus the Battery Increment variable and minus the Battery Decrement variable. $\mathrm{SOC}_{\mathrm{unit,n}}$ represents the state of charge of the electric bus at time period n, $\mathrm{ISOC}_{\mathrm{unit,n}}$ denotes the battery charge increment, and $\mathrm{DSOC}_{\mathrm{unit,n}}$ denotes the battery discharge amount during time period n.

doi:10.6342/NTU202502274

$$SOC_{unit,n} = SOC_{unit,n-1} + ISOC_{unit,n} + DSOC_{unit,n}$$

(12)

The battery charge increment $ISOC_{unit,n}$ define the sum of all charging activities for electric bus unit i at time period t, including slow charging from the grid $SC_{i,t}$, fast charging from the grid $FC_{i,t}$, slow charging from solar power $SSC_{i,t}$, and fast charging from solar power $SFC_{i,t}$ at the corresponding depot charging system. This formula captures the total charging behavior during each time period. The binary variables β and γ indicate whether fast charging or slow charging is activated.

$$ISOC_t = SC_{i,t} * \beta + FC_{i,t} * \gamma + SSC_{i,t} * \beta + SFC_{i,t} * \gamma$$

(13)

The battery discharge amount $DSOC_t$ is defined as the sum of all discharging activities for electric bus unit i at time period t, which includes both energy consumed during bus operations and energy discharged back to the grid through V2G services. $Consump_{i,t}$ represents the energy consumption caused by dispatch operations for bus unit i at time period t, and η is the binary variable indicating whether the bus is discharging during operation. $D_{i,t}$ represents the amount of energy discharged to the grid by bus unit i at time period t, and α is the binary variable indicating whether activate the V2G discharging system.

$$DSOC_t = Consumption_{i,t} * \alpha + D_{i,t} * \eta$$

(14)

The incremental battery degradation cost defined the product of the additional battery degradation by V2G discharging and the battery degradation cost per unit of energy. BD_t represents the total amount of battery degradation at time period t, $D_{i,t}$

doi:10.6342/NTU202502274

represents the amount of V2G discharge by electric bus unit i at time t, and α is the binary variable indicating or not.

$$BD_t = BC * \sum_{unit=1}^{units} D_{I,t} * \alpha$$

(15)

According to some of the previous studies, battery degradation models are nonlinear. However, in this research, the battery degradation cost is modeled linearly to simplify computation. This linear assumption is necessary to ensure computational efficiency, given the scale of the model and the need to simultaneously account for multiple interacting variables. [33, 49]

This study refers to the works of Borge-Diez, Manzolli, and Choudhary to compare and integrate different approaches to battery degradation modeling. Based on these references, we define the linear degradation formula adopted in this study as Equation 16. [31, 35, 50] In this formula, when battery degradation reaches a point where it no longer meets operational requirements, battery replacement cost is BAT_{Cost}; The total number of charge-discharge cycles before requiring replacement is DoD_{Cycle}; DoD represents the usage cycle depth for the electric bus battery.

$$BC = \frac{BAT_{Cost}}{DOD_{Cycle} * DOD}$$

(16)

2.7 Objective Function Definition

To define the optimization objective, this study sets the objective function as a minimization problem, targeting the minimization of the total operational cost of the electric bus system. The total cost is calculated by summing all relevant components

doi:10.6342/NTU202502274

across the selected depots, including city power slow charging costs, city power fast charging costs, solar energy fast charging costs, solar energy slow charging costs, and battery degradation costs, as shown in Equation 17. Specifically, SSP represents the total cost of solar-powered slow charging, SFP represents the total cost of solar-powered fast charging, DP represents the total revenue from V2G discharging, and BDP represents the total cost of battery degradation.

$$minimize \sum_{field}^{fields} SP + FP + SSP + SFP - DP + BDP$$

(17)

Among the various cost components, this study first defines the calculation for the total cost of grid-based slow charging. This cost is obtained by multiplying the slow charging amount for each electric bus unit i at each time period t by the corresponding time-of-use electricity price. This cost is obtained by multiplying the slow charging amount for each electric bus unit i at each time period t by the corresponding time-of-use price EVCPt, and then summing across all buses and time periods, as shown in Equation 18. Here, SP represents the total cost of slow charging, $EVCP_t$ are the time-of-use price for EV grid charging at time t, γ is the binary variable indicate slow charging is activated or not, and SCi,t is the slow charging amount for unit i at time t.

$$\mathrm{SP} = \sum_{\mathrm{period}}^{\mathrm{nperiods}} \sum_{\mathrm{unit}}^{\mathrm{units}} \mathrm{EVCP_t} * \mathrm{SC_{i,t}} * \gamma$$

(18)

To define the cost of city power fast charging, this study calculates it by multiplying the fast charging amount of each electric bus unit i at each time period t by the corresponding time-of-use electricity price $EVCP_t$, and then summing across all buses

doi:10.6342/NTU202502274

and time periods, as shown in Equation 19. The price difference between fast and slow charging is reflected by a multiplier SFC, set at 2.41. This adjustment accounts for the higher infrastructure requirements for fast charging since it need transfer from city power's alternating current to direct current for EVs.

$$\mathrm{FP} = \mathrm{SFC} * \sum_{\mathrm{period}}^{\mathrm{nperiods}} \sum_{\mathrm{unit}}^{\mathrm{units}} \mathrm{EVCP_t} * \mathrm{FC_{i,t}} * \beta \quad \textbf{(19)}$$

To define the cost of building-based solar slow charging, this study calculates it by multiplying the solar slow charging amount of each electric bus unit i at each time period t by the corresponding building solar electricity selling price BSoP, and summing across all buses and time periods, as shown in Equation 20. Here, SSP represents the total cost of solar-powered slow charging, BSoP is the price at which surplus building-generated solar energy could otherwise be sold back to the grid, with a baseline rate of NT$3 per kWh as previously mentioned.

$$\mathrm{SSP} = \sum_{\mathrm{period}}^{\mathrm{nperiods}} \sum_{\mathrm{unit}}^{\mathrm{units}} BSoP * \mathrm{SC_{i,t}} * \gamma \quad \textbf{(20)}$$

To define the revenue generated from V2G discharging by electric buses, this study calculates it by multiplying the V2G discharge amount of each electric bus unit *i* at each time period *t* by the corresponding time-of-use electricity price TP_t, and then summing across all buses and time periods, as shown in Equation 21. Here, DP represents the total revenue from V2G discharging, TP_t is the three-tier time-of-use electricity price at time t, $D_{i,t}$ is the V2G discharge amount for unit i at time t, and η is the binary variable indicating whether discharging is activated.

doi:10.6342/NTU202502274

$$\mathrm{DP} = \sum_{\text{period}}^{\text{nperiods}} \sum_{\text{unit}}^{\text{units}} TP_t * \mathrm{D_{i,t}} * \eta$$

(21)

To define the cost caused by battery degradation, this study calculates it as the sum of battery degradation costs over all time periods. Specifically, BDP represents the total battery degradation cost across all periods, and $\mathrm{BD_t}$ represents the battery degradation cost at time period t.

$$\mathrm{BDP} = \sum_{\text{period}}^{\text{nperiods}} \mathrm{BD_t}$$

(22)

2.8 Capital Cost and Infrastructure Allocation

To allocate the number of capital equipment, this study incorporates constraints based on three depots into the model to modify the optimization results, as shown in Equation 23. This study does not consider the actual limitations of depot space on the number of charging systems; instead, it focuses solely on analyzing the investment cost of the systems and the profits generated through the V2G system.

$$\sum_{\text{unit}}^{\text{units}} \beta + \sum_{\text{unit}}^{\text{units}} \gamma + \sum_{\text{unit}}^{\text{units}} \eta \ \leq \text{Charging System Amount}$$

(23)

Equation 23 incorporates the binary variables β, γ, and η, which represent fast charging, slow charging, and V2G discharging activities. The sum of these three binary variables at any given time should not exceed the number of available charging stations

doi:10.6342/NTU202502274

at the depot which give us an opportunity to study the changing of amount on charging systems with the ultimate payback years of the V2G system. When we changing the system constraint the behavior will be like what we can see in **Figure 16** as the heat map.

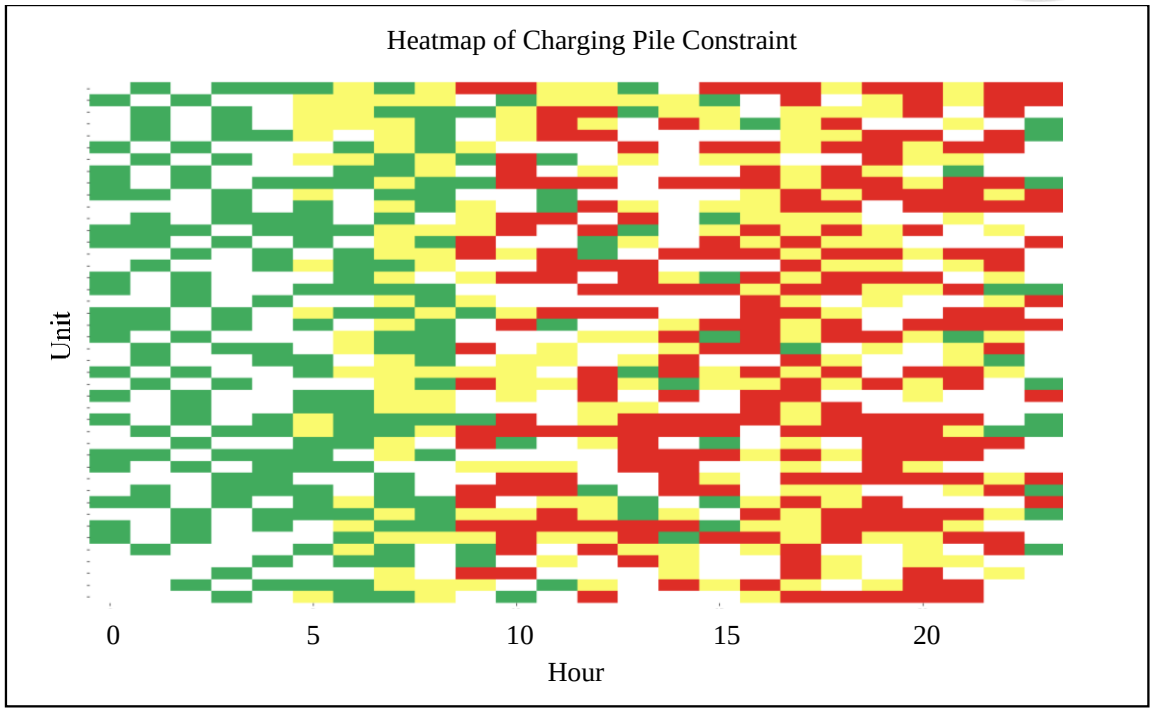

Figure 16 Heat Map Example of Charging Pile Constraint for Buses Behavior

2.9 Parameter Sampling Strategy

After obtaining the optimal solution through the Gurobi optimization model based on the model settings, this study aims to plan future urban power grids by adjusting the model parameters. There are three sampling methods available for sensitive analysis: Monte Carlo Sampling, Latin Hypercube Sampling, and Quasi-Monte Carlo Sampling, the example of distribution of three different sampling method as shown in **Figure 17**. Then we try to used the sampling method with optimization model to conduct sensitive analysis.

To be more specific, Monte Carlo methods rely on random sampling within a defined range, where each sample is randomly distributed based on its probability

doi:10.6342/NTU202502274

distribution. The Monte Carlo sampling method randomly places samples within the defined range and reconstructs the input distribution by repeated sampling after completing the specified number of iterations. However, due to the randomness and slower convergence, this method is less efficient for our study. In contrast, Latin Hypercube Sampling cut the input distribution into equal intervals, ensuring uniform sampling across each dimension. This approach requires fewer iterations and reduces computational costs when combined with Gurobi optimization. Quasi-Monte Carlo methods, such as Sobol sequences, fill the space with low-discrepancy sequences, making them ideal for high-dimensional sensitive analysis and numerical integration. Therefore, in this study, we adopt Latin Hypercube Sampling for one-dimensional analysis to cover a broader range of parameters while minimizing redundant optimization computations and utilize Quasi-Monte Carlo Sampling for higher-order indices.

To sum up, the reason we do not choose Monte Carlo as our sampling method is that it is random-based, which can significantly increase computational pressure. In contrast, Latin Hypercube Sampling and Quasi-Monte Carlo Sampling are more efficient, as they divide the interval into segments and place each sample at equal intervals, ensuring better coverage of the required range showed in **Figure 17**.

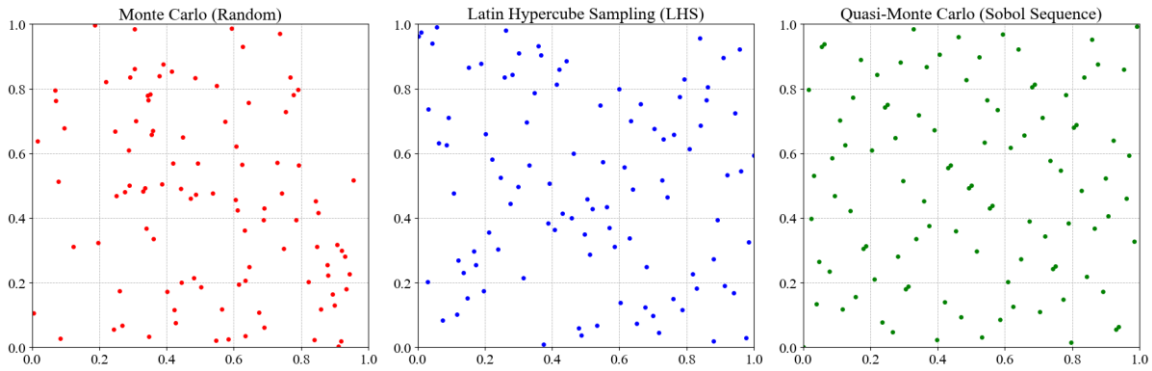

Figure 17 Sampling Method of Parameters

doi:10.6342/NTU202502274

2.10 Global Sensitive Analysis Method

To analyze the influence of multiple parameters on optimization outcomes, this study first extends the Latin Hypercube Sampling (LHS) method used in one-dimensional analysis to two-dimensional cases. However, when more than two parameters interact, the combined effect on the objective function is often nonlinear and cannot be captured accurately by local sensitive approaches. LHS, as a form of local sensitive analysis, exhibits monotonicity and threshold limitations, and its results are highly dependent on the initial sampling points. As reported in prior studies, such limitations may lead to biased interpretations of parameter influence, underestimation of system capacity, or overly optimistic economic forecasts, thereby compromising the system's robustness and flexibility under uncertainty [51, 52].

To address this, the study incorporates a global sensitive analysis approach using the Sobol method, a variance-based sensitive analysis (VBSA) technique. Sobol analysis leverages low-discrepancy sequences for uniform sampling across the entire input space, enhancing the coverage and reliability of sensitive results. This method constructs two independent sample matrices, each with n samples and d variables as shown in **Figure 18**, to evaluate both first-order and total-order sensitive indices. Unlike LHS, the Sobol method is capable of identifying nonlinear relationships and high-order interactions between parameters, offering a more comprehensive understanding of how combinations of uncertain variables jointly affect system performance. This enables more conservative and resilient system design, particularly in energy-related applications with high parametric uncertainty.

doi:10.6342/NTU202502274

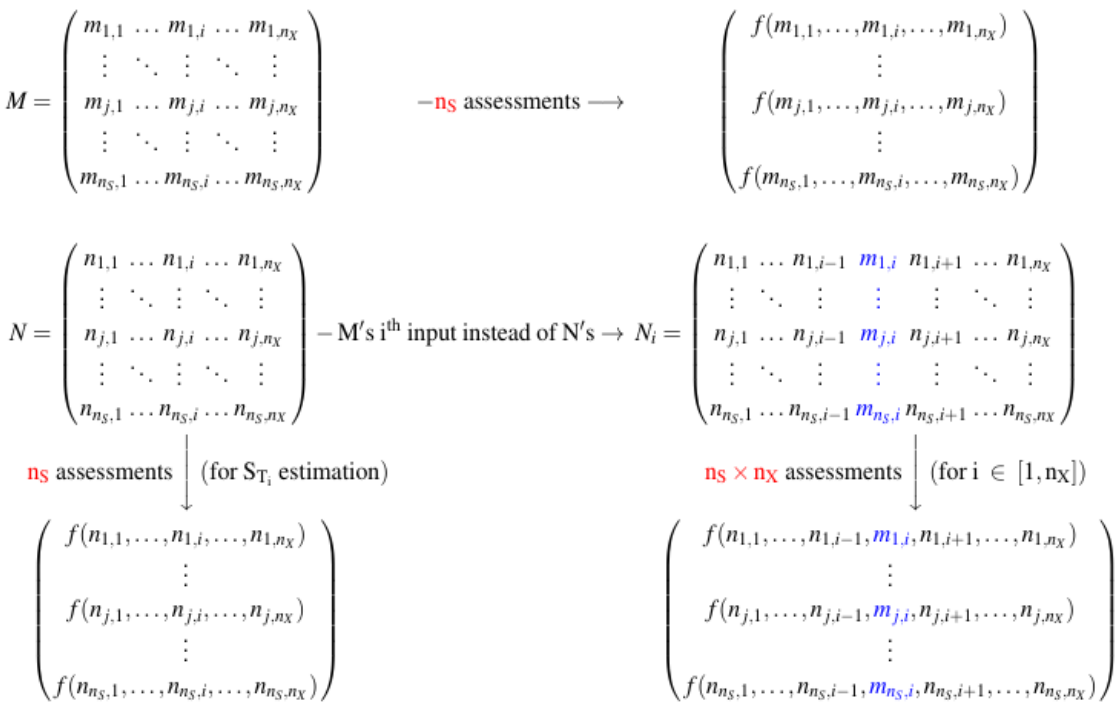

Figure 18 Sobol Computaional Matrix [53]

Next, a mixed matrix is created by sequentially swapping rows [53]. For instance, the “i" row of matrix N is swapped with the “i" row of matrix M to form a new mixed matrix. This process results in an n × (d + 2) dimensional sample matrix where n is the number of samples and d is the number of variables, which serves as the sample space for sensitive index estimation. This method allows for the evaluation of multi-variable interaction effects, as discussed by several studies. [54-56]

This swapping method effectively avoids the traditional method of fixing one parameter and performing sampling integration on another, which would require N × N evaluations. With the Sobol method, the number of samples becomes N + N + N × d, or N × (d + 2). [54]

Here are some examples of the outcome with the sobol analysis, due to its’ variance based we introduce the meaning of indices from these analysis with following equations. In the results analysis, we will use first-order sensitive matrices, second-order sensitive

doi:10.6342/NTU202502274

matrices, and global sensitive indices to analyze the outcomes of the relevant parameters. Equation 24 defines the first-order Sobol sensitive indices, which measures the contribution of a single input variable to the variance of the output variable. Here, V represents variance, E represents expectation, Y represents the output variable, and X_i represents the i input variable. The numerator represents the variance in the model output Y when X_i changes, which reflects the main effect strength of a single variable X_i on the global model output. The denominator represents the total variance contributed by all variables in the model.

$$\mathbf{S1} = \frac{\mathbf{V|E(Y|X_i)|}}{\mathbf{V(Y)}} \tag{24}$$

Equation 25 defines the second-order Sobol sensitive index, which measures the contribution of two input variables to the variance of the output variable. Here, X_i and X_j represent two different input variables. The second-order Sobol index S2 quantifies the interaction effect between X_i and X_j on the variance of the model output. After removing the main effects of both variables from the total variance, the remaining portion represents the interaction effect. If S2 approaches 0, it indicates that the two variables have minimal interaction.

$$\mathbf{S2} = \frac{\mathbf{V|E(Y|X_i, Xj)|} - \mathbf{V|E(Y|X_i)|} - \mathbf{V|E(Y|Xj)|}}{\mathbf{V(Y)}} \tag{25}$$

Equation 26 defines the total Sobol sensitive index, which helps us understand the overall effect of a coefficient, including its interaction effects. In practice, this is calculated by fixing other variables and then performing a reverse calculation to observe

doi:10.6342/NTU202502274

the total impact of X_i. If the total effect of a coefficient, defined as ST - S_1, is large, it indicates significant interaction effects for that variable in the model.

$$\mathbf{ST} = \mathbf{1} - \frac{\mathbf{V|E(Y|X_{\sim i})|}}{\mathbf{V(Y)}}$$

(26)

In the original definition of the total index, if there are no interaction effects in the model, it is referred to as an additive model, where the sum of all first-order sensitive indices equals 1.

$$\mathbf{ST} = \mathbf{S1} + \mathbf{S2} + \cdots$$

(27)

doi:10.6342/NTU202502274

doi:10.6342/NTU202502274

3 Results and Discussion

3.1 Baseline Optimization Outcomes

Based on the baseline parameter settings used in **Section 2.5**, we obtained the baseline optimal solution for the V2G system at three electric bus stations, which is $422,615. In the optimization process, using the June 1st, 24-hour schedule of the Songshan High School station as an example as **Figure 19**, each line is determined by balancing both the bus dispatch demand and the charging/discharging optimization model to decide how the battery behavior should change. Through the analysis of this result, we can also ensure that this optimization model system adheres to the bus dispatch constraints.

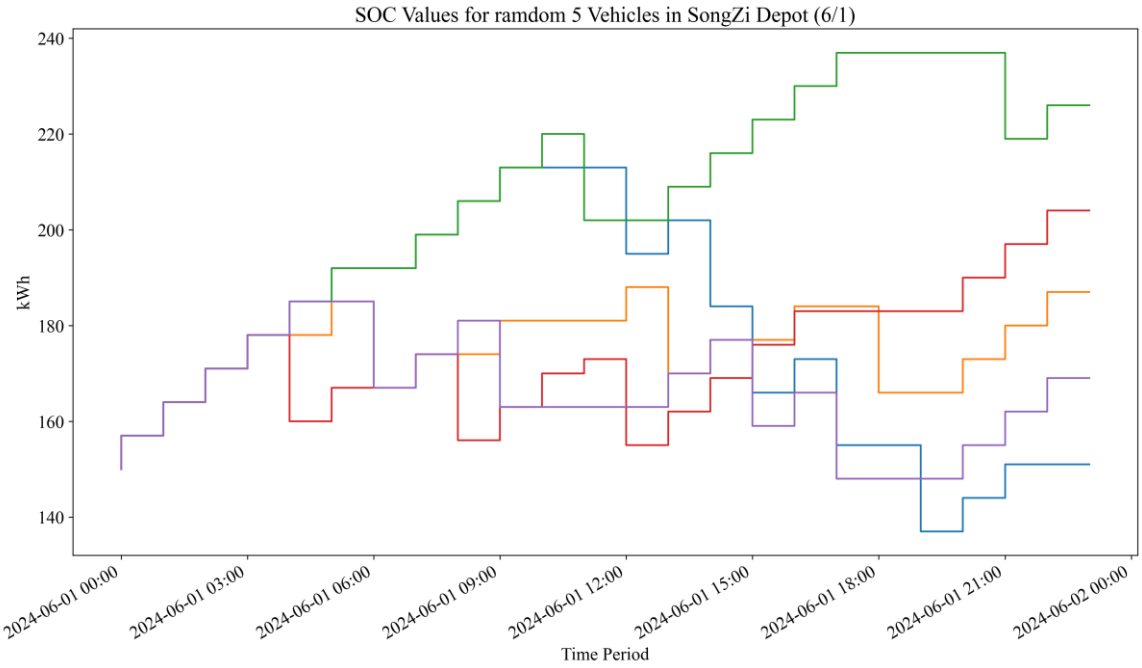

Figure 19 State of Charge for each vehicle in SongShan Vocational School Station

The input weather data in the model is presented in a graphical format as shown in **Figure 20**. From this, we can observe that at the beginning of June, the blue-marked area shows a significant drop in temperature due to the influence of frontal systems, which also brought some rainfall. In such climatic conditions, the solar power generation of the

doi:10.6342/NTU202502274

buildings used by the electric buses is significantly low as indicated by the yellow line. However, when the Pacific high pressure strengthens, as shown in the yellow-marked area, the environmental temperature rapidly rises. During this period, the solar power generation of the buildings used by the electric buses increases significantly. Meanwhile, the city power fast charging system was activated during the frontal weather in early June, as shown in the blue-highlighted area. Meanwhile, towards the end of June, with the strengthening of the Pacific higher pressure, as shown in the yellow area, more solar power was generated, leading to a lower operation of the city power fast charging system in this period as shown in **Table 3.**

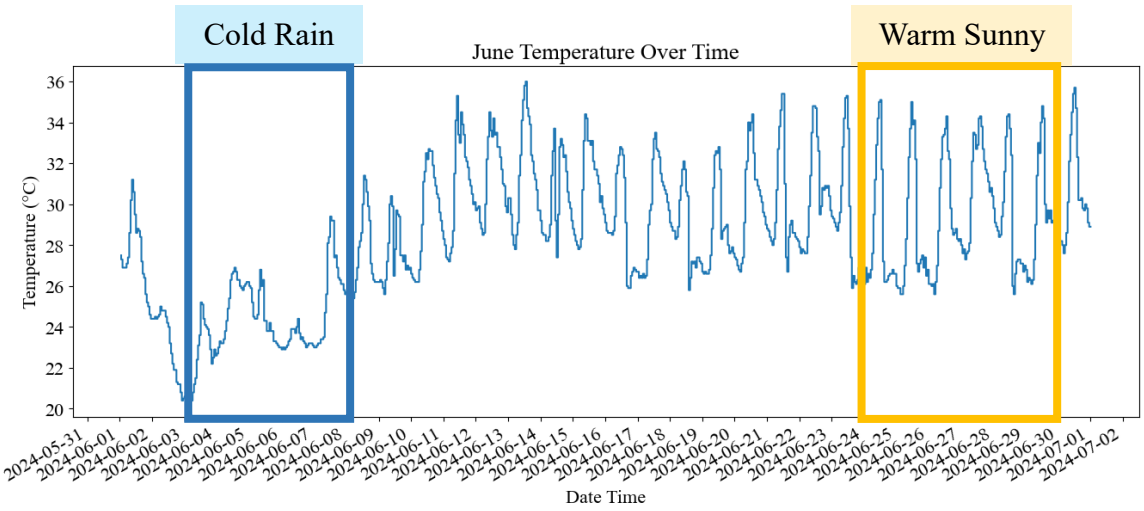

Figure 20 Taipei's June Weather

Table 3 demonstrates that the model can effectively adjust the solar power generation from buildings based on weather patterns. The discharging behavior is strongly positively correlated with the three-stage TOU peak pricing for the V2G system, we can see that during weekends, the model does not discharge because the TOU peak price settings define these periods as off-peak. On the other hand, during weekdays, discharging occurs due to the peak-off-peak differences, which aligns with the original expectations, proving the model's effectiveness.

doi:10.6342/NTU202502274

This study also analyzes the daily energy usage, taking June 3rd for a station energy schedule as an example, as shown in **Figure 21**. Based on the time-of-use electricity pricing, the day is divided into three time periods: off-peak, semi-peak, and peak hours. First, from 11:00 PM to 9:00 AM, this period is off-peak and designated for discharging. During this time, the electricity grid also operates in off-peak hours, so the discharging system remains inactive. Simultaneously, the grid's slow charging system operates at a low power level, often referred to as trickle charging. Next, from 9:00 AM to 4:00 PM, this is the semi-peak period. During this time, it is also the key charging period for building solar systems. Some electric buses charge using the building's solar power, while others discharge to the grid, responding to the higher semi-peak time-of-use rates. Finally, from 4:00 PM to 11:00 PM, this is the peak period, when the discharging system is most active due to the higher time-of-use rates. Simultaneously, the building's solar power charging and the grid's charging systems are typically turned off to align with the high electricity demand during the evening peak period. Meanwhile, we can observe that the daily results vary on other days. As shown in **Figure 22**, when solar energy is insufficient, the daytime charging schedule shifts to the city power fast-charging system, represented by the red line. This behavior differs from that of solar fast charging, as the power level does not reach the same peak when solar energy is unavailable. This is because, in the optimization model, the system shifts to using cheaper nighttime electricity instead of relying on higher-priced daytime city power.

doi:10.6342/NTU202502274

Table 3 Charging Status for EVs

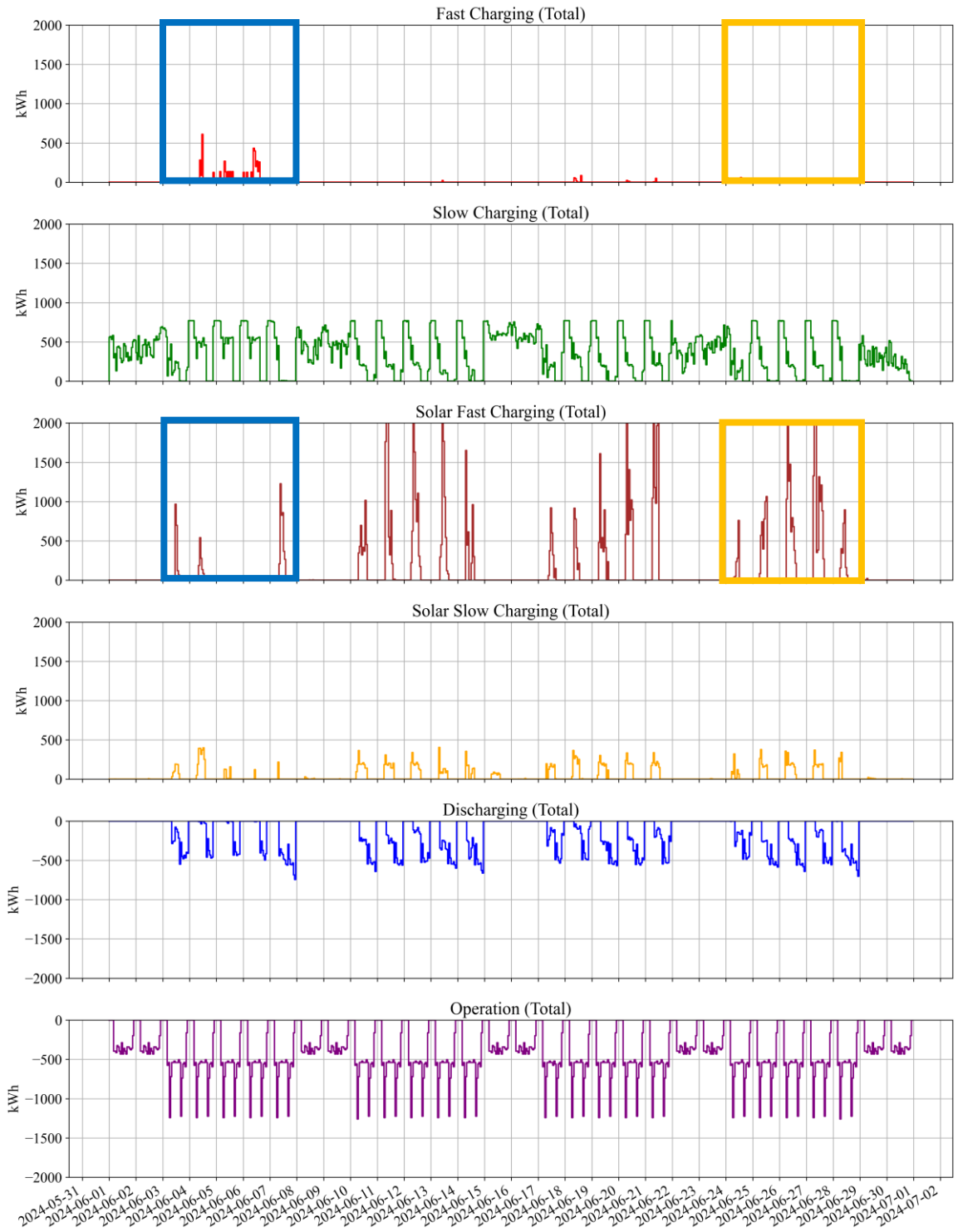

doi:10.6342/NTU202502274

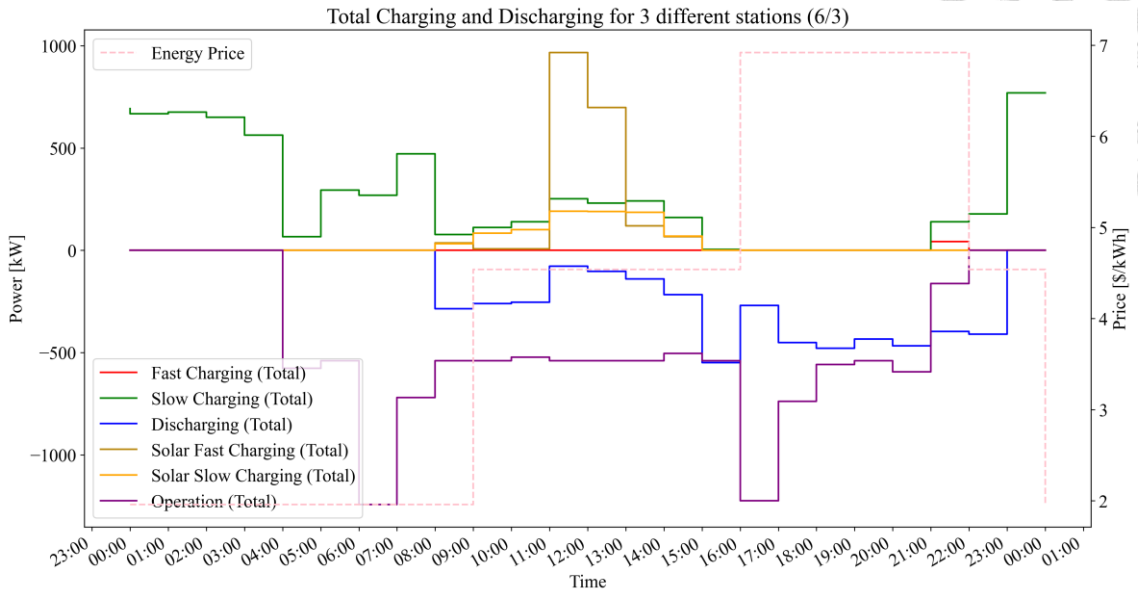

Figure 21 Typical Daily Charging Schedule of V2G system

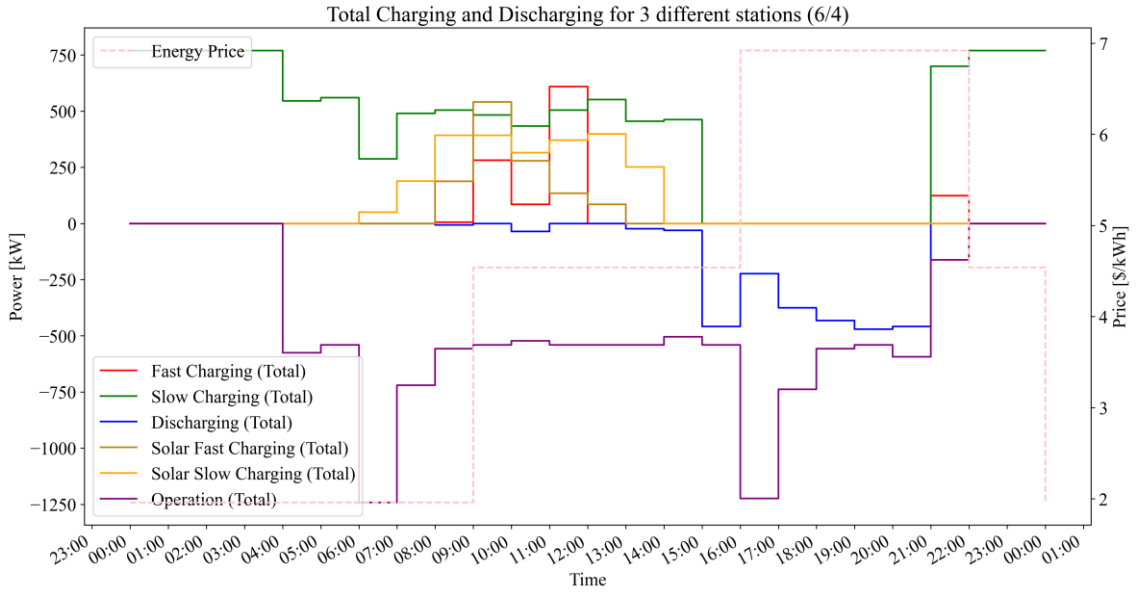

Figure 22 Rainy Daily Charging Schedule of V2G system

In addition to the weather changing has influence on the daily result, shows that the weekday/ weekend's electricity policy changing cause different result. In weekend's scenario, daily result tends to utilize slow charging to deal with the transportation operation need instead of discharging.

doi:10.6342/NTU202502274

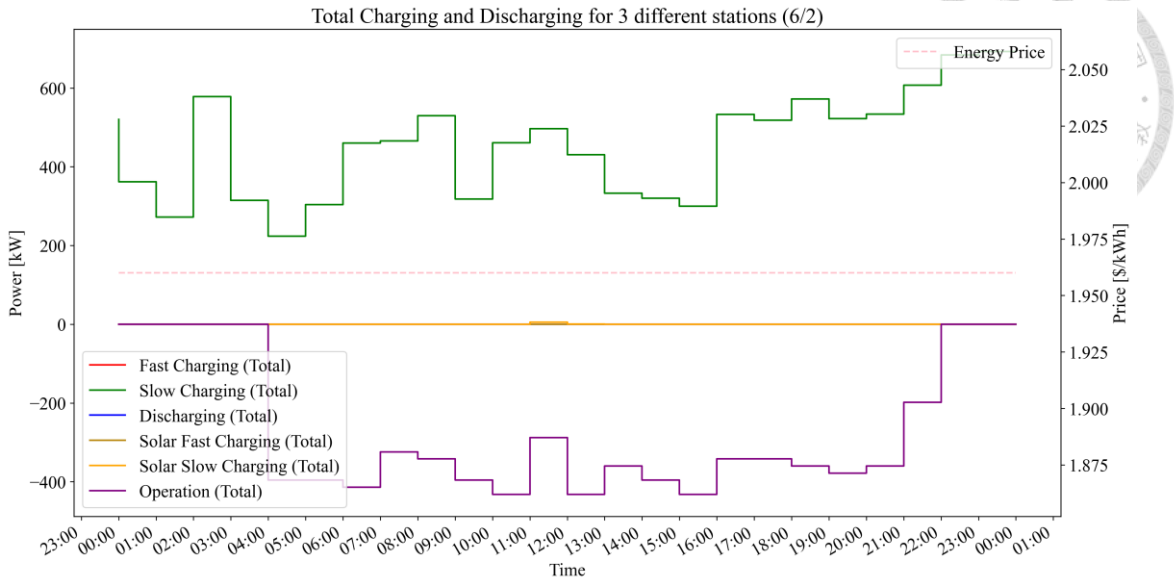

Figure 23 Weekend Daily Charging Schedule of V2G system

In the discussion of the baseline optimization results, this study also analyzes the total cost through graphical representation, as shown in **Figure 24**. The original model is compared with a scenario where the V2G system is not involved, referred to as V1G (No discharging). The chart displays the individual costs for V1G and V2G. From the chart, it is evident that when the discharging system is inactive, V1G primarily relies on trickle charging to meet the operational needs, as it only needs to satisfy the bus scheduling requirements. Therefore, the charging demand is relatively low. According to the current operation of electric buses, charging typically occurs during nighttime trickle charging and in small time slots during daytime scheduling intervals. Additionally, the building's solar charging costs are slightly higher than the nighttime trickle charging costs due to the electricity sales price, so during low charging demand, only a small portion of the charging time utilizes the solar charging system. Furthermore, as seen in **Figure 24**, the number of cost categories increases rapidly, and this can be attributed to the addition of the discharging system. As a result, the charging demand rises, requiring more extensive and varied charging during the appropriate time slots. With the integration of the Vehicle-to-Grid (V2G) system, the building's solar power system generates energy during the day,

doi:10.6342/NTU202502274

while the grid charges during the night, with excess energy sold back to the grid based on the grid's demand.

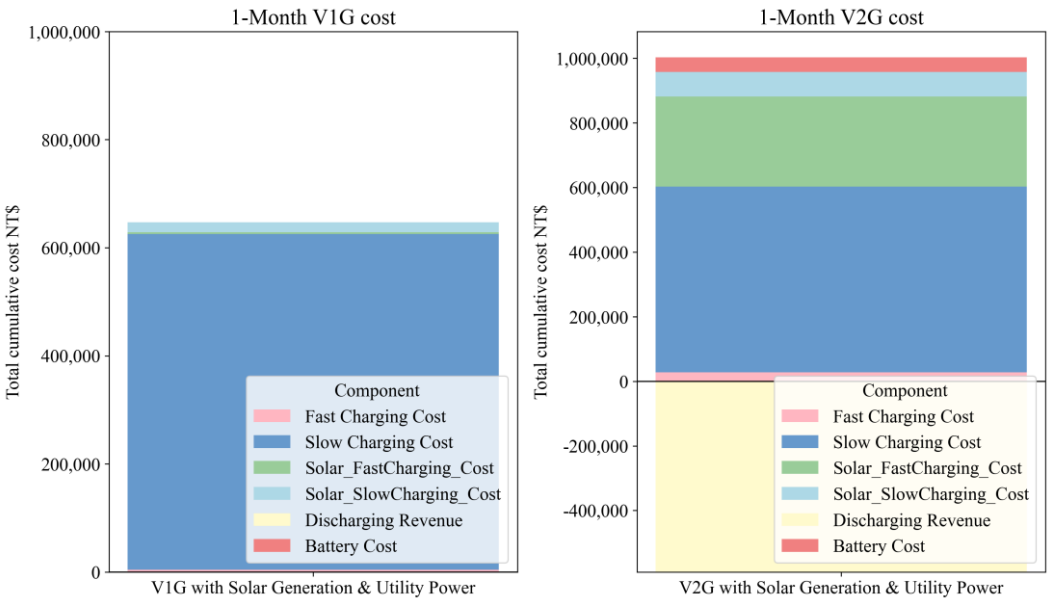

Figure 24 Monthly for V2G Revenue

The baseline optimization result obtained from the V2G system shows a monthly value of NT$422,615. The payback periods is calculated as shown in **Figure 24.** Comparing V1G and V2G, the total operating cost across the three bus stations has decreased by NT$224,383 per month. This result demonstrates that via V2G system can increase the utilization of solar energy generation which meet our goal in the initial mindset. What's more, in the baseline V2G optimization our estimation of the battery degradation cost is about 4% which imply that the policy-related parameter may took the important role in the V2G development.

In the initial construction phase, the cost of the V2G system is estimated per unit. The construction of the V2G system includes a power control system, inverter, converter, and package engineering (EPC), with each system priced at NT$435,000 per system. The charging pile costs NT$135,000 refer to per system [57], bringing the total to approximately NT$570,000 per system. Similar cost estimates from First Student Inc.

doi:10.6342/NTU202502274

which is a school buses operator in North America, their estimate for electric buses used as school buses range from NT$300,000 to NT$900,000 per system [58]. Therefore, our total initial V2G capital cost with 110 systems will be NT$47,850,000 and charging pile in total will be NT$14,850,000. For the operation and maintenance cost, we refer to Razmjoo and estimated it will be 1% of total initial cost [59].

In the Equation 28, the capital cost payback periods is calculated, by dividing the total cost of implementing the V2G system by the monthly reduction in total operating costs achieved after transitioning to V2G operations. Specifically, UCap refers to the capital cost for infrastructure setup, CharCap is the capital cost for installing bidirectional V2G charging piles, UO&M represents the monthly operation and maintenance (O&M) cost of the infrastructure system, CharO&M is the monthly O&M cost of the bidirectional V2G charging piles, and Rev denotes the monthly cost savings like profit from V2G-enabled system operations. The payback periods is thus defined as the number of months required for the cumulative cost savings (Rev) to recover the combined capital and ongoing O&M expenditures of the V2G system.

$$\text{Payback periods} = \frac{\text{Ucap} + \text{CharCap}}{\text{Rev} - \text{UO\&M} - \text{CharO\&M}} \quad \textbf{(28)}$$

According to the chart, the calculated payback periods is 432 months in **Table 4**, meaning it would take 36 years to break even. However, based on the study by Razmjoo the typical service life of relevant infrastructure is approximately under 20 years [59]. Therefore, we set up our payback periods should be under 10 years which is 120 months since our weather data background is based on June.

doi:10.6342/NTU202502274

Table 4 Payback periods Calculation of V2G system in Baseline Scenario

V2G SAVING	
V1G Scenario Cost	NT$646,998
V2G Scenario Cost	NT$412,615
Total per month saving with V2G	NT$234,383
V2G Capital Cost	
V2G Installed Capital Cost	NT$47,850,000
V2G Charging Pile Capital Cost	NT$14,850,000
V2G Installed O&M Cost	NT$39,875
V2G Charging Pile O&M Cost	NT$12,375
V2G ROI (months)	344.25

3.2 Battery Parameter Sensitive Analysis

In the baseline optimization results, battery degradation cost emerges as an optimizable parameter. In the previous study, battery degradation cost shows its dominant influence to total cost. Therefore, this study analyzes trends in electric vehicle (EV) battery applications over the past decade. While solid-state batteries possess the highest energy density and stability, they are not yet commercially viable and are thus excluded from this study. Instead, the analysis focuses on three commercially available battery types: Lithium Iron Phosphate (LFP), Nickel Manganese Cobalt oxide commonly known as ternary lithium batteries (NMC), and Lithium Titanate (LTO). This study aims to assess whether these different battery chemistries, under varying material properties and contextual conditions, can effectively reduce the costs associated with V2G system integration. Compared to the baseline battery type LTO both LFP and NMC batteries exhibit higher energy density measured in Wh/kg, as shown in **Table 5**. Consequently, major EV manufacturers such as Tesla, Volkswagen, and Kia Motors have increasingly adopted NMC batteries in their passenger vehicles. Meanwhile, the Chinese EV giant BYD has continued to expand its market share by leveraging its proprietary blade type LFP battery technology.

doi:10.6342/NTU202502274

Table 5 2024 Energy Density Data

	Energy Density(Wh/Kg)
LTO	50–110 Wh/kg
LFP	140–200 Wh/kg
NMC	200–350 Wh/kg

3.2.1 Electric Buses Battery Degradation Prices Impact

Following the comparative analysis of different electric bus battery types, this study references financial reports on the EV battery market to obtain by year projected prices per kilowatt-hour (NT$/kWh) for each battery type, as illustrated in **Figure 25**.

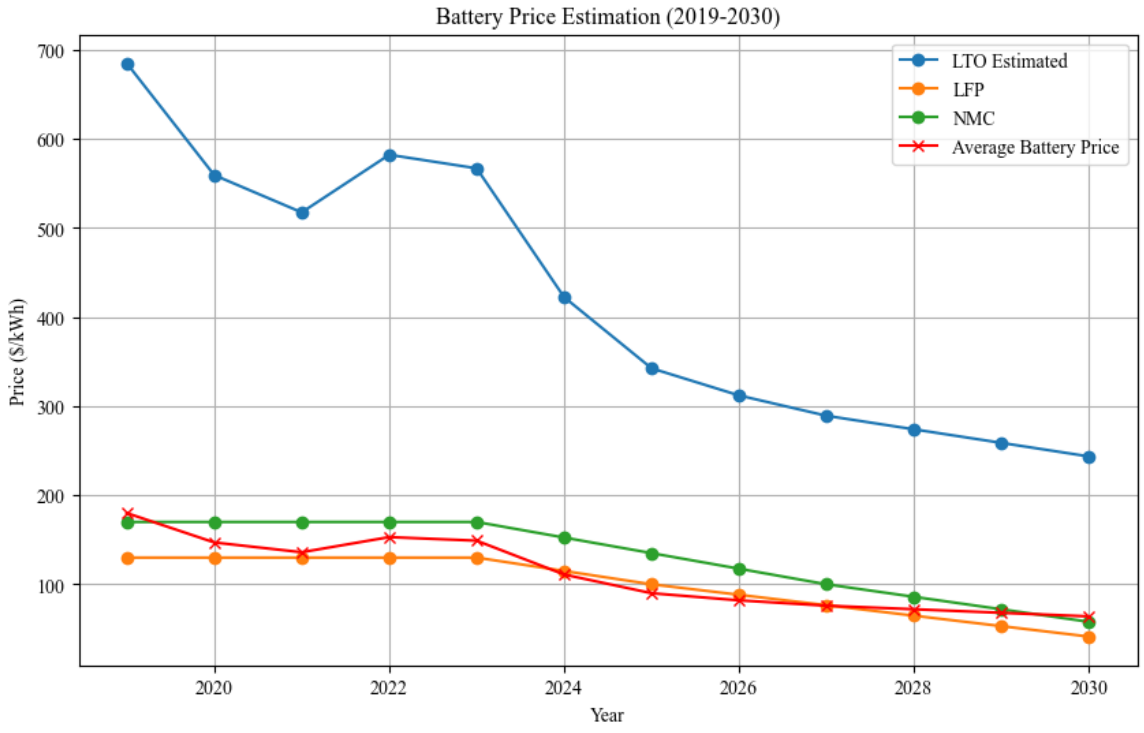

Figure 25 Battery Degradation Price (NT$/kWh)

Among the three, lithium-titanate (LTO) batteries show significantly higher unit capacity costs due to their lower energy density. Specifically, because LTO batteries store

doi:10.6342/NTU202502274

less energy per unit of weight, more material is required to achieve the same energy capacity, driving up the cost per kWh [60]. Furthermore, LTO battery prices exhibit wider fluctuations; the baseline optimization in this study uses the lowest observed price for LTO. Nickel Manganese Cobalt (NMC) batteries, on the other hand, have slightly higher prices due to the volatility in nickel (Ni) supply a critical rare-earth element in their composition resulting in less stable pricing. In contrast, Lithium Iron Phosphate (LFP) batteries benefit from broader adoption and extensive research and development, leading to more stable and generally lower per-kWh costs compared to the other two types [61, 62]. Based on the annual price trends of electric vehicle (EV) batteries per unit capacity (NT$/kWh) obtained in earlier sections, and using the cost formulation defined in Equation 16 which links the cost per unit of discharged energy to the battery's unit capacity cost this study calculates the degradation cost of different battery types under the V2G scenario. A critical parameter in this calculation is the battery's lifecycle, measured in terms of the number of charge-discharge cycles it can endure. To estimate this, we refer to the experimental data from Ager-Wick Ellingsen, in which various EV batteries were subjected to repeated destructive charge-discharge testing: discharging from a State of Charge (SOC) of 90% to 10%, followed by charging back to 90%. This full 90%-10%-90% sequence is defined as one complete cycle. The process continued until the battery's capacity dropped to 80% of its original manufacturing capacity. Using the average cycle life of each battery type (LFP, NMC, LTO) as reported in that study, summarized in **Table 6**, we integrate these values with year-specific battery prices to estimate the battery degradation cost per unit of discharged energy for each type. This provides the basis for the sensitive analysis on alternative battery materials in the V2G system [32].

doi:10.6342/NTU202502274

Table 6 Discharge of Depth Table

	Depth of Discharge Cycle
LTO	20000 times
LFP	6000 times
NMC	4000 times

By incorporating the battery life cycle (number of charge-discharge cycles) and the unit manufacturing cost of batteries ($NT/kWh) into Equation 16, and applying the 90%-to-10% State of Charge (SOC) cycling definition from Ager-Wick Ellingsen's work, we derive **Table 7**. This table presents the calculated cost per kilowatt-hour of energy discharged for three different battery types (LFP, NMC, LTO) across the years 2025, 2027, and 2030. Among the results, the Nickel Manganese Cobalt (NMC) battery exhibits the highest cost under the worst-case scenario, reaching 1.266 $NT/kWh. Conversely, under the most favorable scenario, the Lithium Iron Phosphate (LFP) battery achieves the lowest cost, as low as 0.258 $NT/kWh.

doi:10.6342/NTU202502274

Table 7 Battery Degradation Scenario

Discharge Degradation $NT/kWh	LTO	LFP	NMC
2025	0.642	0.625	1.266
2027	0.542	0.478	0.938
2030	0.457	0.258	0.543

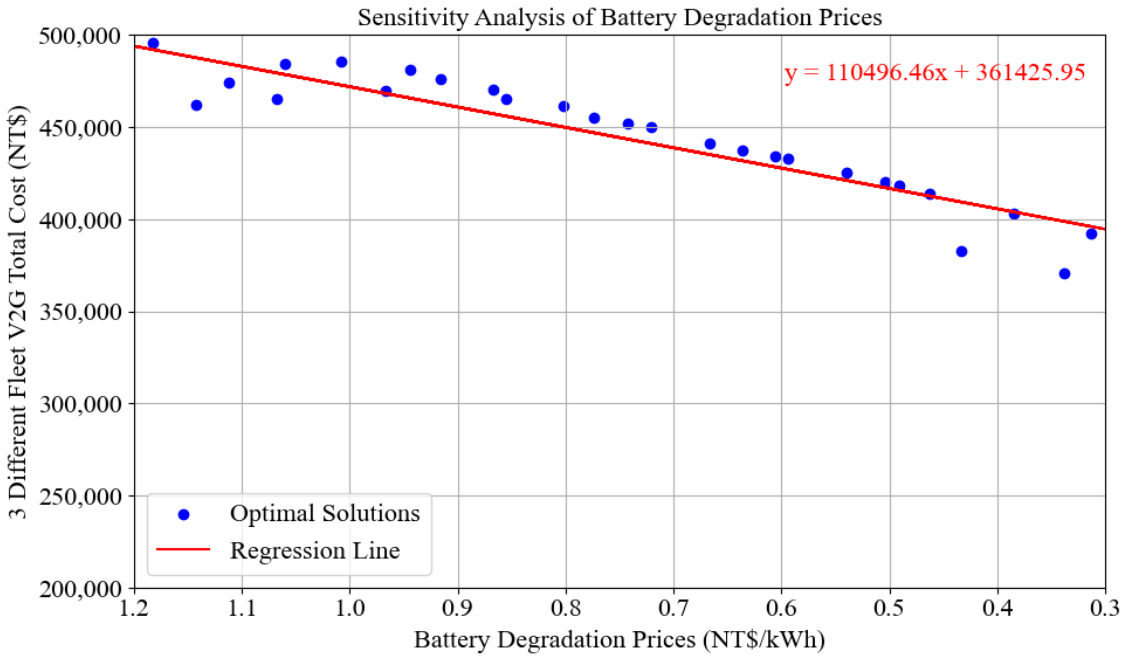

Figure 26 Battery Degradation Prices Sensitive Analysis

Using the data from **Table 7** and the Latin Hypercube Sampling (LHS) method described in **Section 2.9**, a monotonic sensitive analysis was conducted, resulting in **Figure 26** reveals that within the global parameter space, reducing battery degradation cost could lower the total operational cost by up to 24%. Compared to the 38% reduction reported in the study by Manzolli, this highlights the regional differences in the impact of battery degradation costs [35]. In our assumption, today's battery degradation is about

doi:10.6342/NTU202502274

NT0.45/kWh which means it is limited to improve by 2030 meanwhile it is significant right now for monopoly test.

For the year 2025, the discharge cost per kilowatt-hour for Lithium Iron Phosphate (LFP) and Lithium Titanate (LTO) batteries does not differ significantly, whereas Nickel Manganese Cobalt (NMC) batteries exhibit a notably higher cost. Referring to **Figure *26***, when using NMC batteries at NT$1.266/kWh, the total optimized operational cost reaches approximately NT$490,000. In contrast, for LTO and LFP batteries, the optimized operational cost is around NT$420,000. In the baseline scenario used in this study, the degradation cost aligns with that of LTO batteries projected for 2030, estimated at NT$0.45/kWh. If the material were switched to the most favorable case, LFP batteries with a cost of NT$0.26/kWh the optimized total operational cost could drop to approximately NT$390,000. This would further reduce the payback periods by roughly 291 months, bringing the payback period down to 24 years.

3.2.2 Electric Buses Battery Capacity Impact

Beyond battery degradation cost, the total energy capacity of the battery also significantly influences the operational benefits of electric buses, as it determines the maximum storable energy. In this study, the baseline battery capacity for electric buses is set at 300 kWh. Based on data from previous literature, we investigate the feasible capacity ranges for Lithium Titanate (LTO), Lithium Iron Phosphate (LFP), and Nickel Manganese Cobalt (NMC) batteries, with the corresponding minimum and maximum capacities summarized in **Table 8**. These variations in battery capacity are considered under the assumption of technological advancements that improve energy density (Wh/kg), rather than simply increasing battery mass. As shown in **Table 8**, the minimum capacity for LTO batteries is approximately 50 kWh, while the maximum capacity reaches nearly 300 kWh, consistent with this study's baseline and it can recalled to

doi:10.6342/NTU202502274

Behnia's paper mentioned under 300 kWh already worked for V2G structure [2]. Sensitive analysis based on these values is illustrated in **Figure 27**.

Table 8 Estimated Battery Capacity Table

	Estimated Minimize Capacity(kWh)	Estimated Maximize Capacity(kWh)
LTO	50	330
LFP	170	600
NMC	200	1050

Starting from the baseline battery capacity of 300 kWh, the corresponding optimized total operating cost is approximately NT$410,000. When using Nickel Manganese Cobalt (NMC) batteries with a maximum capacity of up to 1000 kWh, the optimized cost can be reduced to around NT$310,000 representing a cost reduction of NT$100,000 so as approximately 23.4% of the total operating cost. This study further reveals that in the monotonic optimization analysis, the most rapid decline in operating cost occurs within the range of 300 ~ 600 kWh. Beyond 600 kWh, the rate of cost reduction begins to plateau, forming a quadratic-like decline curve. This phenomenon is likely attributed to limitations in the total renewable energy available and the maximum allowable charging power.

doi:10.6342/NTU202502274

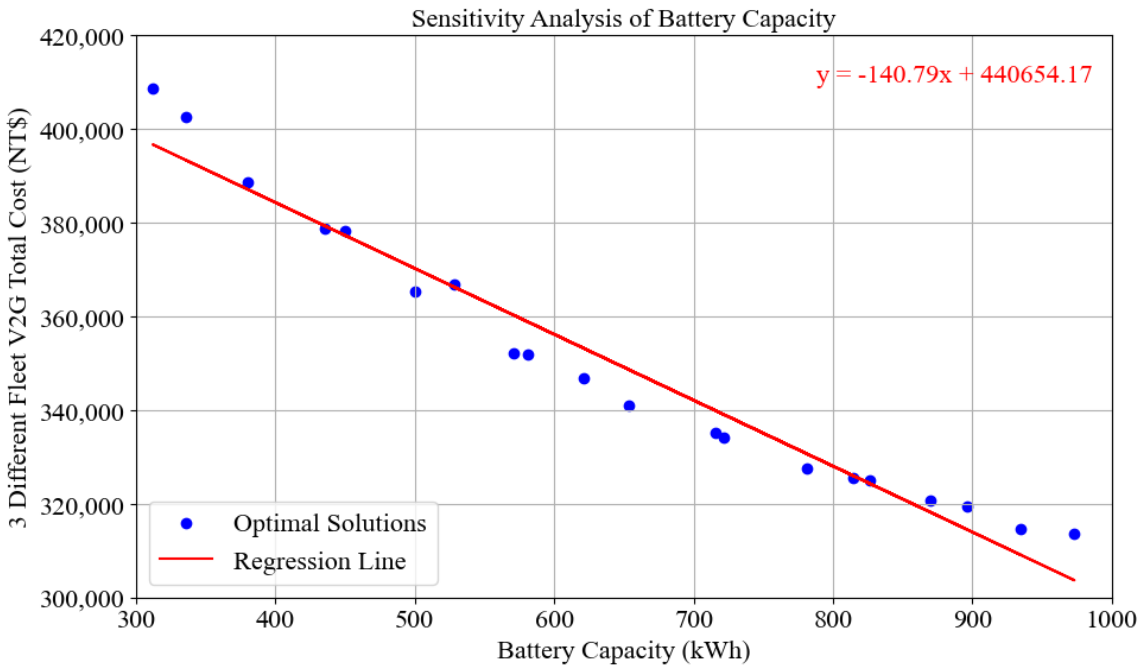

Figure 27 Battery Capacity Sensitive Analysis

3.3 Solar Energy Parameter Sensitive Analysis

In the model design, the original intent of this study was to store surplus solar energy generated by buildings during midday via the V2G system, enabling effective energy dispatch. However, in the baseline optimization results, a portion of the charging behavior still relies on grid-based slow charging to meet demand. This outcome diverges somewhat from the initial design goal of daytime charging and nighttime discharging. Therefore, this study further conducts a sensitive analysis on various solar-related parameters associated with the buildings.

3.3.1 Conversion Transfer Rate Impact

To analyze the impact of building-integrated solar energy, this study first investigates the parameter of photovoltaic (PV) conversion efficiency. By examining variations in this conversion rate, we aim to understand how different levels of solar generation influence the reduction in total operating costs. Based on the literature [63], the current range of solar PV conversion efficiencies spans from 15% to 30%, as

doi:10.6342/NTU202502274

summarized in **Table 9**, covering five commonly used photovoltaic materials. The lowest conversion efficiency, at 15%, is found in Organic PV, which has gained popularity due to its flexibility, making it suitable for curved glass surfaces. Some startups have applied this material to the roofs of electric vehicles. Next is Perovskite PV, which offers partial transparency and is often integrated into curtain walls of high-rise buildings, enabling vertical solar power generation without compromising indoor daylight autonomy. Silicon PV, the most widely used in building rooftop installations, is known for its high reliability and widespread deployment. Finally, the highest conversion efficiencies are achieved by III-V compound PVs, particularly Gallium Arsenide (GaAs) cells, which are commonly used in power systems for space stations due to their higher power output per unit area. In the 30% conversion rate field, we also found out that with Silicon PV and Perovskite PV to absorb lower/longer wave length can meet this conversion rate as shown in **Figure 28** which λ means wavelength of sunlight.

Figure 28 Solar PV Combination of Increasing Conversion Rate

This study conducts a sensitive analysis based on the aforementioned solar conversion efficiencies. Under the assumption that the baseline feed-in tariff for building-generated solar power remains constant regardless of the photovoltaic (PV) material used, we aim to evaluate how variations in solar energy conversion efficiency attributed to different PV technologies affect the total operating cost of the system.

Furthermore, if space-grade materials such as gallium arsenide solar cells are adopted as the building-integrated photovoltaic system in this study, and their production costs are significantly reduced due to technological advancements allowing building

doi:10.6342/NTU202502274

owners to sell the generated electricity to the V2G system at a rate of NT$3 per kilowatt-hour the total operating cost could be further reduced to NT$385,000. This scenario corresponds to a 7.8% reduction in total operating cost in the monotonic sensitive analysis as shown in **Figure 29**.

Table 9 Commercial Solar Transfer Rate Technology

	A	B	C	D	E
Solar energy transfer rate	15%	18%	20%	25%	30%
Material	Organic PV	Perovskite PV	Silicon PV	III–V cells PV	GaAs (thin film cell) *III–V cells PV*
Pros and Cons	Lower cost Flexible (ex. Curve)	Fit for 3D architecture design	Tradition Reliable		Higher cost, Extreme Environment (ex. Space)

doi:10.6342/NTU202502274

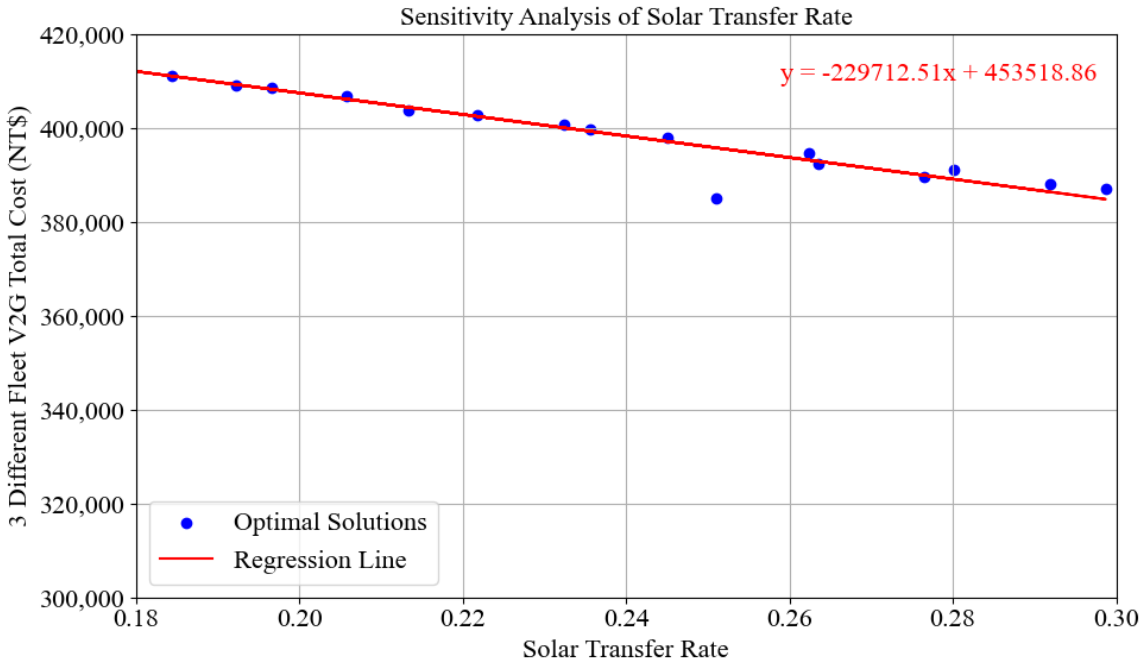

Figure 29 Building Solar Energy Transfer Rate Sensitive Analysis

3.3.2 Building Solar Energy Seasonal Variability

Similar to the seasonal V2G system analysis conducted by Z. He [16], this study also performs a seasonal solar energy assessment for the Taipei region. Specifically, the solar generation and building electricity consumption data for December are compiled to evaluate whether seasonal variations in solar output and building demand significantly affect the total operating cost. The analysis reveals that the total surplus solar generation in June reaches 261,824 kWh, while in December, it drops to 176,237 kWh which represent a decrease of approximately 100,000 kWh which is similar to energy transfer rate effect from 18% to 16%. However, in the June optimization model, the total energy demand for electric bus charging is 149,545 kWh, of which only 51,000 kWh is supplied through the building's solar system. This indicates that the current model is not utilize daytime solar resources, resulting in insufficient reliance on building-integrated photovoltaics. To sum up, this study further discusses possible improvements to better align with the original objective of "charging during the day, discharging at night."

doi:10.6342/NTU202502274

3.3.3 Building Solar Energy Surface Area Coverage Impact

After understanding the impact of building-integrated solar systems, this study further considers the application of perovskite solar cells as mentioned in **Table 9** for building façades and curtain wall designs. Specifically, we examine the effect of expanding the solar coverage area on a cube-like building structure, assuming a fixed solar conversion efficiency of 18%. The analysis ranges from solar panels installed on a single surface to a maximum of five surfaces of the cube. In the context of façade-integrated solar system design, there are several research, in higher latitude like Adelaide in Australia, Zhao estimated that about 9.8% of façade/rooftop solar potential in the integrated solar system [64]. However, Yu estimated that the potential solar energy generated from curtain wall glass can reach approximately 68.2% of the rooftop solar capacity [65]. Based on this estimation, the total realistic solar energy generation potential of a building can be approximated at 168.2%. As shown in **Figure 30**, when the effective solar panel area reaches 1.5 to 2 times the rooftop area, the total operating cost of the V2G system achieves its lowest value in the monotonic sensitive analysis. This further demonstrates that under the current parameter settings, promoting façade-integrated photovoltaic design in buildings can result in a win-win outcome for both architectural energy efficiency and electric bus V2G operations. Specifically, when the solar-enabled area reaches 1.6 times that of the rooftop, the total operating cost of the V2G system can be reduced by approximately 2.3%.

doi:10.6342/NTU202502274

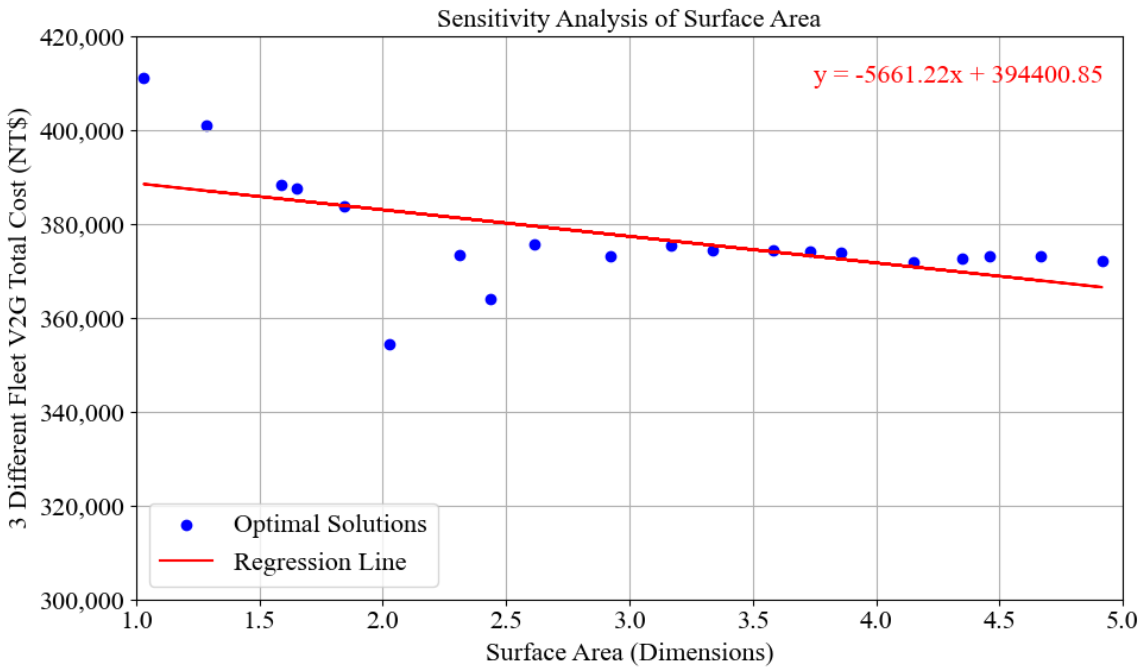

Figure 30 Building Solar Energy Surface Area Sensitive Analysis

3.4 Infrastructure and Fleet Configuration

In addition to battery types and building-integrated solar parameters, the configuration of physical infrastructure at bus depots may also significantly influence the total operating cost of a V2G system. Therefore, this chapter defines and adjusts key hardware related parameters such as the number of charging piles and the size of the bus fleet and conducts sensitive analyses to evaluate their impact on system performance and cost. The findings provide valuable insights for infrastructure planning and investment decision-making in future V2G deployments.

3.4.1 Maximum Charging Power Impact

In the previous sensitive analysis on battery capacity, this study observed that beyond a certain threshold, increases in battery size result in diminishing returns in terms of reducing total operational costs. Meanwhile, many electric vehicle manufacturers have recently developed so called Megawatt Charging Systems (MCS), aiming to significantly reduce charging time by increasing power output. In light of this trend, this study also

doi:10.6342/NTU202502274

investigates the potential impact of increasing the maximum power capacity of charging piles on the optimization results of electric bus operations and the V2G system. A corresponding sensitive analysis is conducted to assess the effects of enhanced charging power infrastructure. According to **Figure 31**, the monotonic sensitive analysis reveals that under the current parameter settings, increasing the maximum charging power yields minimal impact on the total operational cost. This suggests that, within the context of this study, high charging power capacity is not a critical factor in achieving V2G profitability. Instead, operational effectiveness relies more heavily on optimizing charging scheduling and managing the rate of energy transfer.

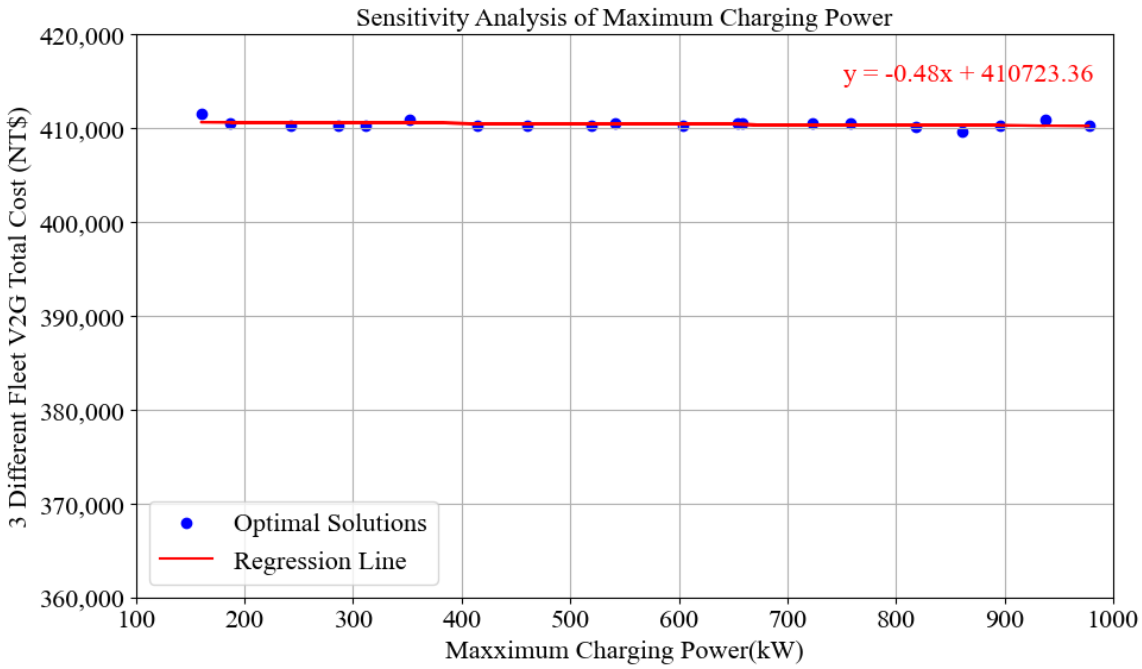

Figure 31 Maximum Charging Power Sensitive Analysis

3.4.2 Electric Buses Fleet Scale Impact

In terms of depot configuration, this study also examines the impact of electric bus fleet size on total operational costs. For a single depot, the energy supply capacity is positively correlated with the fleet size, which is itself constrained by available space and closely related to the operational strategies of depot and bus operators. Through sensitive

doi:10.6342/NTU202502274

analysis, this study aims to explore how variations in fleet size affect operational efficiency, with a particular focus on identifying the threshold at which meaningful operations become feasible and analyzing the associated cost-saving or profit-generating potential.

As illustrated in **Figure 32**, the model begins to generate valid operational cost results when the fleet size reaches 75% of the baseline setting. This situation is likely due to the minimum dispatch requirement for buses which means below this level, the optimization model cannot meet operational constraints and therefore fails to converge.

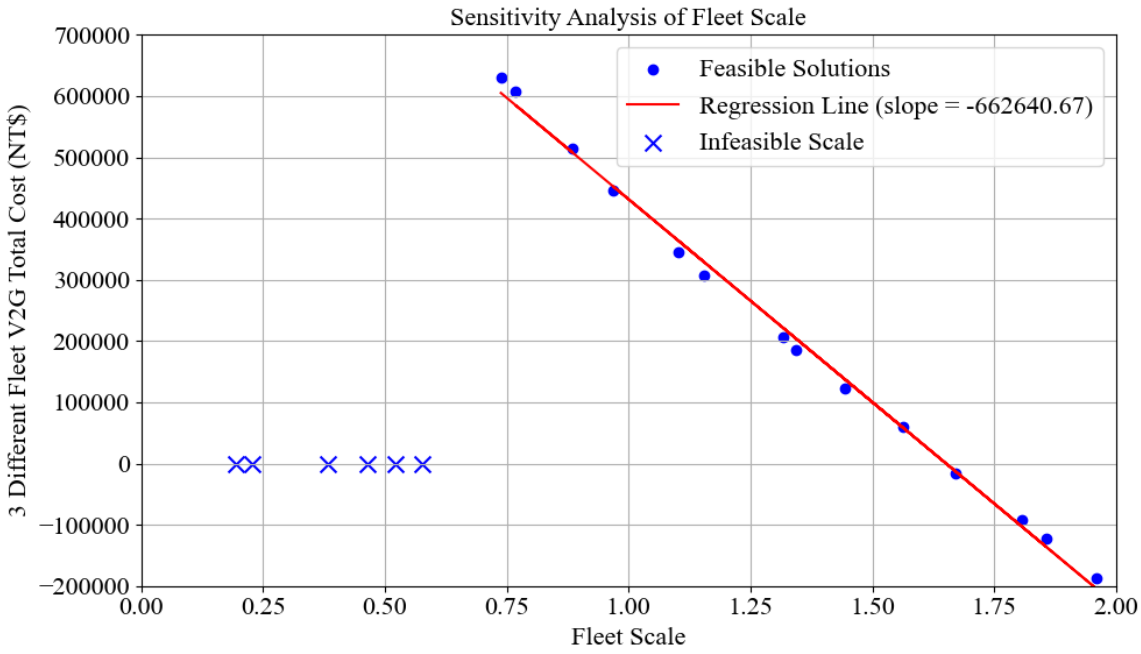

Figure 32 Fleet Scale Sensitive Analysis

Further analysis reveals that doubling the baseline fleet size can lead to a total operational cost reduction of up to 161.6%, highlighting the potential benefits of larger fleets in supporting grid participation and energy management. While this finding offers valuable insight for bus operators when considering fleet expansion or depot development, the actual number of buses deployed must still account for factors such as depot space

doi:10.6342/NTU202502274

limitations, route density, and passenger demand. As such, the results of this analysis should be interpreted as a reference for exploring potential operational improvements.

3.5 Policy-Oriented Parameters

This chapter focuses on adjusting policy-related parameters governing the charging and discharging operations of electric buses. Unlike the previous chapters, which emphasize technological improvements, this section concentrates on parameters influenced by government interventions, such as subsidies and pricing mechanisms. By conducting sensitive analyses on various policy-related factors, this study aims to identify which adjustments can most effectively reduce the total operating cost of the system, thereby providing insights into the most impactful policy measures.

3.5.1 Building Solar Electricity Selling Price Impact

In previous sections, this study found that setting the building-integrated solar electricity selling price at NT$3 per kWh may cause the V2G system from adopting the intended charging pattern of "charging during the day and discharging at night." This pricing strategy limits the effective utilization of solar power. For instance, under the baseline optimization result, the building sold 51,288 kWh of solar energy to the bus operator. However, this electricity could alternatively be sold to Taiwan Power Company. Taipower currently faces a severe financial deficit, with cumulative losses exceeding NT$420 billion. Continuing to purchase solar energy at a price higher than its resale price would exacerbate its financial challenges. As a result, Taipower has gradually reduced its feed-in tariff (FIT) for solar electricity, from NT$11.75/kWh in 2010 to as low as NT$3.5/kWh in 2023 [66].

$$\text{Solar}_{\text{price per kwh}} = \frac{\text{Installation Price}}{\eta_{\text{PV}} * \text{I}_{\text{day}} * \text{kWp per m}^2} \quad \textbf{(29)}$$

doi:10.6342/NTU202502274

This trend is consistent with global cost reductions. According to Lazard , the levelized cost of solar energy ranges from NT$0.72/kWh to NT$3.51/kWh depending on system type and scale [67]. There also has a report for Taiwan's Bureau of Energy, also projected that the cost of solar electricity would fall below NT$2/kWh by 2026 [68]. In Taipei, local solar generation potential is estimated at 3.25 kWh/m²/day. Using this irradiance level with an 18% panel conversion efficiency, 80% system efficiency, a 25-year lifetime, and a rooftop area requirement of 6.7 m² per kWp with Equation 29, the annual output is estimated at 28,616 kWh per kWp. According to PRO360 , installation costs per kWp range between NT$40,000 and NT$70,000 [69]. From this, the levelized cost of electricity (LCOE) for rooftop solar in Taipei is approximately NT$1.39 to NT$2.45/kWh.

Based on these findings, this study recommends setting the building solar electricity selling price from buildings to V2G bus operators within a reasonable range of NT$1 to NT$3/kWh, balancing optimization performance with financial feasibility.

Based on the above assumptions, this study sets NT$3 per kWh as the baseline building solar electricity selling price for building integrated solar power and conducts a sensitive analysis within a range from NT$1 to NT$3 per kWh. It is further assumed that future advancements in solar technology will enable solar power generation costs to drop below those of most other energy sources. The analysis reveals that when the price is reduced to NT$2/kWh, the optimized total operating cost rapidly decreases to NT$200,000. If the price drops to NT$1/kWh, the total operating cost even becomes negative and reach NT$25,000, indicating a surplus. This demonstrates that the building solar electricity selling price is an extremely sensitive policy parameter, influencing up to 125.1% of the total operating cost across the global interval.

doi:10.6342/NTU202502274

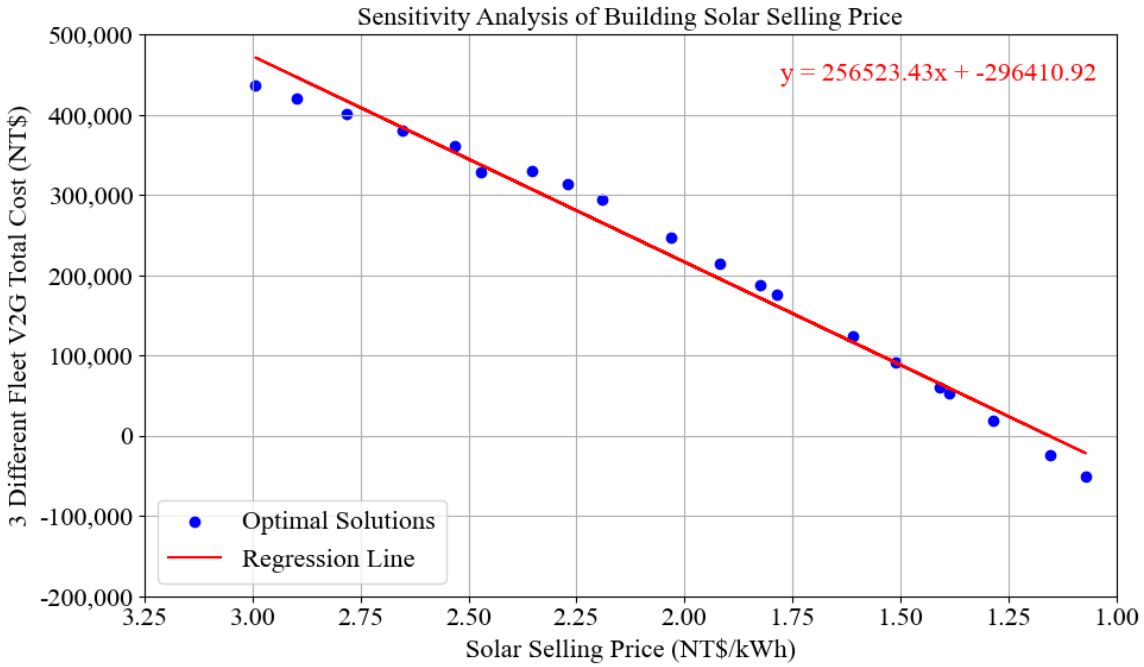

Figure 33 Building Solar Electricity Selling Price Sensitive Analysis

3.5.2 TOU Peak Price and Duration on V2G Operations Impact

Beyond adjusting the charging price, one of the most intuitive strategies to realize the "charging during the day, discharging at night" model is to increase the peak time discharging electricity price, thereby creating more room for V2G system profitability. Therefore, this study conducts a sensitive analysis on the discharging price of the V2G system.

In the baseline optimization scenario, the peak-time electricity price is set at NT$6.92 per kilowatt-hour (kWh), based on the 2024 time-of-use pricing scheme from Taipower's report. To define a reasonable analysis range, this study considers two distinct scenarios. First, based on electricity pricing data from 2025, countries such as the U.S. (both Texas and other states), British, Germany, report peak-time electricity prices averaging around NT$10/kWh according to each countries' electricity market and policy. Second, during previous energy crises such as natural gas shortages and extreme weather events the peak prices in several countries surged above NT$30/kWh. Anticipating future

doi:10.6342/NTU202502274

instability driven by geopolitical and climate-related factors, this study sets the upper limit of discharging prices at NT$30/kWh as shown in **Figure 34**.

When the TOU peak-time price is increased to NT$10/kWh, the optimized total operating cost in this study decreases from approximately NT$400,000 to NT$200,000, achieving a significant cost reduction of NT$200,000 which can reduce 42.7% of operation cost. This finding can be compared with the study by Moradipari, which analyzed a V1G electric bus fleet in California, showing a total operating cost reduction of 62.5% under optimized charging strategies [25].

Under extreme scenarios as high as NT$270/kWh due to supply shortages and privatized market dynamics. To simulate such critical conditions, this study analyzes the V2G system under a peak-time electricity price of NT$30/kWh. The results reveal that under this scenario, the optimized total operating cost drops to NT$910,000 which give us about 320.2% of operational cost reduction and indicating not only full cost recovery but also a substantial profit margin.

In addition to TOU peak price, peak price period is also what we concerned about. We started with 6 hours of peak time step, and increase it into 9 hours of peak time step as shown in Figure 35 which give us 17.2% of total operational cost reduction.

doi:10.6342/NTU202502274

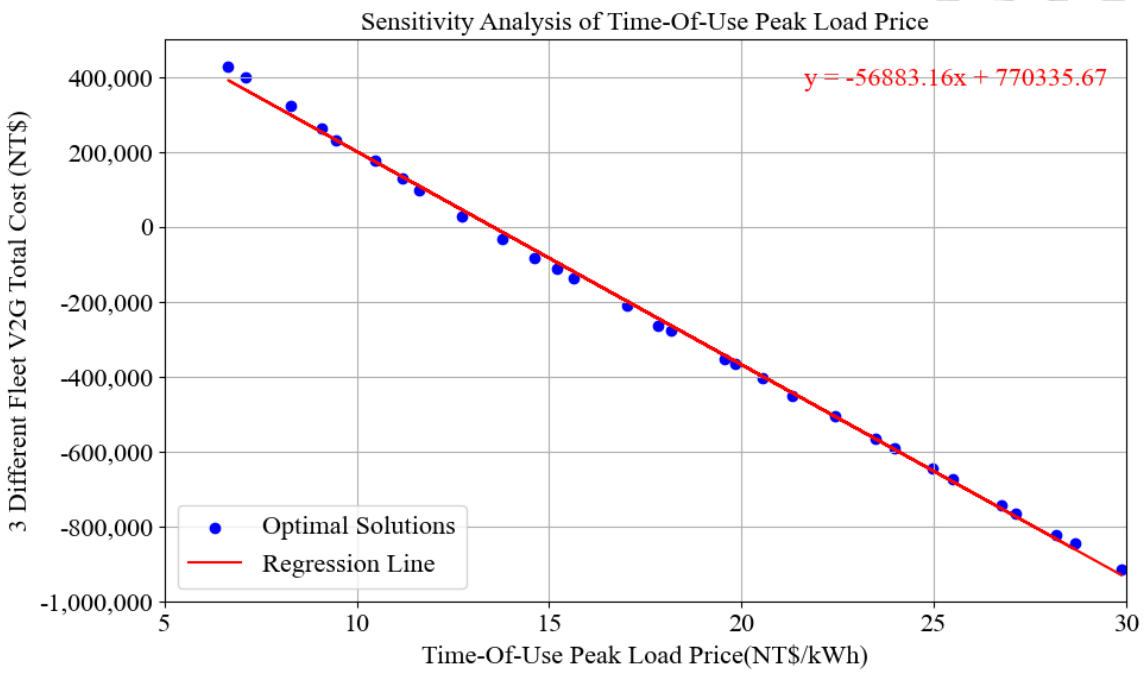

Figure 34 Time-Of-Use Peak Price Sensitive Analysis

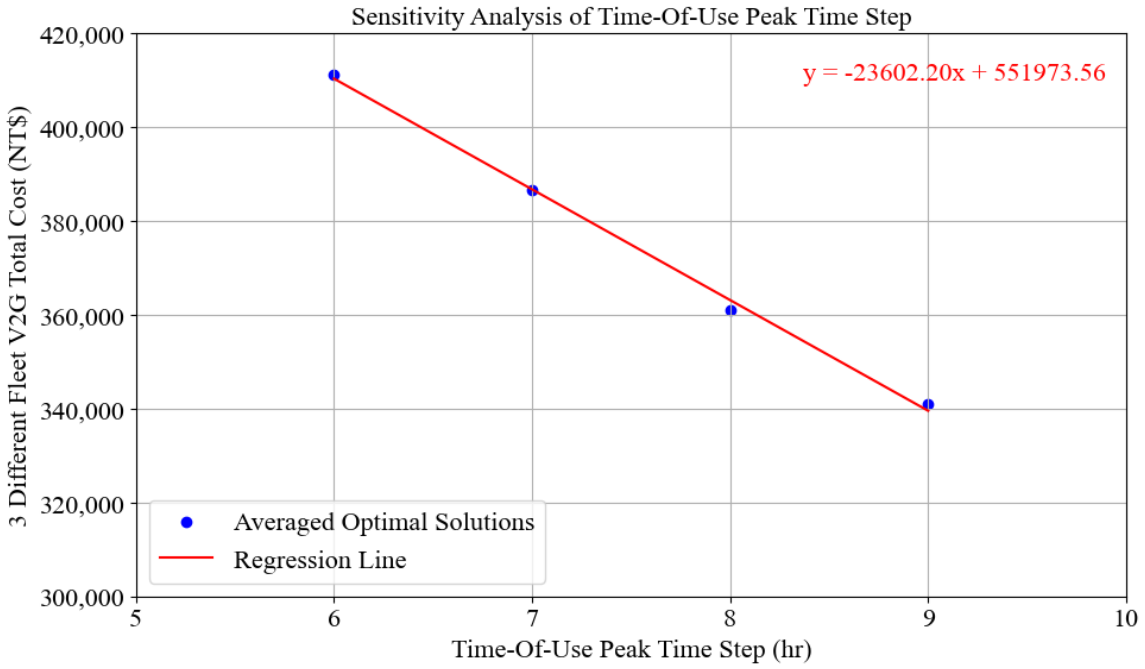

Figure 35 Time-Of-Use Peak Time Step Sensitive Analysis

doi:10.6342/NTU202502274

3.6 Comparative Results of Monopoly Sensitive Analysis

To sum up the V2G monopoly test with Latin Hyper Cube Sampling, we found out that there are several things we can analysis as shown as **Figure 36**. First, we can find out that policy-related parameter like TOU peak price and building solar electricity selling price are the most dominant parameter. Science-Oriented parameters shows it influence but not that effective. This table can give us a primal understanding about each parameter relation with V2G system.

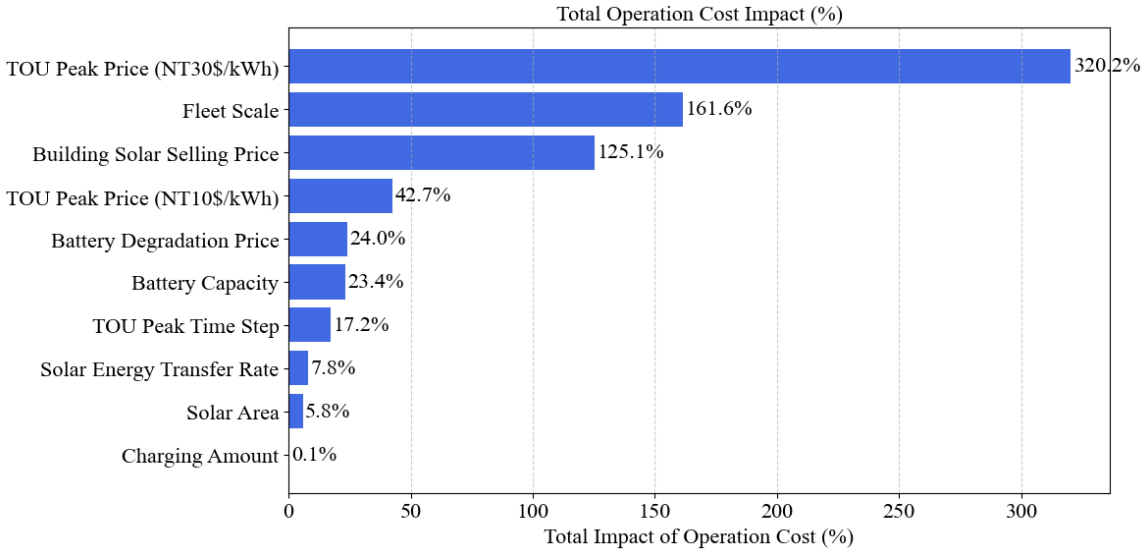

Figure 36 Total Operation Cost Impact of LHS Sampling Sensitive Analysis

3.7 Capital Investment Impact

In addition to previously discussed factors such as battery type, building solar energy generation, and TOU peak electricity pricing, one of the most direct ways to influence the return on investment is by reducing the system's initial capital expenditures. Lowering upfront costs has a significant impact on shortening the payback year and enhancing overall financial feasibility. First, we consider system sizing and deployment configuration.

doi:10.6342/NTU202502274

In this study, we adjusted the number of installed charging systems to assess its impact on the payback periods. First, we reconfigured the number of V2G charging systems at each site to 10 units at Songzhi Station, 5 units at Jiuzhuang Station, and 5 units at Wuxing Station. Compared to the original setup 44 systems at Songzhi, 39 at Jiuzhuang, and 27 at Wuxing, the reduced configuration significantly increased the total operating cost of the V2G system. Specifically, the optimized operating cost rose by NT$440,000, from the baseline NT$412,615 to approximately NT$855,597. Consequently, the net profit margin dropped from NT$234,383 in the baseline scenario to NT$56,604, resulting in a decrease of approximately NT$180,000. While reducing the number of charging systems effectively lowers capital expenditures, it also leads to a substantial reduction in potential operating savings from V2G participation. Based on the payback periods calculation shown in **Table 10**, the payback period under the reduced system configuration extends to 281 payback months (about 23 years), significantly longer than the baseline scenario.

Table 10 Capital Investment Sensitive Analysis Scenario 1

V2G SAVING	
V1G Scenario Cost	NT$912,301
V2G Scenario Cost	NT$855,697
Total per month saving with V2G	NT$56,604
V2G Capital Cost	
V2G Installed Capital Cost	NT$10,875,000
V2G Charging Pile Capital Cost	NT$3,375,000
V2G Installed O&M Cost	NT$4,531
V2G Charging Pile O&M Cost	NT$1,406
V2G ROI (months)	281.25

As shown in **Table 11**, the system configuration was set to 15 units at Songzhi Station, 8 units at Jiuzhuang Station, and 8 units at Wuxing Station. Under this configuration, the total optimized operating cost of the V2G system increased to

doi:10.6342/NTU202502274

approximately NT$670,000 which gave an increase of NT$260,000 compared to the baseline. The profit margin was consequently reduced from NT$234,383 (baseline) to NT$85,165, resulting in a loss of approximately NT$150,000 in profit. However, compared to the more conservative setup of 10, 5, and 5 systems at the respective stations, this configuration improved profitability by about NT$30,000. Despite the improved operating margin, the increased capital expenditure associated with installing more systems led to a slightly longer payback periods. As shown in **Table 11**, the payback period rose from 281 months to 254 months.

Table 11 Capital Investment Sensitive Analysis Scenario 2

V2G SAVING	
V1G Scenario Cost	NT$756,999
V2G Scenario Cost	NT$671,834
Total per month saving with V2G	NT$85,165
V2G Capital Cost	
V2G Installed Capital Cost	NT$16,530,000
V2G Charging Pile Capital Cost	NT$5,130,000
V2G Installed O&M Cost	NT$13,775
V2G Charging Pile O&M Cost	NT$4,275
V2G ROI (months)	254.54

In **Table 12**, we examine another configuration by increasing the number of V2G charging systems to 20 units at Songzhi Station, 10 units at Jiuzhuang Station, and 10 units at Wuxing Station, to evaluate its impact on the payback periods. Under this configuration, the baseline total operating cost of the V2G system increases by approximately NT$180,000, reaching NT$590,000. Despite the higher system cost, the profit margin improves significantly compared to the previous case (15, 8, and 8 systems), increasing from NT$85,165 to NT$201,061. This value approaches the baseline optimization result as NT$234,383, indicating that this configuration recovers much of

doi:10.6342/NTU202502274

the economic benefit while keeping the system investment relatively close to the original. As a result, the payback periods is reduced to 160.73 months, or approximately 13 years.

Table 12 Capital Investment Sensitive Analysis Scenario 3

V2G SAVING	
V1G Scenario Cost	NT$793,084
V2G Scenario Cost	NT$592,023
Total per month saving with V2G	NT$201,061
V2G Capital Cost	
V2G Installed Capital Cost	NT$21,750,000
V2G Charging Pile Capital Cost	NT$6,750,000
V2G Installed O&M Cost	NT$18,125
V2G Charging Pile O&M Cost	NT$5,625
V2G ROI (months)	160.73

Continuing the adjustment of the number of V2G charging systems, this scenario sets the configuration to 25 units at Songzhi Station, 25 units at Jiuzhuang Station, and 13 units at Wuxing Station to examine the resulting changes in Return on Investment. The analysis shows that the profit margin does not increase under this configuration. However, due to the continued rise in capital expenditures, the payback periods gradually declines, reaching 218 months equivalent to 18 payback years as shown in **Table 13**.

Table 13 Capital Investment Sensitive Analysis Scenario 4

V2G SAVING	
V1G Scenario Cost	NT$697,741
V2G Scenario Cost	NT$502,845
Total per month saving with V2G	NT$194,896
V2G Capital Cost	
V2G Installed Capital Cost	NT$27,405,000
V2G Charging Pile Capital Cost	NT$8,505,000
V2G Installed O&M Cost	NT$22,838
V2G Charging Pile O&M Cost	NT$7,088
V2G ROI (months)	217.67

doi:10.6342/NTU202502274

Based on the comparison of charging system quantities and their corresponding payback years, summarized in the **Figure 37**, this study finds that payback periods follows a quadratic trend as the total number of charging systems increases suggesting the existence of an optimal number of charging units. This outcome can be attributed to the limited number of electric buses in operation. When the number of charging stations exceeds a certain threshold, the utilization rate of charging piles decreases, diminishing their overall value. Conversely, when the number of systems is too low, the V2G system cannot fully leverage electricity price fluctuations to discharge and resell energy, thus missing out on potential revenue. This study estimates that the optimal number of charging systems is approximately 36% of the total electric bus fleet, where the capital investment and the economic return from V2G operations are most effectively balanced.

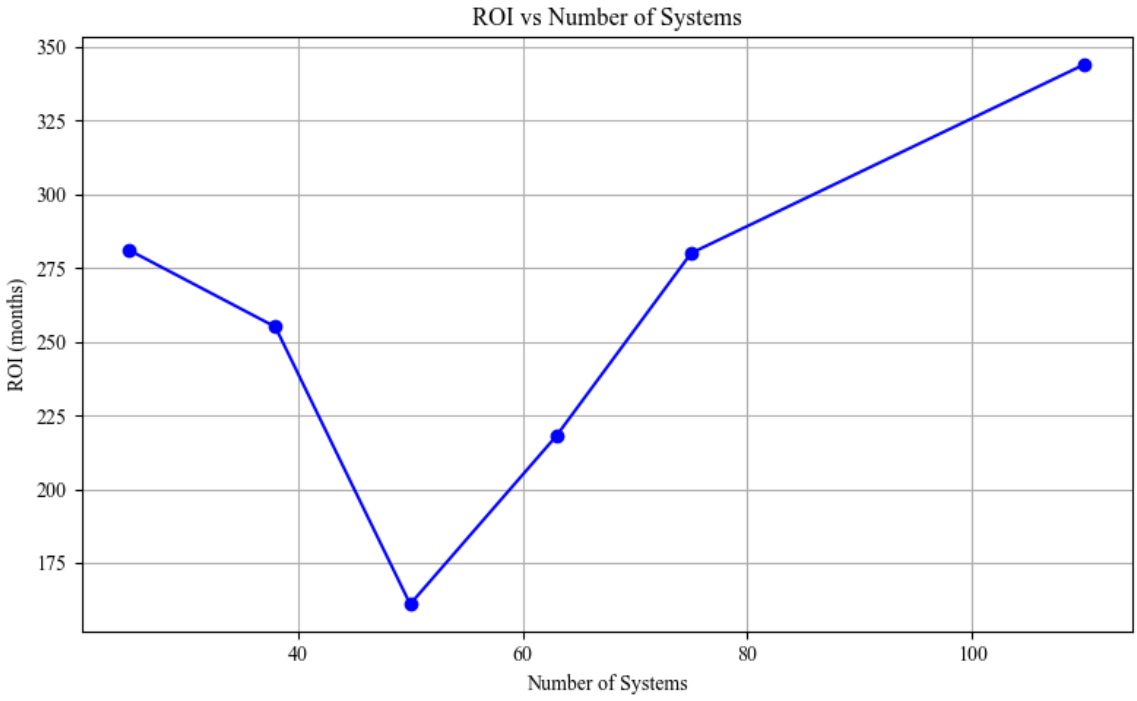

Figure 37 Payback Years considered with Installation Capital Investment

doi:10.6342/NTU202502274

3.8 Multi-Parameter Sensitive Analysis of Interacting V2G Factors

This chapter will explore the trends and related conclusions from the one-dimensional sensitive analysis using a multi-parameter approach, aiming to provide further constructive recommendations for the electric bus system. Based on the one-dimensional LHS sensitive analyses, the time-of-use electricity pricing parameter emerged as the most sensitive. Therefore, this study will first focus on the time-of-use pricing parameter and pair it with other sensitive parameters to explore the global impact of time-of-use pricing.

Next, a multi-parameter sensitive analysis will be conducted using parameters other than the time-of-use pricing to discuss the sensitive levels of various parameters in a global context. By using methods like iteration, the study will define the degree of influence of each parameter, providing valuable insights for future electric bus V2G system planning.

3.8.1 Interaction Analysis between TOU Peak Pricing and Battery Parameters

In this second-order sensitive analysis, regardless of whether the peak time-of-use electricity price is set at NT$30/kWh or NT$10/kWh, the interaction effects between the peak pricing parameter and the battery degradation cost, as well as between the peak pricing and battery capacity, remain minimal, as shown in **Figure 38** and **Figure 39**. In contrast, a slight interaction is observed between the battery degradation cost and battery capacity in the second-order Sobol indices under the three-parameter setting when the maximum of time-of-use price is NT$30/kWh.

doi:10.6342/NTU202502274

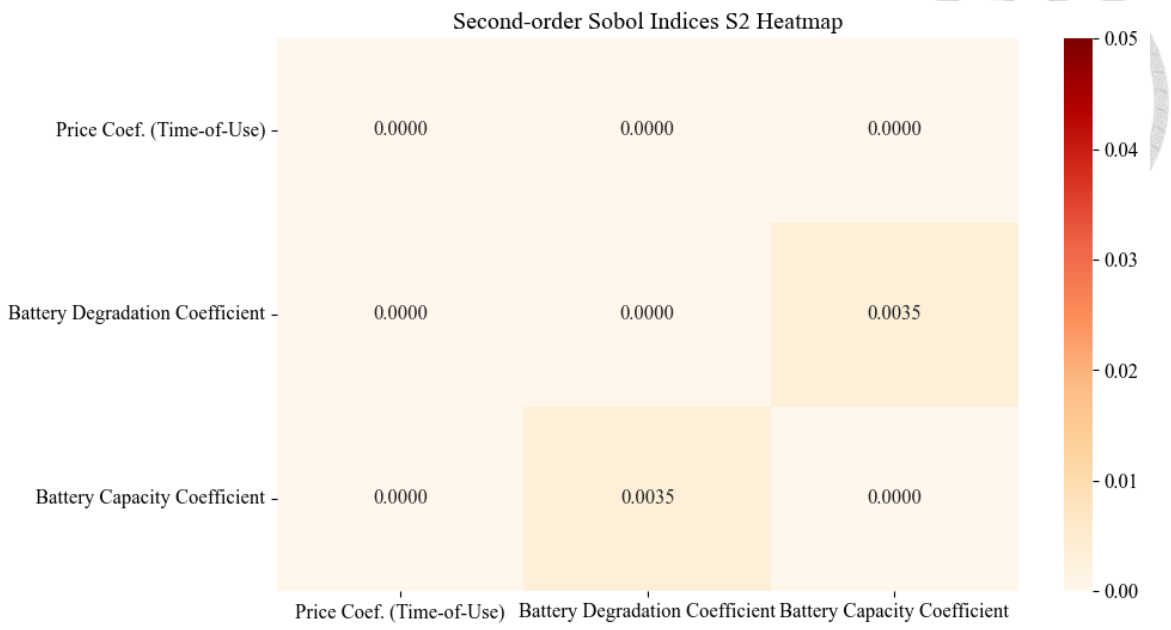

Figure 38 Time-of-use price max in NT$30/kWh with Battery Related Parameter Second-order Heatmap

Figure 39 Time-of-use price max in NT$10/kWh with Battery Related Parameter Second-order Heatmap

doi:10.6342/NTU202502274

By summing the first-order and second-order sensitive results, we obtain the total sensitive indices. The analysis reveals that the time-of-use peak pricing parameter exerts the most influence on the model, followed by the battery degradation cost and then the battery capacity showed as **Figure 40** and **Figure 41**. Due to the insignificance of the second-order effects, this parameter combination exhibits characteristics of an "additive model", where the time-of-use pricing parameter serves as the dominant driver. This phenomenon, commonly referred to as the "showing effect" in sensitive analysis, indicates that the model output variance is primarily governed by a single input parameter, with minimal contribution from interactions. We can also see this dominant situation if we put battery degradation parameter and TOU peak price into LHS sampling with two dimension to give us a 3D graphing in **Figure 42**.

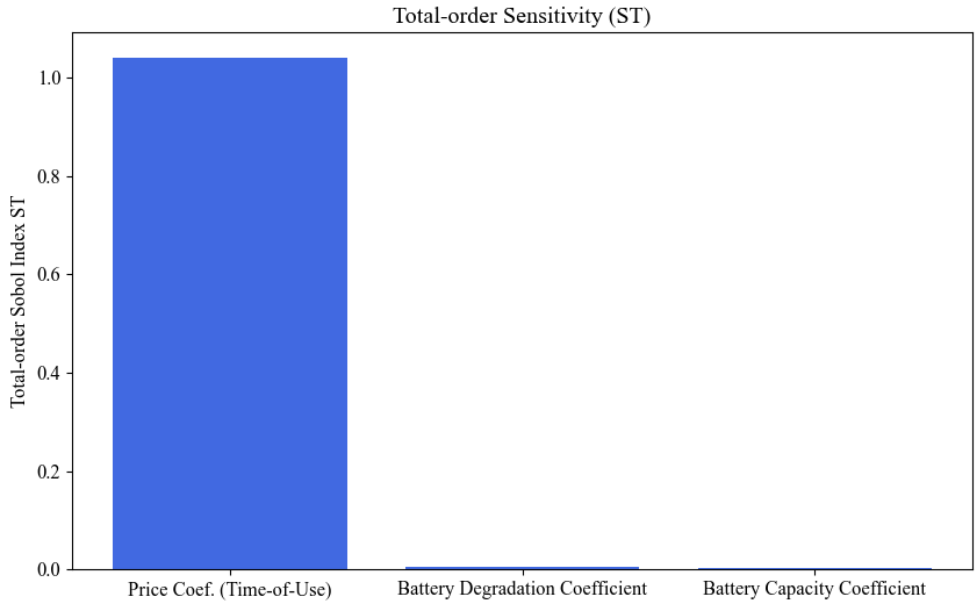

Figure 40 Time-of-use price max in NT$30/kWh with Battery Related Parameter Total Sensitive Analysis Bar chart

doi:10.6342/NTU202502274

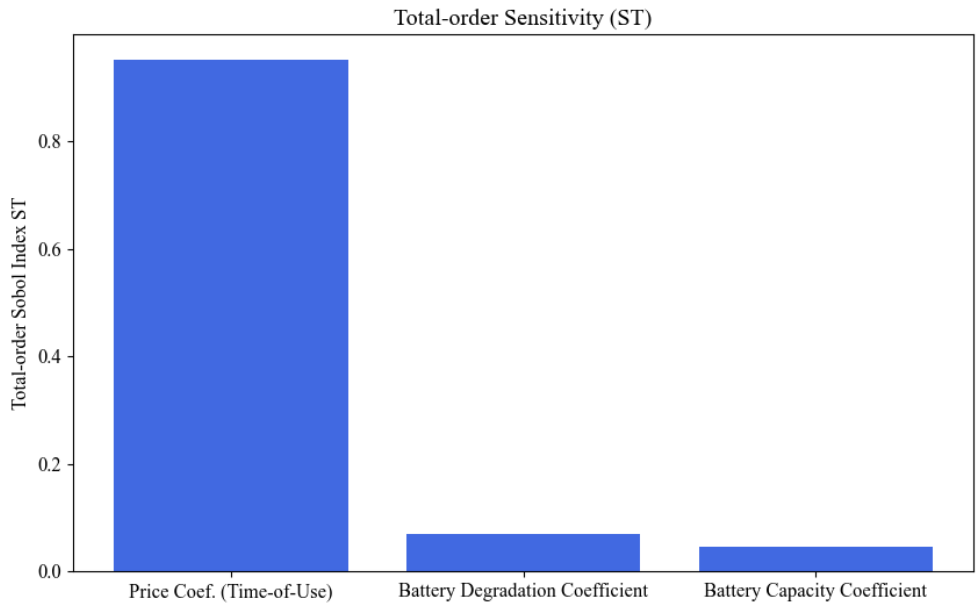

Figure 41 Time-of-use price max in NT$10/kWh with Battery Related Parameter Total Sensitive Analysis Bar chart

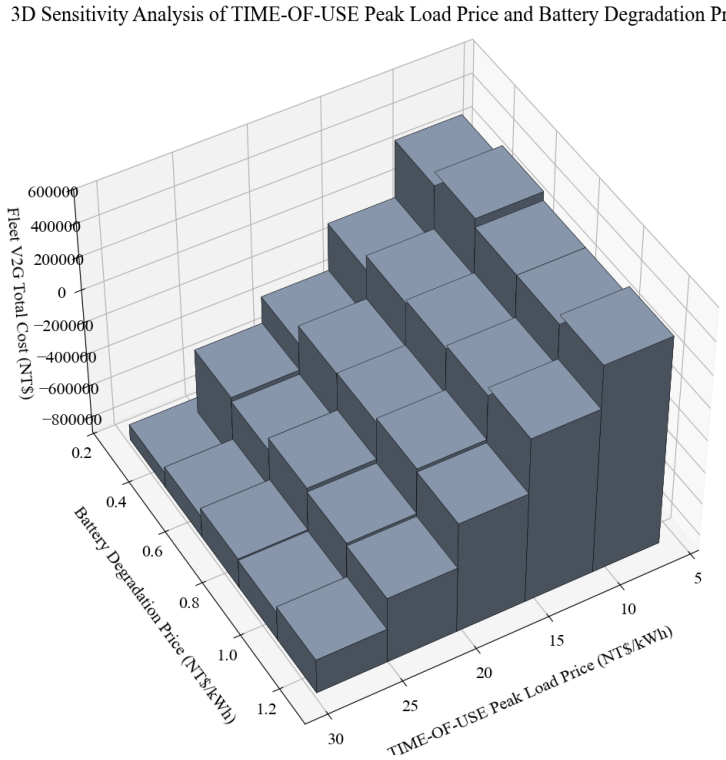

Figure 42 3D LHS Sampling Sensitive Analysis in Battery Degradation Prices and TOU peak prices

doi:10.6342/NTU202502274

3.8.2 Interaction Analysis between TOU Peak Pricing and Solar Energy Parameters

Similar to previous sections, in the three-parameter sensitive analysis involving time-of-use pricing and battery-related parameters, the peak electricity price coefficient remains the dominant factor when set at its maximum value of NT$30/kWh. Under this setting, the building solar electricity selling price coefficient shows greater global sensitive than the solar conversion rate, indicating its more critical role in the system's response as shown in **Figure 45**. In the second-order Sobol sensitive analysis, the interaction effect (S2) between the time-of-use peak price and the building solar electricity selling price is 0.0114, suggesting a weak relationship. Meanwhile, the S2 value between the building solar electricity selling price and the solar conversion rate is 0.0324, which is the most prominent interaction in this analysis, indicating relatively higher joint sensitive as shown in **Figure 43**.

When the peak electricity price is reduced to NT$10/kWh, its influence on the system decreases. As a result, the building solar electricity selling price coefficient accounts for a larger share in the total sensitive index (ST), and its interaction with the solar conversion rate becomes more significant like **Figure 44**. This reflects the increased explanatory power of this parameter pair under such conditions. Considering the total Sobol indices (ST), the building solar electricity selling price shows a higher total sensitive than the peak electricity price, making it the second most influential factor as shown in **Figure 46**. Notably, both parameters are policy-adjustable, suggesting that future policy interventions aiming to improve system performance should prioritize adjustments to building solar electricity selling prices and peak electricity pricing.

doi:10.6342/NTU202502274

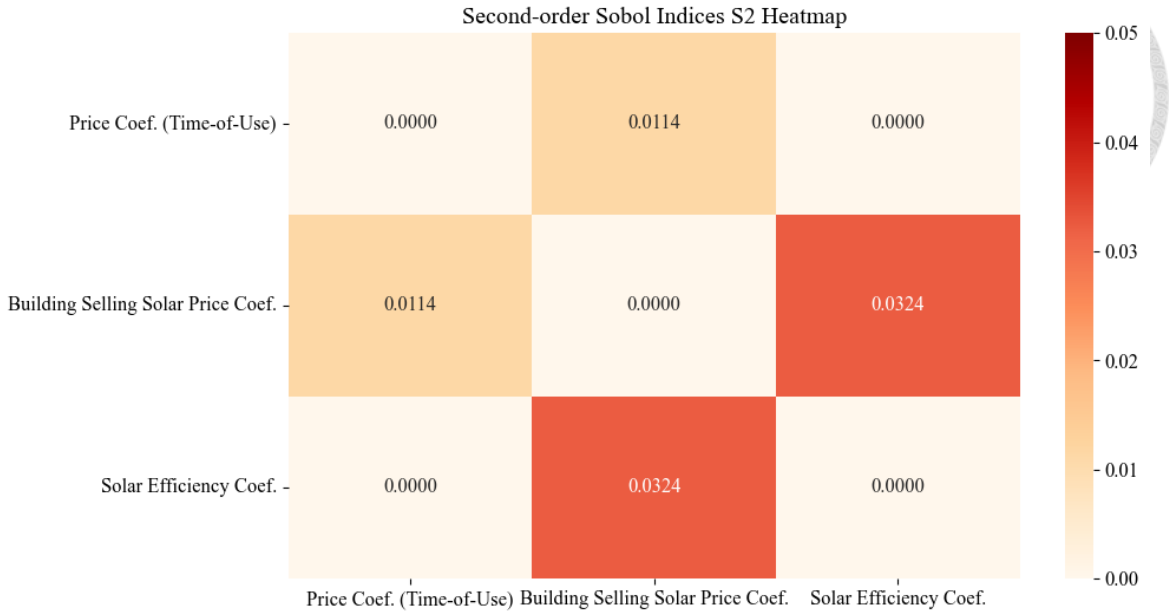

Figure 43 Time-of-use price max in NT$30/kWh with Solar Energy Related Parameter Second-order Heatmap

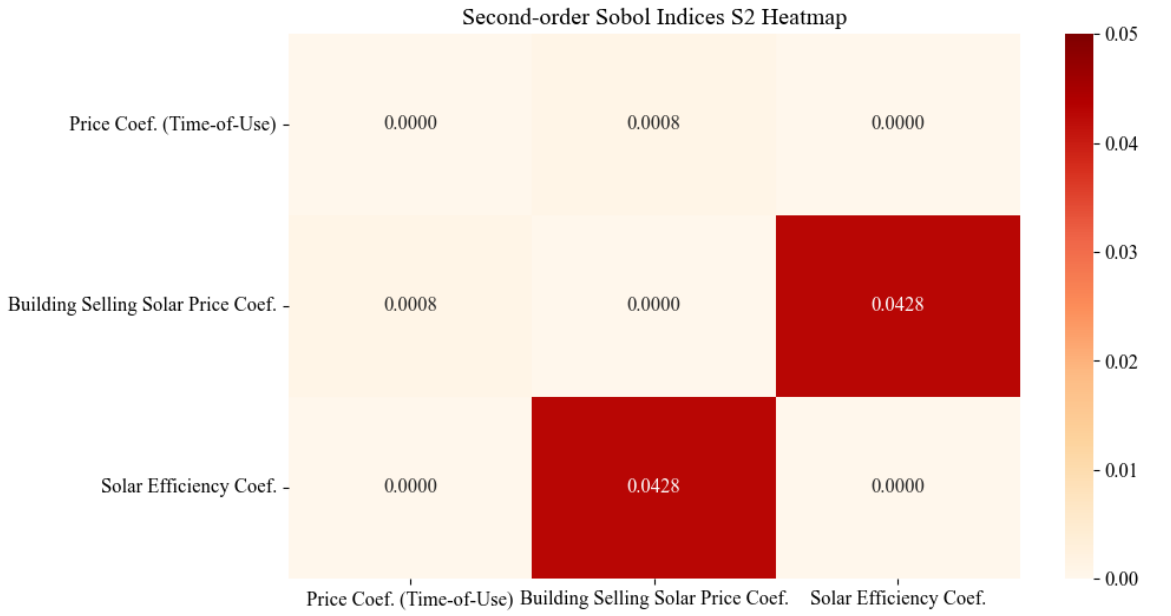

Figure 44 Time-of-use price max in NT10/kWh with Solar Energy Related Parameter Second-order Heatmap

doi:10.6342/NTU202502274

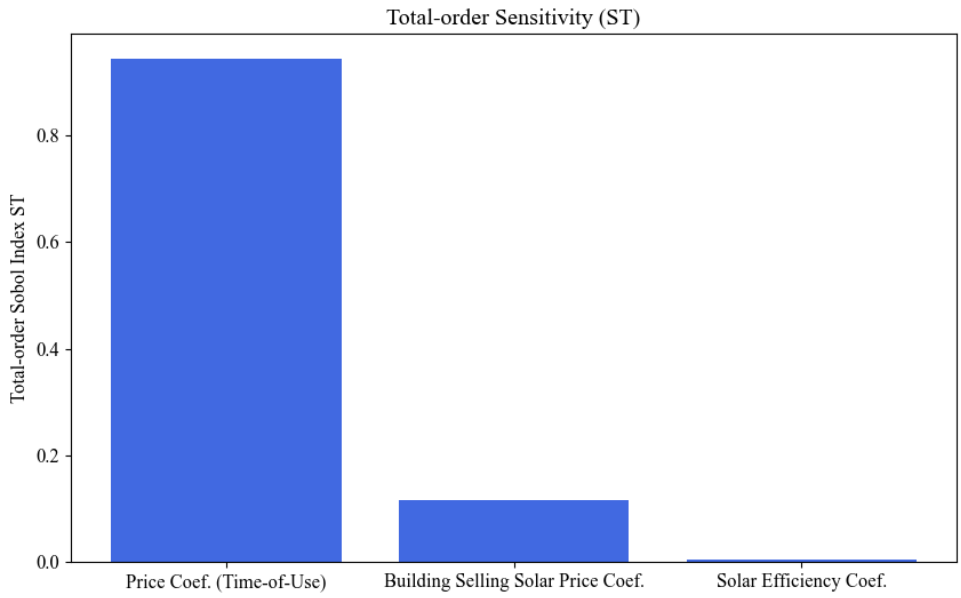

Figure 45 Time-of-use price max in NT$30/kWh with Solar Energy Related Parameter Total Sensitive Analysis Bar chart

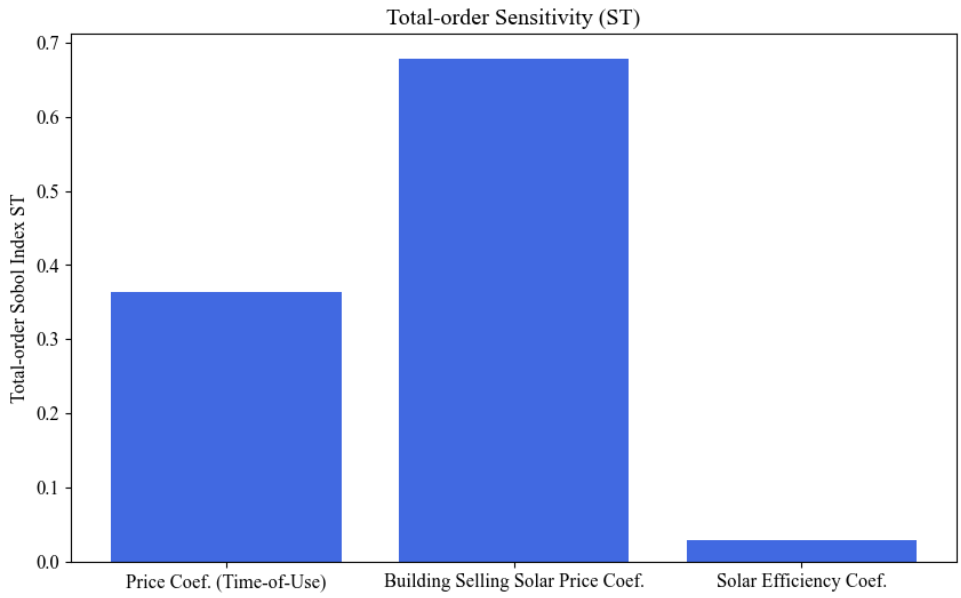

Figure 46 Time-of-use price max in NT$10/kWh with Solar Energy Related Parameter Total Sensitive Analysis Bar chart

doi:10.6342/NTU202502274

3.8.3 Interaction Analysis between Battery and Solar Energy Parameter

In this section, we've eliminated TOU peak price parameter, and found out that the Building Selling Solar Price Coefficient emerged as a new dominant coefficient according to the SoBoL analysis as shown in **Figure 47**.

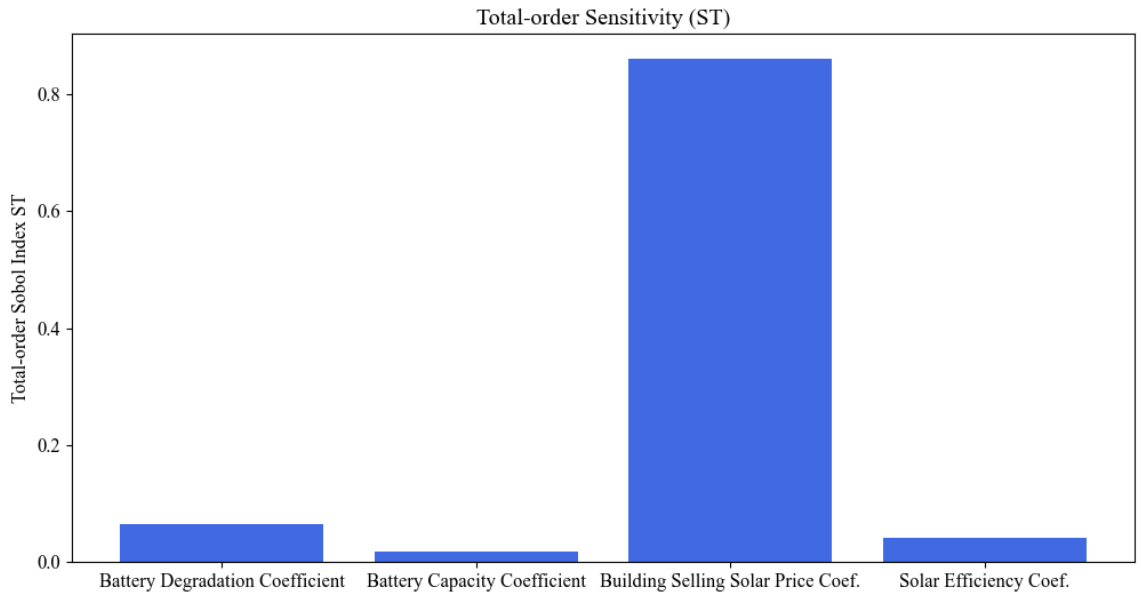

Figure 47 Battery and Solar Energy Related Parameter

Total Sensitive Analysis Bar Chart

Additionally, in the second-order SoBoL sensitive index, after removing the influence of the TOU peak price parameter, the Battery Degradation Coefficient exhibited interaction effects with other parameters. The relationship between the Building Solar Price Coefficient and the Solar Conversion Efficiency also maintained a certain level of interaction, consistent with the previous analysis. The Battery Degradation Coefficient is the most likely to cause second-order effects on other parameters as shown in **Figure 48**.

doi:10.6342/NTU202502274

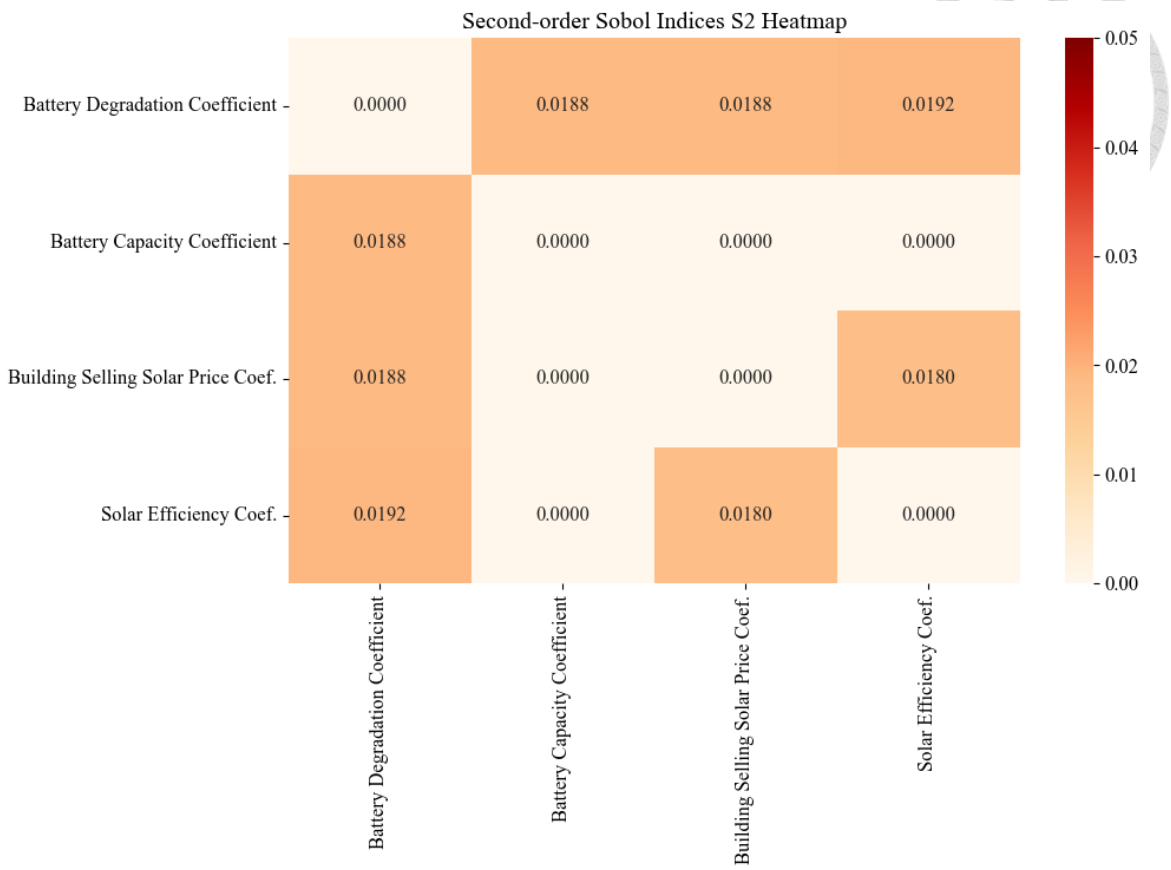

Figure 48 Time-of-use price max in NT$30/kWh with Solar Energy Related Parameter Second-order Heatmap

In order to compared the dominant parameter and its influence on the operational cost, we've tried to utilize the energy and solar related parameter to found out the sequence of the dominant total sensitive indices. What we did is we eliminate the dominant parameter step by step, to gradually give the result. And we found out the dominant sequence from **Figure 49** and **Figure 50** that the parameters are ranked as follows: TOU peak price > Building Selling Solar Price Coefficient > Solar Conversion Efficiency = Battery Degradation > Battery Capacity by different combination . Among this sequence, the solar efficiency coefficient and Battery Degradation efficiency showed it complex result with the background data in the SoBoL analysis.

doi:10.6342/NTU202502274

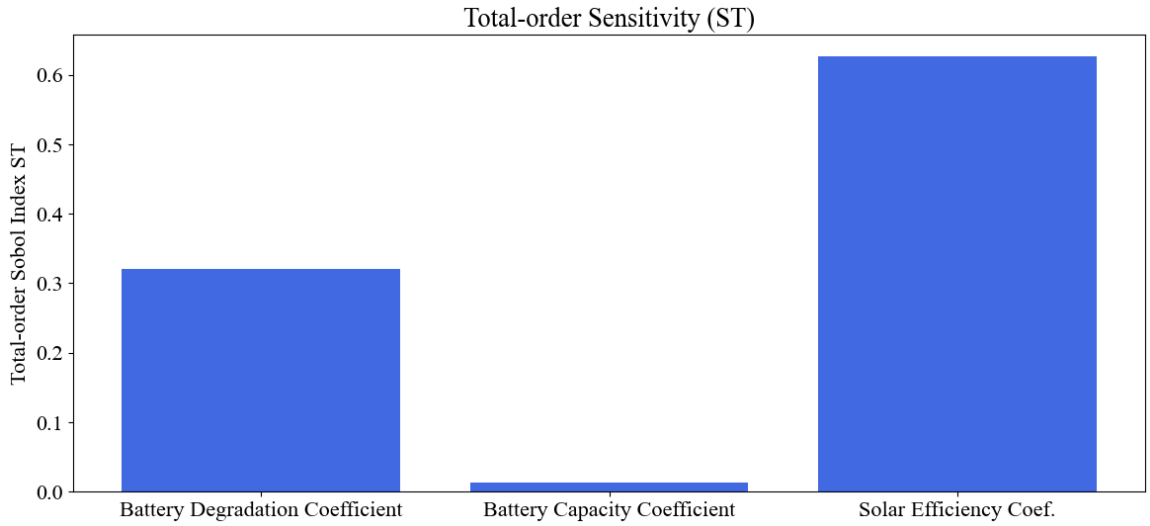

Figure 49 Battery and Solar Energy Related Parameter Total Sensitive Analysis Bar Chart Eliminate Building Solar Electricity Selling Price Coef.

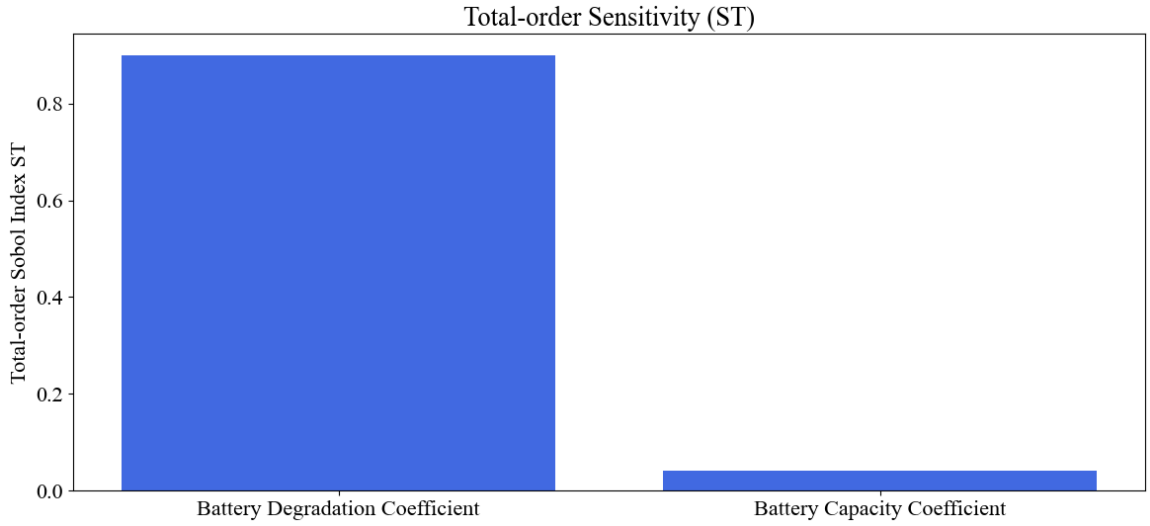

Figure 50 Battery and Solar Energy Related Parameter Total Sensitive Analysis Bar Chart Eliminate Building Solar Electricity Selling Price and Solar Efficiency Coef.

doi:10.6342/NTU202502274

3.8.4 Interaction Analysis of Battery, Solar, and Fleet Scale and Charging Power Parameters

Aside from battery and solar energy-related parameters, this study also incorporates utility-related parameters into the Sobol sensitive analysis, expanding the scope to five parameters as shown in **Figure 51**. The heatmap reveals that the battery degradation price coefficient and solar efficiency coefficient exhibit dominant second-order interactions with other parameters. This aligns with observations made in the earlier Latin Hypercube Sampling (LHS) sensitive analysis, where battery capacity was found to interact with maximum charging power. However, the influence of this interaction remains relatively limited and does not significantly alter the global sensitive ranking of the maximum charging power parameter. From **Figure 52**, it is evident that the charging maximum power consistently holds the lowest sensitive index among all parameters in the global sensitive analysis. Additionally, the ranking of battery and solar energy-related parameters remains unchanged, confirming their dominant influence in the system across different configurations.

doi:10.6342/NTU202502274

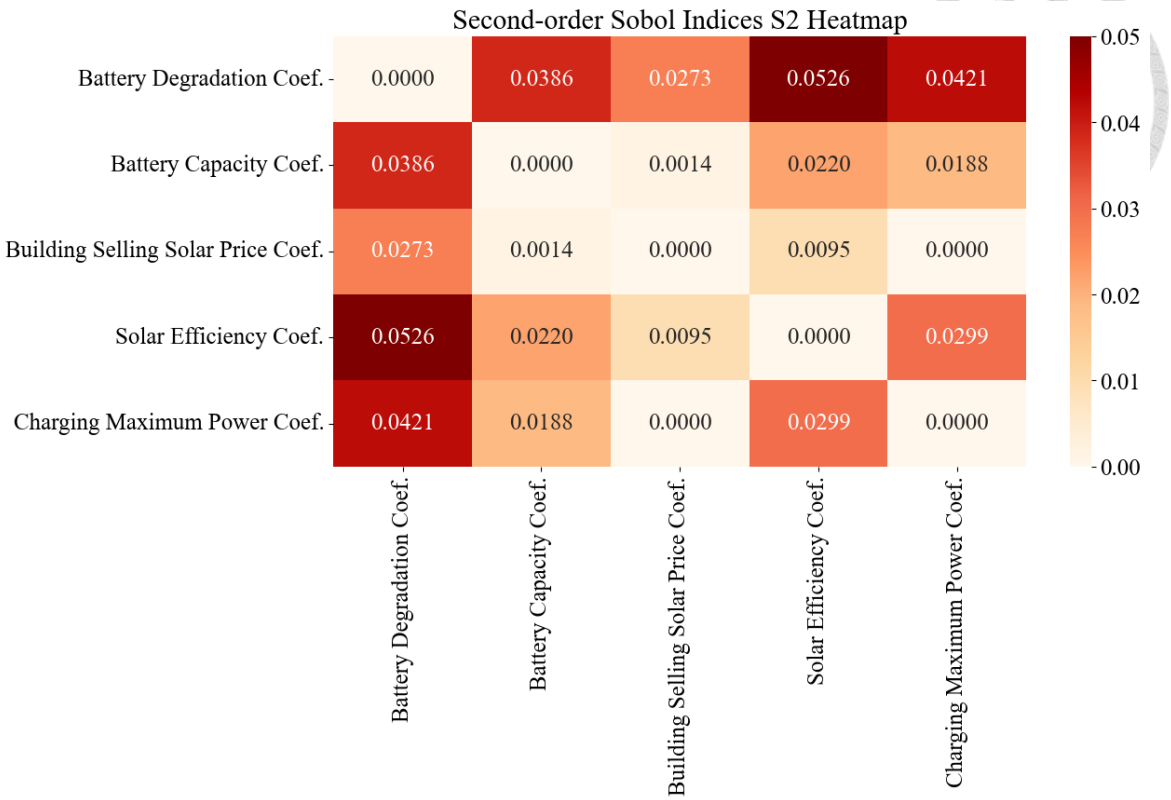

Figure 51 Battery, Solar Energy and Utility Related Parameter Second-order Heatmap

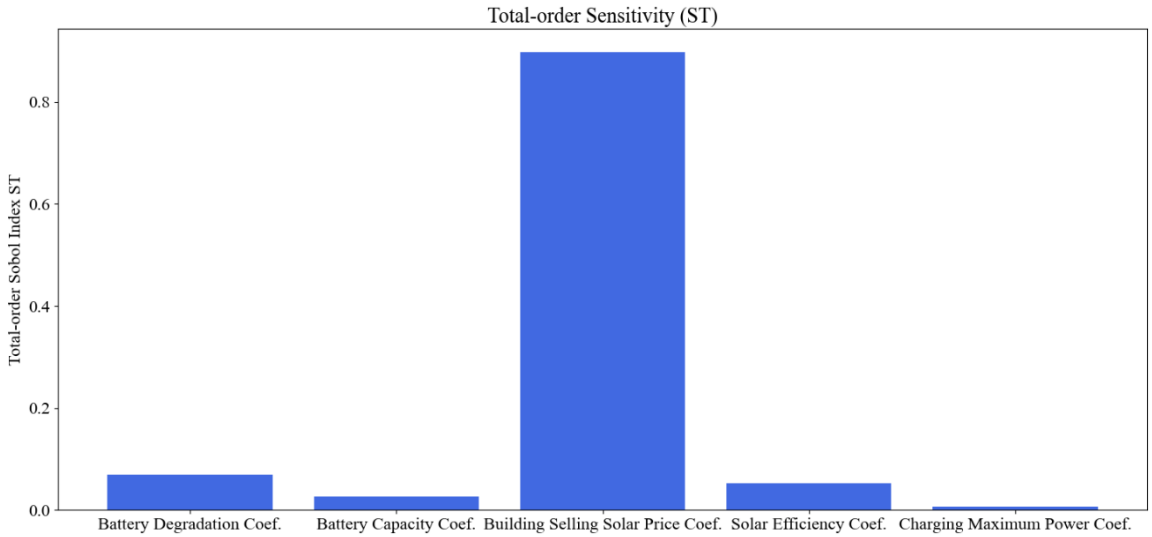

Figure 52 Battery, Solar Energy and Utility Related Parameter Bar Chart

doi:10.6342/NTU202502274

3.8.5 Interaction Analysis of Battery, Solar Energy and Fleet Scale Parameters

From the **Figure 53**, we observe that when the fleet scale parameter is included in the Sobol analysis, several sensitive indices decrease in significance. However, the interaction between the fleet scale coefficient and the building solar electricity selling price coefficient becomes prominent, suggesting that as the fleet size expands, the building solar electricity selling price emerges as the most influential second-order factor. We also did a total sensitive analysis with this coefficient in **Figure 54**, fleet scale coefficient shows it dominant within this combination. We also try to compared it with following experiment with time-of-use prices.

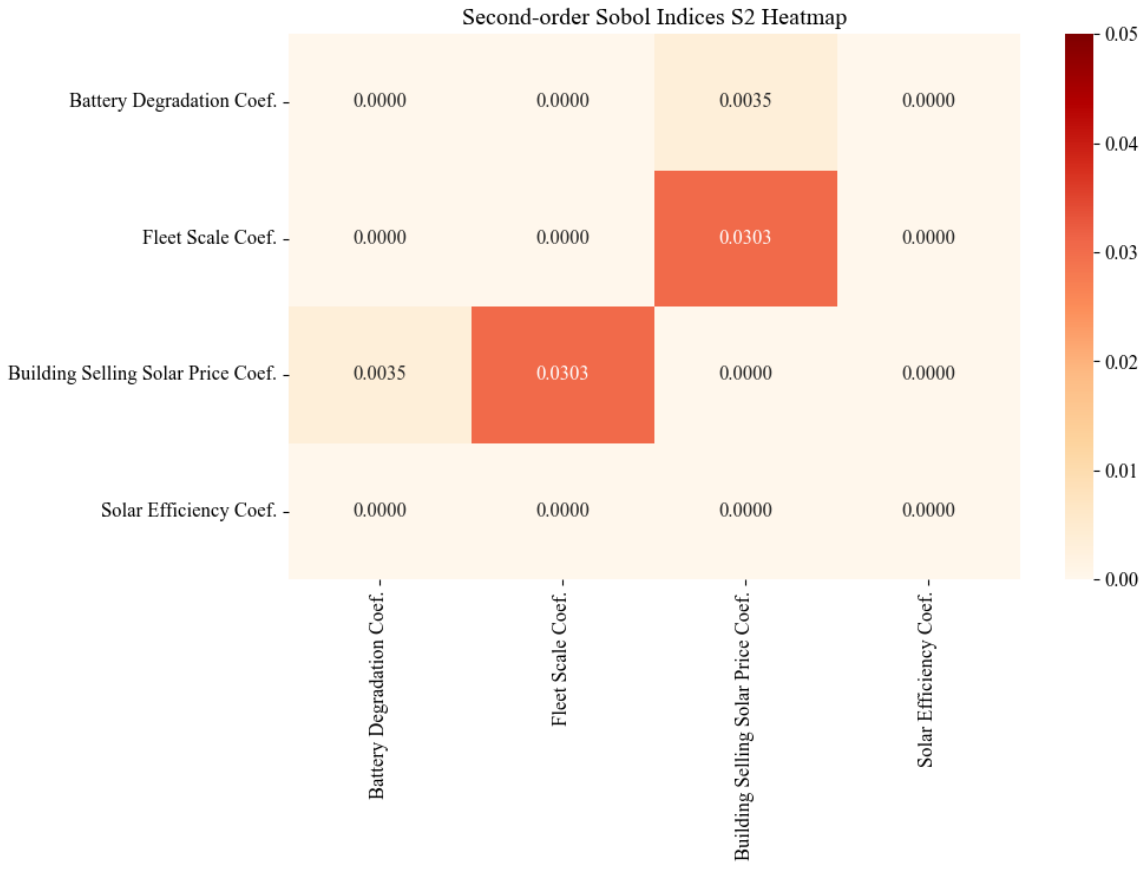

Figure 53 Battery, Solar Energy and Fleet Scale Related Parameter Second-order Heatmap

doi:10.6342/NTU202502274

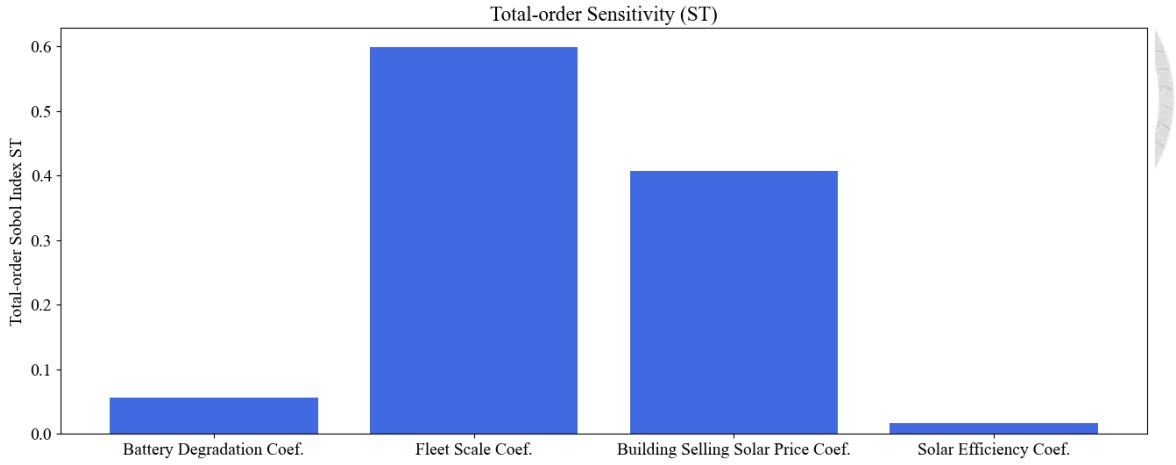

Figure 54 Battery, Solar Energy and Fleet Scale Related Parameter Bar Chart

Proceed with the previous knowledge, we conduct the Sobol analysis with TOU peak price, Fleet Scale and Building Selling Solar Price Coefficient in the following research. First, in second-order interaction fleet scale continued its interaction with fleet scale shown as **Figure 55**.

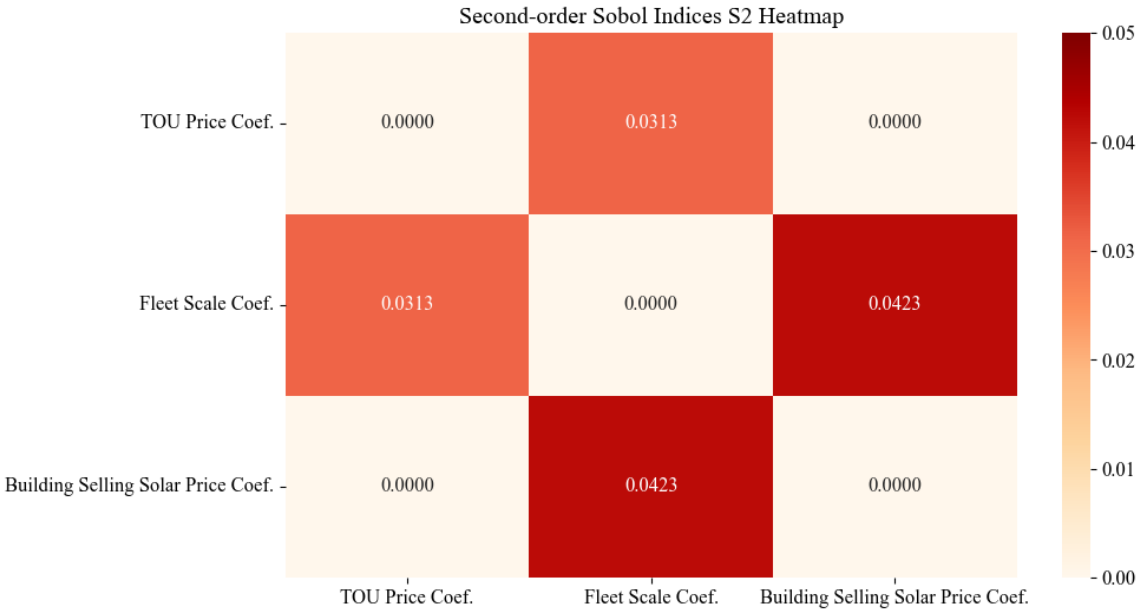

Figure 55 Policy-Orientated and Fleet Scale Related Parameter Second-order Heatmap

doi:10.6342/NTU202502274

This total sensitive analysis demonstrated the previous understanding, in this combination it is in the order of fleet scale, building solar electricity selling price and TOU peak price coefficient.

Based on our earlier study, we set the highest TOU peak price at NT$30/kWh. We saw a clear rise in the second-order effect between fleet size and TOU peak price, which supports the past finding that policy-related factors interact strongly with fleet size as shown in **Figure 57**. In this case, the building solar electricity selling price of electricity only went down a little.

In **Figure 58** we found out that the result has changed from **Figure 56**, when the TOU prices goes to NT$30/kWh as maximum then the sequence of each parameter has change which means the define of TOU peak price can lead to different background for V2G urban operation.

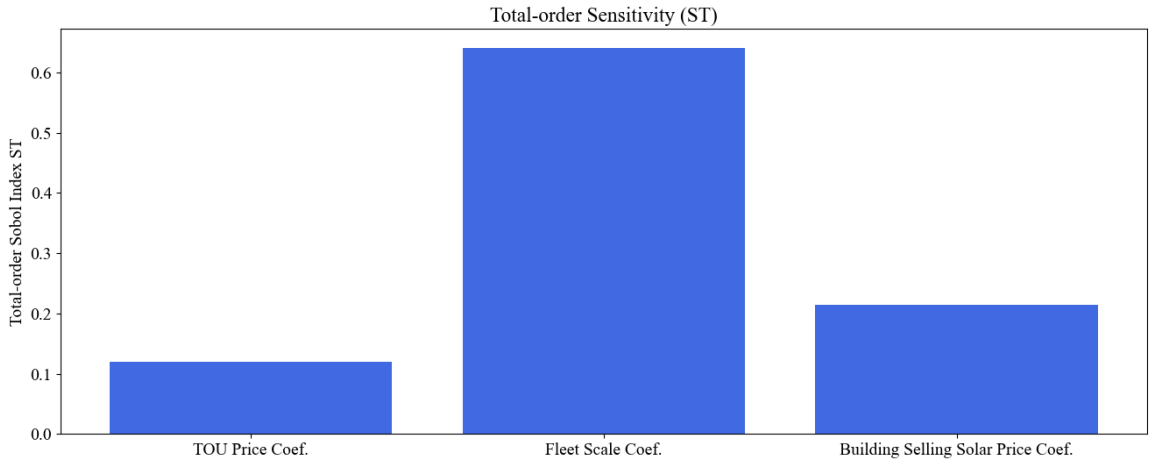

Figure 56 Policy-Orientated and Fleet Scale Related Parameter Bar Chart

doi:10.6342/NTU202502274

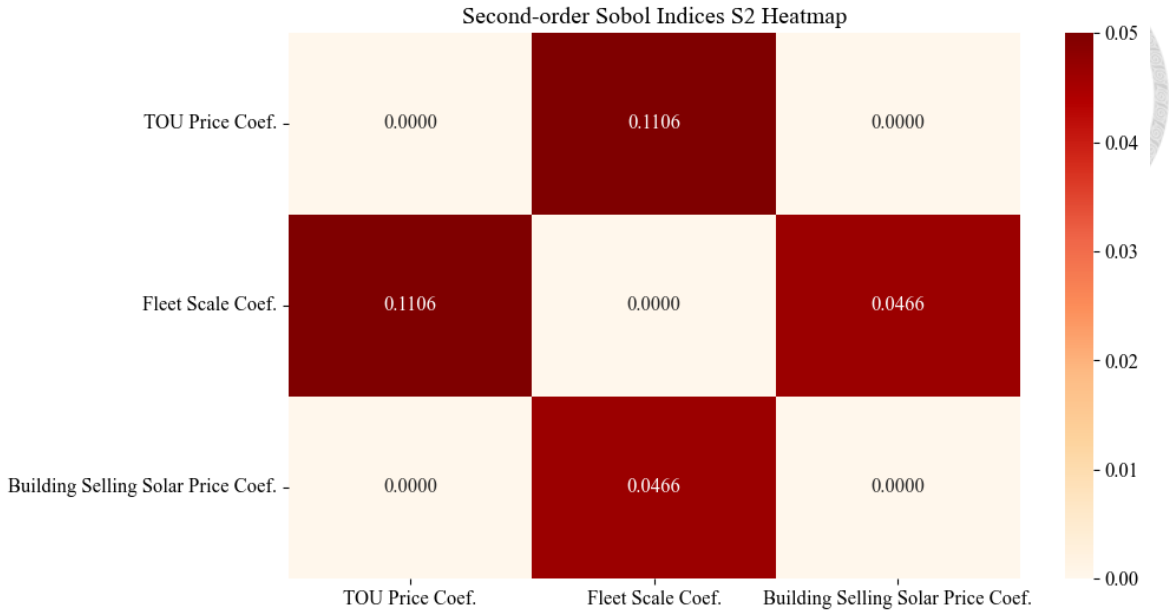

Figure 57 Policy-Orientated and Fleet Scale Related Parameter Second-order Heatmap when TOU peak prices set in NT$30/kWh

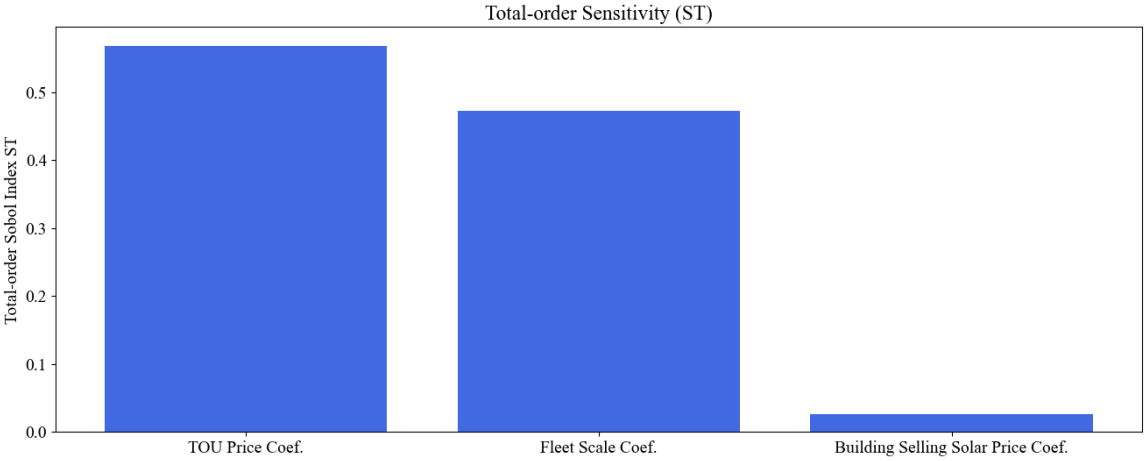

Figure 58 Policy-Orientated and Fleet Scale Related Parameter Bar Chart when TOU peak prices set in NT$30/kWh

3.9 Depot Design Discussion

In this research we survey 3 different depots with its' associate school rooftop as its renewable resource. In order to V2G discharging revenue. We found that in general when redundance goes up it will lead to higher V2G amount as **Table 14**. However, the actual solar charging amount associate to bus depot behavior, if most of bus are occupy when solar energy has redundance will lead to lower utilization of building redundance energy.

doi:10.6342/NTU202502274

Table 14 Depot Design Comparison

	Building Solar Energy Amount (kWh/bus)	Solar Charging Amount (kWh/bus)	V2G Discharging Amount (kWh/bus)
Songzhi Depot	5,951	1,178	955
Jiuzhuang Depot	1,315	751	781
Wuxing Depot	3,982	1,603	1,052

Moreover, a higher operational demand for bus routes increases the need for solar energy, even when the battery discharging capacity is nearly saturated. Based on this understanding, we estimate the optimal integration of rooftop solar resources and bus depot operations under various scenarios. For instance, in locations such as JiuZhuang Station, where available rooftop solar energy is relatively limited, the system tends to rely more heavily on city power to support V2G operations. Conversely, in areas with greater solar potential, the focus shifts toward optimizing charging and discharging behavior to effectively manage the surplus energy.

To expand this concept across other bus depots in Taipei City, the availability of nearby surplus solar energy plays a critical role in the effectiveness of a V2G system. While some depots benefit from adjacent public school's rooftops, others lack such opportunity. For instance, the Xinxin Bus Zhongxing Depot, located in a suburban area of Taipei, serves as a major bus charging facility. As shown in **Figure 59**, it is situated next to abandoned Taipei steel plant with large rooftop areas. Although these rooftops offer solar potential, they involve more complicated coordination due to private ownership and the diversity of stakeholders which is different from the relatively straightforward use of publicly owned school buildings. In contrast, urban depots surrounded by dense residential neighborhoods often lack accessible public rooftops altogether. In such cases, the absence of public building infrastructure such as schools or government facilities means that solar energy must be sourced from privately-owned residential buildings. This leads to even higher fragmented ownership and makes revenue

doi:10.6342/NTU202502274

sharing and infrastructure coordination more complex, posing a significant barrier to V2G deployment in these urban contexts.

Figure 59 Charging Allocation with Electric Buses in Xinxin Bus Zhongxing Depot

3.10 Discussion Summary

These findings not only validate the effectiveness of the proposed model but also offer actionable insights for policymakers and transit operators. First, policy-related parameters emerge as the most influential factors in both primary and advanced sensitive analyses. Unlike previous studies in the literature review, our analysis identifies the solar conversion efficiency as a critical physical parameter with long-term influence. While it may not be the most dominant factor initially, its impact becomes increasingly significant under varying parameter conditions, ultimately exerting a strong influence on the system's outcomes.

doi:10.6342/NTU202502274

We conduct second-order interaction with sobol analysis. Battery degradation prices parameter shows notable second-order interactions in the Sobol sensitive analysis. Meanwhile, solar conversion efficiency interacts significantly with building solar electricity selling price, underscoring the need to co-optimize both policy and technical variables to maximize system-level benefits. The building electricity selling price and TOU peak price shows its significant second interaction with fleet scale as well. Fleet-scaled parameters also exhibit strong second-order interactions with policy-related variables, such as TOU peak pricing and feed-in tariffs. Importantly, our analysis reveals that V2G deployment becomes economically feasible when at least 75% of the current fleet is electrified. Additionally, our findings highlight that optimizing the charger bus ratio be 1:2.22 can significantly reduce payback periods by 15 years.

It is also important to acknowledge the model-included parameters such as fleet size, available rooftop area, and maximum charging power, which are primarily determined by fleet operators or building owners and are not directly modifiable by public policy. Furthermore, our analysis indicates that the influence of charging power on payback periods is relatively limited. Taken together, these findings highlight the importance of prioritizing pricing mechanisms especially feed-in tariffs and TOU peak price rate design in energy policy to guide market behavior and promote efficient resource allocation.

3.11 Limitation

This study faces several limitations related to model simplifications, data availability, and real-world deployment considerations. First, the optimization framework incorporates certain mathematical assumptions and simplifications, which combined with limited access to real-world operational data, constrain the model's ability to fully capture actual system behavior. Additionally, the analysis is conducted using a one-month time

doi:10.6342/NTU202502274

horizon, rather than a full-year scope, which may limit the generalizability of the results across seasonal variations. In terms of bus operations, the dispatch schedule is randomly generated without incorporating realistic constraints such as a minimum dispatch interval, and the absence of real-time floating dispatch data hinders accurate simulation of operational dynamics. For renewable energy modeling, the system does not fully capture the nonlinear characteristics of solar generation, nor does it consider efficiency losses caused by dust urban form factors such as building-induced shading. Similarly, Battery degradation is modeled as a linear cost, without considering nonlinear factors such as temperature variation. On the policy side, the model only includes a single electricity pricing mechanism, omitting important market structures such as contracted capacity, demand response strategies, and frequency-based ancillary services. The physical design of charging infrastructure is also simplified, without accounting for actual station layout, equipment deployment, or spatial constraints. Moreover, the model does not distinguish between alternating current (AC) and direct current (DC) configurations, which may introduce additional complexity in practical V2G depot designs due to conversion equipment requirements. From an economic perspective, inflation, depreciation, and long-term financial risks are not considered, and capital and operational expenditures are treated independently rather than through an integrated financial framework. Additionally, the study excludes the participation of private electric vehicles (PEVs) in the V2G system. While PEVs may offer additional grid flexibility, their involvement depends heavily on user willingness, introducing uncertainty and potential complications in system control. Lastly, the study focuses solely on urban electric buses within metropolitan areas and does not extend to other types of electric vehicles or regional contexts, potentially limiting the generalizability of the finding.

doi:10.6342/NTU202502274

In addition to these modeling limitations, the practical implementation of V2G systems in Taiwan faces systemic and regulatory barriers. According to interviews with transportation research institutions, public bus operators continue to adopt diesel-based operational logic, which impedes the strategic transition toward V2G-enabled fleet management. Moreover, in the discussions with local industry stakeholders revealed that Taiwan's V2G ecosystem is still under development. For instance, only the CHAdeMO charging standard currently supports bidirectional charging, while other protocols commonly used in electric bus systems remain incompatible. Communication mismatches between charging stations and control systems further complicate integration. Equipment vendors in Taiwan have yet to commercialize certified V2G products, and regulatory frameworks such as fire safety codes and energy dispatch laws remain rigid. These standards often fail to address issues like cable thermal fatigue under high-frequency charging and discharging, which are critical for safe and scalable V2G deployment. Together, these institutional and infrastructural gaps highlight the need for comprehensive policy updates and industry coordination to enable real-world implementation of the proposed optimization framework.

doi:10.6342/NTU202502274

4. Conclusion

This study developed a MILP model focused on evaluating the economic feasibility of integrating rooftop solar energy and V2G systems in urban electric bus operations. The model incorporates real-world operational constraints, including dispatch scheduling, solar resource availability, battery degradation costs, and TOU electricity peak pricing. Through both first-order and second-order sensitive analyses, the research identifies the key drivers influencing operational costs and payback periods.

Under current conditions, V2G deployment can reduce monthly operational costs by approximately NT$ 220,000 in our case. However, the estimated payback periods may exceed 30 years, indicating limited economic incentive. When adopting the recommended scenario proposed in this study, put policy-related parameter into building solar electricity selling price of NT$2/kWh, TOU peak price of $10/kWh if science-oriented parameters battery degradation cost of $0.258/kWh, and a solar transfer rate of 30% and battery capacity of 500 kWh, this can lead to the payback periods payback period be shortened to within 12 years. This combination shown as **Table 15**.

Table 15 Combination of V2G economic feasible solution

	Solar Selling Price ($/kWh)	TOU peak Price ($/kWh)	Battery Capacity (kWh)	Battery Degradation ($/kWh)	Solar Transfer Rate
Recommend Scenario	2	10	500	0.258	30%

Further optimization of capital installation with a charger-to-bus ratio of 1:2.22 can reduces payback periods by an additional 15 years, and when combined with operational scheduling optimization, the payback periods can be reduced to just 6 years. We found out this scenario also contributes to a monthly emission of -4.5 tCO_2-eq, while the conventional one-way V1G system by 13.4 tCO_2-eq, aligning with Taiwan's 2030 net-zero carbon targets.

doi:10.6342/NTU202502274

This study confirms that both policy-related variables like TOU pricing and building solar electricity selling price and science-oriented factors like battery degradation and solar efficiency rate play complementary roles in influencing system performance and economic outcomes. It is important to note that parameters such as fleet size, available rooftop area, and maximum charging power while included in the model are largely determined by fleet operators or building owners and are not directly modifiable by public policy. Furthermore, the impact of charging power on payback periods is relatively limited. Therefore, this study emphasizes that government policies should focus on pricing mechanisms such as building solar selling price which usually is FIT and TOU rate design to effectively guide market behavior and promote resource allocation.

In the future work we think it can be multi stakeholder dimensions analysis, include external and resilience benefits to see the robust optimized solutions. As demonstrated in the Nissan project in Ishikawa, Japan, V2G systems have shown their potential to support black-start capabilities during disaster-induced grid failures. Such resilience applications highlight the importance of expanding V2G evaluation frameworks beyond pure economic measurement[70]. In addition, future research should incorporate real-time robust optimization frameworks that can adapt dynamically to fluctuating inputs such as energy demand, renewable generation, and electricity pricing. By integrating real-time data and uncertainty modeling, the system will be able to generate recommendations that are both resilient and context-aware, improving decision-making accuracy under diverse operational scenarios.

To sum up, despite our contributions, the model simplifies certain technical and financial aspects, which should be addressed in future research to enhance applicability and robustness.

doi:10.6342/NTU202502274

Reference

1. Council, N.D., Taiwan's 2050 Net-Zero Pathway and Strategy Overview. 2024.
2. Behnia, F., B.-A. Schuelke-Leech, and M. Mirhassani, Optimizing sustainable urban mobility: A comprehensive review of electric bus scheduling strategies and future directions. Sustainable Cities and Society, 2024. **108**: p. 105497.
3. Manzolli, J.A., J.P.F. Trovão, and C. Henggeler Antunes, Electric bus fleet charging management: A robust optimisation framework addressing battery ageing, time-of-use tariffs, and energy consumption uncertainty. Applied Energy, 2025. **381**: p. 125137.
4. Liu, X., et al., A solar-powered bus charging infrastructure location problem under charging service degradation. Transportation Research Part D: Transport and Environment, 2023. **119**: p. 103770.
5. Najafi, A., et al., Integrated optimization of charging infrastructure, electric bus scheduling and energy systems. Transportation Research Part D: Transport and Environment, 2025. **141**: p. 104664.
6. Thorne, R.J., et al., Facilitating adoption of electric buses through policy: Learnings from a trial in Norway. Energy Policy, 2021. **155**: p. 112310.
7. Guschinsky, N., et al., Fleet and charging infrastructure decisions for fast-charging city electric bus service. Computers & Operations Research, 2021. **135**: p. 105449.
8. Wei-Ting Hung, I.D.D., Automotive Research & Testing Center (ARTC), Overview of Taiwan's Electric Bus Manufacturing Industry under the 2050 Net-Zero Transition. 2023.

doi:10.6342/NTU202502274

9. Kuo-Yueh Chen, T.-L.W., and Yi-Cheng Chang, T.I. Division, and M.o.T.a.C.I.M. Institute of Transportation, Taiwan, A Preliminary Study on the Impact of Smart Charging on Electric Buses. 2021.
10. Lee, C.-Y., The study of Scheduling Problems for Battery Charging Electric Buses, in Submitted to Department of Transportation and Logistics Management. 2015, National Chiao Tung University: Hsinchu, Taiwan.
11. Lin, C.-C., The Study of Electronic Bus Scheduling Problems Considering the Charging Demands, in Degree Program of Transportation and Logistics. 2023, National Yang Ming Chiao Tung University: Taiwan.
12. CHEN, Y.-M., Electric bus vs diesel bus cost-benefit analysis for public transportation company, in Executive Master's Program of Business Administration (EMBA). 2024, Feng Chia University: Taiwan.
13. Commission, C.E., California E-Bus to Grid Integration Project. 2021.
14. Government, T.C., Sustainable Energy Taipei. 2020.
15. Wellik, T.K., et al., Utility-transit nexus: Leveraging intelligently charged electrified transit to support a renewable energy grid. Renewable and Sustainable Energy Reviews, 2021. **139**: p. 110657.
16. He, Z., J. Khazaei, and J.D. Freihaut, Optimal integration of Vehicle to Building (V2B) and Building to Vehicle (B2V) technologies for commercial buildings. Sustainable Energy, Grids and Networks, 2022. **32**: p. 100921.
17. Yeoh, J.H., K.-Y. Lo, and I.Y.L. Hsieh, Optimizing urban energy flows: Integrative vehicle-to-building strategies and renewable energy management. Energy Conversion and Management: X, 2025. **26**: p. 100974.

doi:10.6342/NTU202502274

18. Tian, X., et al., Carbon emission reduction capability assessment based on synergistic optimization control of electric vehicle V2G and multiple types power supply. Energy Reports, 2024. **11**: p. 1191-1198.
19. Elliott, M. and N. Kittner, Operational grid and environmental impacts for a V2G-enabled electric school bus fleet using DC fast chargers. Sustainable Production and Consumption, 2022. **30**: p. 316-330.
20. Yang, K., et al., A new model for comprehensively evaluating the economic and environmental effects of vehicle-to-grid(V2G) towards carbon neutrality. Journal of Energy Storage, 2024. **98**: p. 113067.
21. Lee, J., G. Razeghi, and S. Samuelsen, Utilization of Battery Electric Buses for the Resiliency of Islanded Microgrids. Applied Energy, 2023. **347**: p. 121295.
22. Liao, Z., M. Taiebat, and M. Xu, Shared autonomous electric vehicle fleets with vehicle-to-grid capability: Economic viability and environmental co-benefits. Applied Energy, 2021. **302**: p. 117500.
23. Shirazi, Y., E. Carr, and L. Knapp, A cost-benefit analysis of alternatively fueled buses with special considerations for V2G technology. Energy Policy, 2015. **87**: p. 591-603.
24. Jyh-Yih Hsu, C.-F.K., Chih-Hsiang Tsai, Fa-Ming Yeh, Cost Effectiveness Analysis of “Electric Bus-to-Grid (B2G)” Operation Model: Taking Taipei City Bus as an Example. Journal of Taiwan Energy, 2021. **Volume 8**(No. 2): p. pp. 117-132.
25. Moradipari, A., et al. Mobility-Aware Smart Charging of Electric Bus Fleets. in 2020 IEEE Power & Energy Society General Meeting (PESGM). 2020.
26. Pilotti, L., et al., Optimal E-fleet charging station design with V2G capability. Sustainable Energy, Grids and Networks, 2023. **36**: p. 101220.

doi:10.6342/NTU202502274

27. Fei, F., et al., Exploring the profitability of using electric bus fleets for transport and power grid services. Transportation Research Part C: Emerging Technologies, 2023. **149**: p. 104060.
28. Tian, X., B. Cheng, and H. Liu, V2G optimized power control strategy based on time-of-use electricity price and comprehensive load cost. Energy Reports, 2023. **10**: p. 1467-1473.
29. Arsalan, M., et al., Analyzing the impact of battery technical performance and driving conditions on the overall economic feasibility of a Vehicle-to-Grid (V2G) system implemented in the Japan electric power exchange (JEPX) market. Energy Conversion and Management: X, 2025: p. 100980.
30. He, Y., Z. Liu, and Z. Song, Integrated charging infrastructure planning and charging scheduling for battery electric bus systems. Transportation Research Part D: Transport and Environment, 2022. **111**: p. 103437.
31. Borge-Diez, D., et al., Combined vehicle to building (V2B) and vehicle to home (V2H) strategy to increase electric vehicle market share. Energy, 2021. **237**: p. 121608.
32. Ager-Wick Ellingsen, L., et al., Life cycle assessment of battery electric buses. Transportation Research Part D: Transport and Environment, 2022. **112**: p. 103498.
33. Lee, C.F., et al., Vehicle-to-Grid Optimization Considering Battery Aging. IFAC-PapersOnLine, 2023. **56**(2): p. 6624-6629.
34. Zeng, Z., S. Wang, and X. Qu, On the role of battery degradation in en-route charge scheduling for an electric bus system. Transportation Research Part E: Logistics and Transportation Review, 2022. **161**: p. 102727.

doi:10.6342/NTU202502274

35. Manzolli, J.A., J.P.F. Trovão, and C. Henggeler Antunes, Electric bus coordinated charging strategy considering V2G and battery degradation. Energy, 2022. **254**: p. 124252.

36. Zhu, R., et al., Study of Electric Bus Scheduling Problem Considering V2G and Battery Degradation, in CICTP 2024. 2024. p. 3139-3150.

37. Lo, K.-Y., J.H. Yeoh, and I.Y.L. Hsieh, Towards Nearly Zero-Energy Buildings: Smart Energy Management of Vehicle-to-Building (V2B) Strategy and Renewable Energy Sources. Sustainable Cities and Society, 2023. **99**: p. 104941.

38. Han, J.-Y., Y.-C. Chen, and S.-Y. Li, Utilising high-fidelity 3D building model for analysing the rooftop solar photovoltaic potential in urban areas. Solar Energy, 2022. **235**: p. 187-199.

39. Chang, Y.-J. and I.Y.L. Hsieh, Transitioning from illegal rooftop dwellings to solar PV: Market-based incentive design and techno-economic analysis. Energy Strategy Reviews, 2023. **49**: p. 101154.

40. Li, S.-Y. and J.-Y. Han, The impact of shadow covering on the rooftop solar photovoltaic system for evaluating self-sufficiency rate in the concept of nearly zero energy building. Sustainable Cities and Society, 2022. **80**: p. 103821.

41. Wen-Sheng Ou, M.-C.H., Jui-Ling Chen, Chien-Fu Chen, and Shih-Chi Lo, A Study on Standard Solar Irradiance for Solar Energy System Design in Taiwan. Journal of Architecture, 2008. **No.64**: p. pp.103~118,.

42. Bureau of Energy, M.o.E.A.M., Taiwan. Enhancing Electricity Use Efficiency at Government Agencies and Schools Program. 2024; Available from: https://moeaea.gov.tw.

doi:10.6342/NTU202502274

43. Agarwal, S. Solving an optimization problem. 2022; Available from: https://medium.com/@souravagarwal54321/solving-an-optimization-problem-82c062a967c6.

44. Albert, B.-H., Chen. Lecture Notes for the Operations Research Course at National Taiwan University. 2024.

45. Company, T.P. Load Management Platform. 2023; Available from: https://www.taipower.com.tw/tc/page.aspx?mid=135.

46. Upower. Electric Vehicle Fast-Charging Rates in Taiwan. 2024; Available from: https://www.u-power.com.tw/news/news-20240913.html.

47. Zecar. Charging Guide: Charge times, speed and cost. 2023; Available from: https://zecar.com/resources/polestar-2-charging-guide.

48. Company, T.P. Time-of-Use (TOU) Electricity Pricing. 2023; Available from: https://service.taipower.com.tw/taipowerdsm/residential-and-commercial.

49. Gehbauer, C., D.R. Black, and P. Grant, Advanced control strategies to manage electric vehicle drivetrain battery health for Vehicle-to-X applications. Applied Energy, 2023. **345**: p. 121296.

50. Choudhary, D., R.N. Mahanty, and N. Kumar, A dynamic pricing strategy and charging coordination of PEV in a renewable-grid integrated charging station. Electric Power Systems Research, 2025. **238**: p. 111105.

51. Wang, M., et al., Comparing stochastic programming with posteriori approach for multi-objective optimization of distributed energy systems under uncertainty. Energy, 2020. **210**: p. 118571.

52. Wei, S., et al., Multi-stage Sensitivity Analysis of Distributed Energy Systems: A Variance-based Sobol Method. Journal of Modern Power Systems and Clean Energy, 2020. **8**(5): p. 895-905.

doi:10.6342/NTU202502274

53. URANIE. Methodological reference guide for Uranie v4.9.0. 2024; Available from: https://uranie.cea.fr/documentation/methodology/ch05.

54. Andrea Saltelli, M.R., Terry Andres, Francesca Campolongo, Jessica Cariboni, Debora Gatelli, Michaela Saisana, Stefano Tarantola, Global Sensitivity Analysis. The Primer. 2007.

55. CDSN. Sensitivity Analysis — Sobol Method. 2015; Available from: https://blog.csdn.net/xiaosebi1111/article/details/46517409.

56. Oad, A., et al., Green smart grid predictive analysis to integrate sustainable energy of emerging V2G in smart city technologies. Optik, 2023. **272**: p. 170146.

57. CleanEnergyReviews. Bidirectional EV Chargers Review, Clean Energy Reviews. 2024; Available from: https://www.cleanenergyreviews.info/blog/bidirectional-ev-chargers-review.

58. FirstStudent. Total Cost of Ownership: Determining if Electric Buses are Right for Your District. 2022; Available from: https://firststudentinc.com/resources/electric/total-cost-of-ownership-determining-if-electric-buses-are-right-for-your-district/.

59. Razmjoo, A., et al. A Comprehensive Study on the Expansion of Electric Vehicles in Europe. Applied Sciences, 2022. **12**, DOI: 10.3390/app122211656.

60. SolarTechAdvisor. Lithium Titanate Batteries for Off-grid Solar Systems. 2021; Available from: https://solartechadvisor.com/lithium-titanate-batteries/.

61. Colthorpe, A. LFP cell average falls below US$100/kWh as battery pack prices drop to record low in 2023. 2023; Available from: https://www.energy-storage.news/lfp-cell-average-falls-below-us100-kwh-as-battery-pack-prices-drop-to-record-low-in-2023/.

doi:10.6342/NTU202502274

62. Orangi, S., et al., Historical and prospective lithium-ion battery cost trajectories from a bottom-up production modeling perspective. Journal of Energy Storage, 2024. **76**: p. 109800.

63. Green, M.A., Dunlop, E., Hohl-Ebinger, J., Yoshita, M., Kopidakis, N. and Hao, X., Solar cell efficiency tables (version 56). PROGRESS IN PHOTOVOLTAICS, 2020: p. p. 629-638.

64. Zhao, K. and Z. Gou, Influence of urban morphology on facade solar potential in mixed-use neighborhoods: Block prototypes and design benchmark. Energy and Buildings, 2023. **297**: p. 113446.

65. Yu, Q., et al., Global estimation of building-integrated facade and rooftop photovoltaic potential by integrating 3D building footprint and spatio-temporal datasets. Nexus, 2025. **2**(2): p. 100060.

66. Affairs, M.o.E. Official Announcement of the 2024 Feed-in Tariffs for Renewable Energy. 2024; Available from: https://www.moea.gov.tw/MNS/populace/news/News.aspx?kind=1&menu_id=40&news_id=114036.

67. Lazard. Lazard April LCOE+ (2023). 2023; Available from: https://www.lazard.com/research-insights/2023-levelized-cost-of-energyplus/.

68. Hung, C.-Y. The learning curve of solar photovoltaics continues to decline steadily at a rate of 21%, and the levelized cost of electricity (LCOE) for solar PV is expected to fall to NT$2 per kilowatt-hour by 2026. 2016; Available from: https://km.twenergy.org.tw/Data/db_more?id=1200.

69. Information, P.P. How Much Does Solar Cost Per Ping? A Complete Guide to Installation Costs, Payback Period, and Maintenance Fees. 2025; Available from: https://www.pro360.com.tw/price/solar_system.

doi:10.6342/NTU202502274

70. Portal, N.E.V.E.I. Launch of a Trial to Reduce Energy Costs and CO_2 Emissions in Office Buildings Using EV (V2B) Technology. 2018; Available from: https://global.nissannews.com/ja-JP/releases/190926-02-j.

doi:10.6342/NTU202502274

Appendix

Table A1 Daily Environmental Cost of Northern Taiwan

Hour (hr)	Total Electricity Generation (MW)	Environmental cost ($/kWh)
1	6458.26	1.66
2	6387.75	1.65
3	6329.40	1.63
4	6319.10	1.63
5	6222.36	1.60
6	6207.61	1.60
7	6113.14	1.57
8	6089.09	1.56
9	6388.84	1.63
10	6308.11	1.60
11	6480.23	1.64
12	6548.98	1.66
13	6454.34	1.63
14	6630.75	1.67
15	6709.15	1.69
16	6759.37	1.70
17	6960.37	1.75
18	6994.40	1.76
19	7044.84	1.78
20	7041.81	1.78
21	7062.33	1.79
22	7006.25	1.78
23	6945.10	1.76
24	6625.50	1.69

doi:10.6342/NTU202502274

Table A2 Carbon Dioxide Daily Environmental Cost of Northern Taiwan

Hour (hr)	Total Carbon Emission (kg)	Carbon Emission Amount (kg/kWh)	Carbon Environmental Cost ($/kWh)
1	4073131	0.41	1.63
2	4044805	0.40	1.62
3	4009403	0.40	1.60
4	4003905	0.40	1.60
5	3937911	0.39	1.58
6	3917550	0.39	1.57
7	3851536	0.39	1.54
8	3825610	0.38	1.53
9	3992928	0.40	1.60
10	3927892	0.39	1.57
11	4036258	0.40	1.61
12	4085162	0.41	1.63
13	4011740	0.40	1.60
14	4111681	0.41	1.64
15	4161117	0.42	1.66
16	4184804	0.42	1.67
17	4314065	0.43	1.73
18	4336769	0.43	1.73
19	4376953	0.44	1.75
20	4381879	0.44	1.75
21	4395104	0.44	1.76
22	4366733	0.44	1.75
23	4332154	0.43	1.73
24	4158299	0.42	1.66

doi:10.6342/NTU202502274

Table A3 NOx Daily Environmental Cost of Northern Taiwan

Hour (hr)	Total NOx Emission (kg)	NOx Emission Amount (kg/kWh)	NOx Environmental Cost ($/kWh)
1	1158.24	0.00012	0.01
2	1159.84	0.00012	0.01
3	1157.20	0.00012	0.01
4	1158.30	0.00012	0.01
5	1149.56	0.00012	0.01
6	1142.68	0.00011	0.01
7	1129.01	0.00011	0.01
8	1118.52	0.00011	0.01
9	1136.63	0.00011	0.01
10	1104.60	0.00011	0.01
11	1140.05	0.00011	0.01
12	1150.22	0.00012	0.01
13	1119.92	0.00011	0.01
14	1135.68	0.00011	0.01
15	1144.52	0.00011	0.01
16	1136.32	0.00012	0.01
17	1166.59	0.00012	0.01
18	1169.61	0.00012	0.01
19	1176.08	0.00012	0.01
20	1178.75	0.00012	0.01
21	1180.40	0.00012	0.01
22	1178.14	0.00012	0.01
23	1174.66	0.00012	0.01
24	1156.81	0.00012	0.01

doi:10.6342/NTU202502274

Table A4 Sox Daily Environmental Cost of Northern Taiwan

Hour (hr)	Total SOx Emission (kg)	SOx Emission Amount (kg/kWh)	SOx Environmental Cost ($/kWh)
1	2306.32	0.00023	0.015
2	2311.03	0.00023	0.015
3	2307.13	0.00023	0.015
4	2309.81	0.00023	0.015
5	2294.40	0.00023	0.015
6	2280.70	0.00023	0.015
7	2254.58	0.00023	0.015
8	2233.31	0.00022	0.015
9	2264.22	0.00023	0.015
10	2198.17	0.00022	0.015
11	2269.62	0.00023	0.015
12	2289.06	0.00023	0.015
13	2227.23	0.00022	0.015
14	2256.45	0.00023	0.015
15	2273.06	0.00023	0.015
16	2254.07	0.00023	0.015
17	2313.06	0.00023	0.015
18	2318.40	0.00023	0.016
19	2330.18	0.00023	0.016
20	2335.63	0.00023	0.016
21	2338.50	0.00023	0.016
22	2334.96	0.00023	0.016
23	2329.15	0.00023	0.016
24	2299.04	0.00023	0.015

doi:10.6342/NTU202502274

Table A5 PM10 Environmental Cost of Northern Taiwan

Hour (hr)	Total PM10 Emission (kg)	PM10 Emission Amount (kg/kWh)	PM10 Environmental Cost ($/kWh)
1	179.31	1.80E-05	0.00256
2	180.49	1.80E-05	0.00258
3	179.19	1.80E-05	0.00256
4	179.11	1.80E-05	0.00256
5	175.54	1.80E-05	0.00251
6	173.01	1.70E-05	0.00247
7	169.19	1.70E-05	0.00242
8	166.45	1.70E-05	0.00238
9	170.43	1.70E-05	0.00244
10	165.41	1.70E-05	0.00237
11	170.18	1.70E-05	0.00243
12	173.13	1.70E-05	0.00248
13	167.82	1.70E-05	0.00240
14	170.47	1.70E-05	0.00244
15	172.61	1.70E-05	0.00247
16	172.39	1.70E-05	0.00247
17	178.40	1.80E-05	0.00255
18	179.56	1.80E-05	0.00257
19	182.53	1.80E-05	0.00261
20	183.76	1.80E-05	0.00263
21	184.37	1.80E-05	0.00264
22	184.18	1.80E-05	0.00263
23	183.29	1.80E-05	0.00262
24	179.91	1.80E-05	0.00257

doi:10.6342/NTU202502274